
Methods¹

Expedition 317 Scientists²

Chapter contents

Background and objectives	1
Operations	1
Lithostratigraphy	4
Biostratigraphy	6
Paleomagnetism	10
Physical properties	13
Geochemistry and microbiology	18
Heat flow	25
Downhole logging	27
Stratigraphic correlation	31
References	31
Figures	36
Tables	54

Background and objectives

This chapter documents the procedures and methods employed in the various shipboard laboratories during Expedition 317 of the Integrated Ocean Drilling Program (IODP). This information applies only to shipboard work described in the Expedition Reports section of the Expedition 317 *Proceedings of the Integrated Ocean Drilling Program* volume. Methods for shore-based analyses of Expedition 317 samples and data will be described in individual scientific contributions to be published elsewhere. All shipboard scientists contributed to the completion of this volume.

Operations

Site locations

Global Positioning System (GPS) coordinates from precruise site surveys were used to position the vessel at all Expedition 317 sites. A SyQuest Bathy 2010 CHIRP subbottom profiler was used to monitor the seafloor depth on the approach to each site to reconfirm the depth profiles from precruise surveys. Once the vessel was positioned at a site, the thrusters were lowered and a positioning beacon was dropped to the seafloor. The dynamic positioning (DP) control of the vessel used navigational input from the GPS system and triangulation to the seafloor beacon, weighted by the estimated positional accuracy. The final hole position was the mean position calculated from the GPS data collected over a significant portion of the time the hole was occupied.

Drilling operations

All three standard coring systems—the advanced piston corer (APC), the extended core barrel (XCB), and the rotary core barrel (RCB)—were used during Expedition 317.

The APC system was used in the upper portion of each hole when coring in the top of the hole was the objective. The APC system cuts soft-sediment cores with minimal coring disturbance relative to other IODP coring systems. After the APC core barrel is lowered through the drill pipe and lands near the bit, the drill pipe is pressured up until the two shear pins that hold the inner barrel attached to the outer barrel fail. The inner barrel then advances into the formation and cuts the core. The driller can detect a successful cut, or “full stroke,” from the pressure gauge on the rig floor.

¹Expedition 317 Scientists, 2011. *Methods*. In Fulthorpe, C.S., Hoyanagi, K., Blum, P., and the Expedition 317 Scientists, *Proc. IODP, 317*: Tokyo (Integrated Ocean Drilling Program Management International, Inc.).
doi:10.2204/iodp.proc.317.102.2011

²[Expedition 317 Scientists' addresses.](#)



APC refusal is conventionally defined in two ways: (1) the piston fails to achieve a complete stroke (as determined from the pump pressure reading) because the formation is too hard or (2) excessive force (>60,000 lb; ~267 kN) is required to pull the core barrel out of the formation. When a full stroke could not be achieved, one or two additional attempts were typically made, and each time the bit was advanced by the length of recovered core. Note that this resulted in a nominal recovery of ~100% based on the assumption that the barrel penetrated the formation by the equivalent of the length of core recovered. When a full or partial stroke was achieved but excessive force could not retrieve the barrel, the core barrel was sometimes “drilled over”: after the inner core barrel was successfully shot into the formation, the drill bit was advanced to total depth to free the APC barrel.

Nonmagnetic core barrels were used during all conventional APC coring to a pull force of ~40,000 lb. When the need for drillover was anticipated, standard steel core barrels were used because they are stronger than the nonmagnetic barrels. Most APC cores recovered during Expedition 317 were oriented using the Flexit tool (see “[Paleomagnetism](#)”). Formation temperature measurements were made to obtain temperature gradients and heat flow estimates (see “[Heat flow](#)”).

The XCB system was used to advance the hole when APC refusal occurred before the target depth was reached or when the formation became either too stiff for the APC system or hard substrate such as cemented layers and nodules or chert was encountered. The XCB is a rotary system with a small cutting shoe that extends below the large rotary APC/XCB bit. The smaller bit can cut a semi-indurated core with less torque and fluid circulation than the main bit, optimizing recovery. The XCB cutting shoe (bit) extends ~30.5 cm ahead of the main bit in soft sediments but retracts into the main bit when hard formations are encountered. The XCB system was used extensively during Expedition 317 and to greater depths than anticipated.

The bottom-hole assembly (BHA) used for APC and XCB coring during Expedition 317 was composed of an 11 $\frac{1}{16}$ inch (~29.05 cm) drill bit, a bit sub, a seal bore drill collar, a landing saver sub, a modified top sub, a modified head sub, a nonmagnetic drill collar, five 8 inch (~20.32 cm) control length drill collars, and a tapered drill collar, followed by a 5 $\frac{1}{2}$ inch drill pipe to the surface. A typical tapered drill string was not used during Expedition 317 because of the shallow water depth. A lockable flapper valve was used so that downhole logs could be collected.

The RCB system was deployed when XCB coring rates diminished below an acceptable level or the bit was destroyed by the increasingly hard formation. The RCB is the most conventional rotary drilling system and was used during Expedition 317 to drill and core the deepest sediment hole in the history of the R/V *JOIDES Resolution*. The RCB system requires a dedicated RCB BHA and a dedicated RCB drilling bit.

The BHA used for RCB coring included a 9 $\frac{3}{8}$ inch RCB drill bit, a mechanical bit release, a modified head sub, an outer core barrel, a modified top sub, and seven control length drill collars, followed by a tapered drill collar to the 5 $\frac{1}{2}$ inch drill pipe.

Most cored intervals were ~9.5 m long, which is the length of a standard core barrel and the length of a joint of drill pipe. In some cases, the drill string was drilled or “washed” ahead without recovering sediments to advance the drill bit to a target depth to resume core recovery. Such intervals were typically drilled using a center bit installed within the RCB bit.

IODP depth conventions

In the last few decades, Deep Sea Drilling Project (DSDP), Ocean Drilling Program (ODP), and IODP Phase 1 reports, diagrams, and publications used three primary designations to reference depth: meters below rig floor (mbrf), meters below seafloor (mbsf), and meters composite depth (mcd). These designations were combinations of origin of depth scales (rig floor or seafloor), measurement units (m), and method of construction (composite). The designations evolved over many years based on the needs of individual science parties.

Over the course of ODP and IODP scientific drilling, issues with the existing depth scale designations and the lack of a consistent framework became apparent. For example, application of the same designation to scales created with distinctly different tools and methods was common (e.g., mbsf used for scales measured both by drill string tally and the wireline). Consequently, new scale type designations were created ad hoc to differentiate the wireline logging scale from the core depth scale so that depth-mapping procedures and products could be adequately described. However, the management and use of multiple maps, composite scales, or splices for a hole or a site was problematic, and the requirement to integrate scientific procedures among three IODP implementing organizations amplified the need to establish a standardized and versatile depth framework.

Using the opportunity offered by the hiatus in IODP drilling operations, a new classification and nomenclature for depth scale types was defined in 2006–2007

to provide a starting point from which the implementing organizations could address more specific issues about the management of depth scales, depth maps, and splices (see “IODP depth scales terminology,” version 1.0, available at www.iodp.org/program-policies/, for explanation of IODP depth scale definitions) (Table T1).

The primary depth scale types are based on the measurement of drill string length (e.g., drilling depth below rig floor [DRF] and drilling depth below seafloor [DSF]), length of core recovered (e.g., core depth below seafloor [CSF] and core composite depth below seafloor [CCSF]), and logging wireline (e.g., wireline log depth below rig floor [WRF] and wireline log depth below seafloor [WSF]). All units are in meters (m). The relationship between scales is defined either by protocol, such as the rules for computation of CSF from DSF, or user-defined correlations, such as stratigraphic correlation of cores between holes to create a common CCSF scale from the CSF scales used in each hole. The distinction in nomenclature should keep the user aware that a nominal depth value at two different depth scales usually does not refer to exactly the same stratigraphic interval (also see “[Curatorial procedures and sample depth calculations](#)”).

For editorial convenience, the depth scale type acronym was not repeated with each depth reference in the site chapters. The scale type was declared at the beginning of each section and only mentioned again if a different scale type was used.

Core handling and analysis

The first hole drilled at each Expedition 317 site was a short (<50 m deep) hole dedicated to whole-round sampling for microbiology, geochemistry, and geotechnical studies of the uppermost interval in the hole, where physical and chemical properties change rapidly downhole. Whole-round samples were also taken from cores from the main holes but at much lower frequency. As soon as cores arrived on deck, microbiological whole-round samples as well as headspace samples for contamination testing were taken with sterilized tools (see “[Geochemistry and microbiology](#)”). Additional headspace samples as well as gas void (vacuum tube) samples were also taken for immediate hydrocarbon analysis as part of the shipboard safety and pollution prevention program. Additional whole-round samples were taken for interstitial water analysis. Core catcher samples were taken for biostratigraphic analysis.

Core sections were then placed in core racks in the laboratory. When the cores reached equilibrium with laboratory temperature (typically after ~4 h), whole-round core sections were run through the Whole-

Round Multisensor Logger (WRMSL; measuring *P*-wave velocity, density, magnetic susceptibility, and resistivity) and the Natural Gamma Radiation Logger (NGRL). Thermal conductivity measurements were typically taken at a rate of one per section (see “[Physical properties](#)”).

The cores were then split lengthwise from bottom to top into working and archive halves. Investigators should note that older material may have been transported upward on the split face of each section during splitting. The working half of each core was sampled for shipboard analysis (biostratigraphy, physical properties, carbonate, paleomagnetism, and bulk X-ray diffraction [XRD] mineralogy) and for shore-based studies. The archive half of each core was scanned on the Section Half Imaging Logger (SHIL) and measured for color reflectance and magnetic susceptibility on the Section Half Multisensor Logger (SHMSL). At the same time, the archive halves were described visually and by means of smear slides. Finally, the archive halves were run through the cryogenic magnetometer.

Both halves of the core were then put into labeled plastic tubes that were sealed and transferred to cold storage space aboard the ship. At the end of the expedition, the cores were transferred from the ship to refrigerated trucks and then transported to cold storage at the IODP Gulf Coast Repository in College Station, Texas (USA).

Drilling disturbance

Cores may be significantly disturbed as a result of the drilling process and contain extraneous material as a result of the coring and core handling process. In formations with loose sand layers, sand from intervals higher in the hole may be washed down by drilling circulation, accumulate at the bottom of the hole, and be sampled with the next core. The uppermost 10–50 cm of each core must therefore be examined critically during description for potential “cave-in.” Common coring-induced deformation includes the concave-downward appearance of originally horizontal bedding. Piston action may result in fluidization (flow-in) at the bottom of APC cores. Retrieval from depth to the surface may result in elastic rebound. Gas that is in solution at depth may become free and drive core segments within the liner apart. When gas content is high, pressure must be relieved for safety reasons before the cores are cut into segments. This is accomplished by drilling holes into the liner, which forces some sediment as well as gas out of the liner. These disturbances are described in “[Lithostratigraphy](#)” in each site chapter and graphically indicated on the core summary graphic reports (standard graphic reports or “barrel sheets”).

Curatorial procedures and sample depth calculations

The numbering of sites, holes, cores, and samples followed standard IODP procedure. A full curatorial sample identifier consists of the following information: expedition, site, hole, core number, core type, section number, and interval in centimeters measured from the top of the core section. For example, a sample identification of “317-U1351A-1H-2, 10–12 cm” represents a sample taken from the interval between 10 and 12 cm below the top of Section 2 of Core 1 (“H” designates that this core was taken with the APC system) of Hole A of Site U1351 during Expedition 317. The “U” preceding the hole number indicates that the hole was drilled by the United States Implementing Organization (USIO) platform, the *JOIDES Resolution*.

Cored intervals are defined by the core top depth in DSF and the amount the driller advanced the bit and core barrel in meters. The length of the core is defined by the sum of lengths of the core sections. The CSF of a sample is calculated by adding the offset of the sample below the section top and the lengths of all higher sections in the core to the core top depth measured with the drill string (DSF). A soft to semi-soft sediment core from less than a few hundred meters below seafloor expands upon recovery (typically a few percent to as much as 15%), so the recovered interval does not match the cored interval. In addition, a coring gap typically occurs between cores, as shown by composite depth construction. Thus, a discrepancy between DSF and CSF depths can exist with regard to a stratigraphic interval. Furthermore, when a core recovers more than 100% of the cored interval, the CSF depth of a sample taken from the bottom of a core will be greater than that of a sample from the top of the subsequent core (i.e., the data associated with the two core intervals overlap at the CSF scale).

If a core has incomplete recovery, all cored material is assumed to originate from the top of the drilled interval as a continuous section for curation purposes. The true depth interval within the cored interval is unknown and should be considered a sample depth uncertainty in age-depth analyses and in the correlation of core data with downhole logging data.

Lithostratigraphy

The lithostratigraphic procedures used during Expedition 317, including sediment classification, visual core description, smear slide and thin section preparation and description, and XRD, are outlined below. In addition, please see “[Geochemistry and microbiology](#)” for an explanation of carbonate, major ele-

ment, and trace element analyses carried out on sediments and sedimentary rocks.

Core preparation

After imaging, but prior to description, the quality of the split surface of the archive half of each core was assessed, and when necessary (e.g., the surface was smeared or uneven) the split surface of the archive half was scraped lightly with a glass slide or spatula. Cleaned sections were occasionally reimaged if the visibility of sedimentary structures and fabric improved.

Visual core description

Sediment components and percentages in the core were determined using a hand lens, binocular microscope, smear slide examination, or thin section. Information from macroscopic and microscopic examinations of each core section was recorded by hand on a primary description form (Fig. F1). All handwritten forms were digitally preserved as PDF files (see LITH in “[Supplementary material](#)”). The schemes used for sediment description are detailed below.

Color

Sediment color was determined qualitatively for core intervals using Munsell soil color charts (Munsell Color Company, Inc., 2000).

Lithologic classification

The lithologic classification scheme used during Expedition 317, modified from Shipboard Scientific Party (2004), is based on three end-member grain components: biogenic silica, carbonate, and terrigenous or volcanic grains, along with alternative modifiers determined from smear slides (Fig. F2). This scheme is further divided according to the grain size of the terrigenous component (i.e., the relative proportions of gravel, sand, silt, and clay) (Wentworth, 1922). The term “mud” is used for a mixture of silt and clay (Fig. F2). Adjectives such as “silty” and “clayey” are used to differentiate mixtures of mud. Sand is grouped into very fine to fine sand and medium to very coarse sand fractions for description purposes. Mixtures of mud and sand are divided based on whether sand content is greater than or less than 50% (sandy mud or muddy sand, respectively).

Mixtures of terrigenous, siliceous, and calcareous sediments are named according to the relative proportion of the three components (Fig. F2). “Marl” describes a mixture of sand- to mud-sized carbonate and terrigenous material, whereas sand-sized mixtures with little matrix are referred to as “bioclastic

sand” and similarly “bioclastic gravel” for gravel-sized sediment with little matrix. The term “ooze” is used to describe <2 mm calcareous sediments containing >90% carbonate, whereas “shell hash” denotes >2 mm components. “Ash/tuff” is defined as sediment containing >50% silt- and sand-sized volcanic grains (Mazzullo et al., 1988; Shipboard Scientific Party, 2003b).

Sediment names also indicate the degree of sediment induration (e.g., sand versus sandstone, silt versus siltstone, mud versus mudstone, ooze versus chalk, or limestone). Terrigenous sediments with >2 mm modal grain size are termed “gravel,” whereas “conglomerate” and “breccia” are the principal names for consolidated gravels with well-rounded and angular clasts, respectively.

Sedimentary structures, accessories, and bedding

Sedimentary structures, accessories, and other primary and secondary (diagenetic) features are noted in the core descriptions. Bed thickness was defined according to McKee and Weir (1953):

- Very thick bedded = >100 cm.
- Thick bedded = >30–100 cm.
- Medium bedded = >10–30 cm.
- Thin bedded = >3–10 cm.
- Very thin bedded = 1–3 cm.

Laminae are described as <1 cm thick. For units in which two lithologies are closely interbedded (i.e., the individual beds are <15 cm thick and alternate between one lithology and another), three “interbedded” lithology names are used (Fig. F3): interbedded sand and mud, interbedded silt and mud, and interbedded clay and mud. When beds are scattered throughout a different lithology (e.g., beds of clay several centimeters to tens of centimeters thick within a mud bed), they are logged individually and entered as sedimentary structures, along with their associated thicknesses and textures, into the database using the DESClogik application.

Lithologic accessories noted include the type and proportion of shells and organic material, the presence of glauconite or other minerals, concretions and nodules, veins, and so on (Fig. F3).

Bioturbation

Ichnofabric description analysis included evaluation of the extent of bioturbation and notation of distinctive biogenic structures. To assess the degree of bioturbation semiquantitatively, a modified version of the Droser and Bottjer (1986) ichnofabric index (1–5) scheme was employed (1 = no apparent bioturbation, 2 = slight bioturbation, 3 = moderate bioturbation,

4 = heavy bioturbation, 5 = complete bioturbation [no depositional structure remaining]) (Fig. F4). These indexes are illustrated using the numerical scale in the ichnofabric column of the standard graphic reports (barrel sheets). Sediments without recognizable depositional structures were recorded as Level 1 on this scale. Recognizable biogenic structures and trace fossils were noted and logged in the database.

Drilling disturbance

The type and/or degree of drilling disturbance is indicated using the terminology and intensities defined in Figure F3.

Smear slide analysis

Toothpick samples were taken at select intervals in the core and used to create smear slides according to the method outlined in Mazzullo et al. (1988). One or more smear slide samples were collected from the main or dominant (D) lithology from the archive half of each core. Additional samples were collected from minor (M) lithologies and/or other areas of interest (e.g., laminations, mottles, etc.). Smear slides were viewed with a transmitted-light, petrographic microscope, and the percentages of different mineralogical, biogenic, and authigenic components were estimated along with the proportions of sand, silt, and clay (terrigenous only). These estimations were recorded on smear slide sample sheets, which were digitally preserved as PDF files (see LITH in “[Supplementary material](#)”), and entered into the database. This technique was limited in that sand grains were underemphasized, as were large calcareous components (shells and shell fragments), and the determination of percentages was subjective and varied slightly among different practitioners. Lithology descriptions from smear slides were calibrated by comparison with XRD analysis and calcium carbonate analyses by coulometry.

Thin sections

Thin sections were created on board when representative lithified sediments were encountered (including concretions and nodules). Thin sections generally provide less biased samples of whole rock than do smear slides, and they allow for more accurate identification of the minerals present. However, the limitation of selecting samples from the concretions and nodules present in soft sediments means that there was some bias in the types of lithology sampled, including (1) sampling concretions in one lithology over unlithified sediments from another and (2) recovering concreted horizons at the expense of other sediments.

Lithologies were defined according to the main lithologic classification scheme described above (Fig. F2). Additionally, a smear slide sample worksheet was completed before the results were added to the database. Representative locations for thin sections were selected when the sediments were generally too lithified for smear slide analysis.

DESClogik data capture software

Primary description forms for core sections were compiled and entered into the database using the DESClogik application. Direct entry of descriptive and interpretive information into the DESClogik program was performed using the Tabular Data Capture (TDC) mode. Before core description, a spreadsheet template was constructed in TDC. Tabs and columns were customized to include description from information categories (e.g., lithology, drilling disturbance, and bioturbation). A second template containing category columns for texture and relative abundance of biogenic/mineralogic components was configured specifically for recording smear slide data.

DESClogik includes a graphic display mode for core data (e.g., digital images of section halves and measurement data) that can be used to augment core description.

The data entered in DESClogik were then uploaded into the Laboratory Information Management System (LIMS) database.

Standard graphic report (barrel sheet)

The LIMS2Excel application was used to extract data in a format that could be used to plot descriptive as well as instrumental data in core graphic summaries using a commercial program (Strater, Golden Software). The Strater program was then used to produce a simplified, annotated, publication-quality standard graphic report (also known as a barrel sheet) of each core.

Beginning with the leftmost column, each barrel sheet displays depth scale (m CSF-A), core length, and section information. A fourth column displays the concatenated section-half images adjacent to a graphic lithology column in which core lithologies are represented by graphic patterns illustrated in Figure F3. Subsequent columns provide information on drilling disturbance, sedimentary structures, lithologic accessories, ichnofabric, and shipboard samples (see legend in Fig. F3). Additional columns present age data (see “[Biostratigraphy](#)”) and plots of core logging data such as magnetic susceptibility, natural gamma radiation (NGR), and color measurements (see “[Physical properties](#)”).

X-ray diffraction analysis

Samples for XRD analyses were selected from working halves based on visual core observations (e.g., color variability, visual changes in lithology, and texture) and smear slides. XRD analyses were performed on one sample per core from the dominant lithology in the same interval from which samples were taken for smear slide, carbonate, and carbon content analyses (coulometry, CHNS; see “[Geochemistry and microbiology](#)”). One 5–10 cm³ sample per core was frozen, freeze-dried in the case of unlithified samples, and ground by hand or in an agate ball mill as necessary. Prepared samples were top-mounted onto a sample holder and analyzed using a Bruker D-4 Endeavor diffractometer mounted with a Vantec-1 detector using nickel-filtered CuK α radiation. The standard locked coupled scan was as follows:

Voltage = 40 kV.

Current = 40 mA.

Goniometer scan = 5° to 70°2 θ .

Step size = 0.015°2 θ .

Scan speed = 0.1 s/step.

Divergence slit = 0.3 mm.

Diffractograms of single samples were evaluated with the Bruker DiffracPlus software package, which allowed only for mineral identification and basic peak characterization (e.g., width and maximum peak intensity) and could not deconvolve overlapping peaks, which were commonly observed in samples from all sites. The locations of peaks used for mineral recognition are shown in Table T2. Secondary diffraction peaks were used for certain minerals (e.g., quartz and K-feldspar) because there was interference at the primary diffraction peak position. Relative abundances of various minerals were established on the basis of maximum peak intensity. Quantification of mineral contents was not possible because the samples were not spiked with a defined amount of a mineral standard for calibration and because of a possible preferred orientation caused by top-mounting the samples. Therefore, shipboard results yielded only qualitative results on the relative occurrences and abundances of the most common mineralogical components. Further identification of clay mineralogy from these bulk powder analyses was not attempted on board the ship. Based on the comparison of calcite peak intensity with total carbonate content from coulometry, the minimum detectable peak intensity was set at 60 counts.

Biostratigraphy

The primary focus of the Expedition 317 shipboard paleontological group was to provide robust age and

paleodepth inputs to help constrain the timing and magnitude of global sea level perturbations during the late Eocene to Holocene.

Ages were assigned based on core catcher samples using calcareous nannofossil, planktonic and benthic foraminifer, bolboformid, and diatom biostratigraphy; where fitting, additional section subsamples were taken to better define some bioevents and zonal boundaries. Whole and nearly whole macrofossils in split cores and in the coarse-sized fraction of washed microfossil samples were also routinely sampled and identified. Other fossil material that was monitored in washed samples and/or smear slides included shell fragments from bivalves, gastropods, brachiopods, scaphopods, barnacles, and crabs, as well as ostracods, otoliths, fish teeth, bryozoan fragments, echinoid spines and plate fragments, radiolarians, and silicoflagellates. All micropaleontological data, including relative and total abundances and preservation, were uploaded to LIMS using the DESClogik application.

The 2008 geological timescale (Ogg et al., 2008) was used during Expedition 317, and the base of the Quaternary and Pleistocene were placed at the top of the Gelasian (1.806 Ma). The Pleistocene and Pliocene were divided into early, middle, and late (Fig. F5). All bioevents, including highest occurrences (HOs), lowest occurrences (LOs), highest common occurrences (HCOs), and lowest common occurrences (LCOs), were calibrated to the astronomically calibrated timescale of Ogg et al. (2008). Correlations to the geological timescale will be improved by the integration of postcruise data from more detailed biostratigraphic and magnetostratigraphic analyses, oxygen isotope stratigraphy, and cyclostratigraphic studies of physical property data.

Foraminifers and bolboformids

Foraminifer and bolboformid biostratigraphy provided robust correlations with the New Zealand geological timescale (Cooper, 2004) shown in Figure F5. The ranges of selected foraminifer and bolboformid species are shown in Figure F6. The calibrated ages of planktonic foraminifer and bolboformid datums are given in Table T3, and the recalibrated ages of benthic foraminifer datums are given in Table T4. Foraminiferal criteria for the adopted marine paleoenvironmental classification, modified after Hayward et al. (1999), are shown in Figure F7.

Microfossil preparation

To obtain planktonic and benthic foraminifers and bolboformids from core catcher samples, a 100–200 cm³ whole-round sample was soaked in tap wa-

ter, disaggregated, and washed over a 63 µm sieve. Where disaggregation was incomplete, especially through cemented intervals, selected samples were rewashed to improve microfossil recovery and facilitate microfossil identification. All sieves were cleaned in an ultrasonic tank and rinsed with a methylene blue solution between successive samples as a precaution against cross-contamination. After being washed, all samples were dried at 100°C in a thermostatically controlled drying cabinet. The samples were then divided with a microsplitter into separate aliquots for examination by members of the shipboard micropaleontological team. In most cases, only the >150 µm size fraction was examined; however, for stratigraphic levels where bolboformids were likely to be present, the 125–150 µm size fraction was also examined.

All age- and depth-diagnostic species of planktonic and benthic foraminifers and bolboformids were picked and mounted onto 60-division faunal slides and/or single-hole slides coated with gum tragacanth. As time allowed, other species and microfossils were also picked and mounted onto the same slides.

Planktonic foraminifers

The taxonomy for Neogene planktonic foraminifers follows a modified version of the phylogenetic classification of Kennett and Srinivasan (1983), except subgenera were raised to the status of genera (e.g., *Globorotalia* [*Globoconella*] = *Globoconella*). Abbreviations for genera and species qualifiers are given in Table T5. Species concepts are primarily based on Hornibrook (1981, 1982), Hornibrook et al. (1989), Scott et al. (1990), Hornibrook and Jenkins (1994), and Crundwell and Nelson (2007). Planktonic foraminiferal biostratigraphy from DSDP Site 594 and ODP Site 1119, off the eastern South Island of New Zealand, showed that late Neogene planktonic assemblages were strongly influenced by cold subantarctic water and that many of the age-diagnostic temperate species were either absent or poorly represented. As a consequence, unpublished ages for recently calibrated bioevents at South Tasman Rise (ODP Site 1171, 50°S) (M.P. Crundwell, unpubl. data) were used during Expedition 317 to subdivide and correlate the late middle Miocene. These bioevents include the HO of *Globoconella conica* (12.98 Ma), the LCO of *Paragloborotalia mayeri* s.l. (13.33 Ma), and the LO of *Truncorotalia juanai* (13.72 Ma).

During the shipboard examination of samples for planktonic foraminifers, the abundance of foraminifers, bolboformids, and other fossil groups in the 150–1000 µm grain-size fractions of washed microfossil samples was categorized as follows:

- D = dominant; >50% of the washed sample.
 A = abundant; >20%–50% of the washed sample.
 C = common; >5%–20% of the washed sample.
 F = few; 1%–5% of the washed sample.
 R = rare; <1% of the washed sample.

The percentage of planktonic foraminifers relative to all foraminifers was determined semiquantitatively for all samples from random counts of 100 foraminifers in the 150–1000 μm grain-size fractions of washed microfossil residues. Because planktonic foraminifers were often present in very low numbers, especially at the cored shelf sites, only the presence of each species was recorded using the following categories:

- X = present.
 ? = uncertain or unreliable identification.
 cf. = *confer* (compare with).
 aff. = *affinis* (affinity with).
 sp. = unidentified species assigned to the genus.
 spp. = more than one unidentified species assigned to the genus.

The preservation of planktonic foraminifers was categorized as follows:

- G = good; mostly whole specimens; well-preserved ornamentation and surface ultrastructure; nearly all specimens identifiable at the species level.
 M = moderate; specimens often etched or broken; ornamentation and surface ultrastructure modified; most specimens identifiable at the species level.
 P = poor; most specimens heavily encrusted, recrystallized, diagenetically overgrown, crushed, or broken; most specimens difficult to identify at the species level.

Bolboformids

Bolboformids are an extinct group of microfossils that have generally been interpreted as phytoplanktonic organisms (Spiegler and von Daniels, 1991), although oxygen isotope data from the analysis of bolboformid shells (Poag and Karowe, 1986; Spiegler and Erlenkeuser, 2001) suggest that bolboformids spent at least part of their life cycles below the photic zone in the mid- to lower levels of the water column. Bolboformids are generally made up of a hollow, single-spheroidal or subspheroidal chamber with a wall composed of monocrystalline calcite. They have a simple aperture surrounded by a short neck or collar. Surface morphology ranges from smooth to highly ornamented, with spines, knobs, reticulations, ribs, ridges, and flanges. Shell sizes range from 70 to 240 μm , although most specimens are <150 μm . Because of their small size, simple

form, and often highly ornamented shells, bolboformids have commonly been misidentified as simple single-chambered foraminifers. They are important index fossils that supplement calcareous nannofossil and planktonic foraminiferal zonations in mid- to high-latitude regions of Europe, the Atlantic, the southern Indian Ocean, and the southwest Pacific (Spiegler and von Daniels, 1991; Spiegler and Müller, 1992; Crundwell and Nelson, 2007).

Bolboformid records from oceanic sites around New Zealand, including Site 594 (45.5°S) and ODP Site 1123 (42°S) off the east coast of the South Island, comprise a series of short-lived appearances and disappearances punctuated by intervals without bolboformids (Fig. F6). These occurrences are unusual in that they are generally associated with a single species, often in very large numbers, and each interval is typically associated with a different morphologically distinct species. Similar bolboformid occurrences have been noted in offshore petroleum exploration wells in the Canterbury Basin and at ODP Site 1120 (50°S) on Campbell Plateau (M.P. Crundwell, pers. comm., 2009).

The taxonomic classification scheme for Neogene bolboformids adopted during Expedition 317 follows Spiegler and von Daniels (1991), Spiegler (1999), and the intraspecific morphological variation of Crundwell et al. (2005). All bolboformid events in the Southwest Pacific were age calibrated to the geomagnetic polarity timescale (GPTS) at Site 1123 (Crundwell and Nelson, 2007). The ages of bolboformid datums recalibrated to the timescale of Ogg et al. (2008) are given in Table T3.

Benthic foraminifers

Benthic foraminifers were the primary paleontological tool used for estimating changes in water depths during the shipboard examination of samples. Benthic foraminifers were also used for biostratigraphic dating, especially for the shallow-water sections of cored sites, where planktonic foraminifers and calcareous nannofossils were poorly represented (e.g., Site U1353). The individual benthic foraminiferal datums recognized were mostly regional datums established for onshore and near-shore New Zealand (e.g., Hornibrook et al., 1989). The benthic foraminiferal taxonomy adopted for Expedition 317 follows Vella (1957), Hornibrook (1961), Hornibrook et al. (1989), and Hayward et al. (1999).

The depth distributions of extinct benthic foraminifers were approximated on the assumption that extant species belonging to the same evolutionary lineage occupy a similar depth range. Water depths were estimated for each sample using a qualitative approach based on the diagnostic assemblages listed

in Table T6 and by comparing the fossil assemblages with extant New Zealand benthic foraminiferal assemblages with known depth distributions (Hayward et al., 1999, unpubl. data). The proportion of planktonic to benthic foraminifers was also used as a proxy for paleowater depths.

The abundance of benthic foraminifers relative to the composite fossil group of all foraminifers, ostracods, otoliths, echinoid spines, and micro-mollusks was categorized as follows:

D = dominant; >50% of the total composite fossil group.

A = abundant; >20%–50% of the total composite fossil group.

C = common; >5%–20% of the total composite fossil group.

F = few; 1%–5% of the total composite fossil group.

R = rare; <1% of the total composite fossil group.

The relative abundances of individual benthic foraminiferal species were recorded as follows:

D = dominant; >30% of the benthic foraminiferal assemblage.

A = abundant; >10%–30% of the benthic foraminiferal assemblage.

C = common; >5%–10% of the benthic foraminiferal assemblage.

F = few; 1%–5% of the benthic foraminiferal assemblage.

R = rare; <1% of the benthic foraminiferal assemblage.

Preservation categories for benthic foraminifers follow those of planktonic foraminifers.

Calcareous nannofossils

The calcareous nannofossil zonation of Martini (1971; zonal code numbers NP–NN) was used as a general framework during Expedition 317 (Fig. F8). The biozonal markers of Gartner (1977) were also used to improve biostratigraphic resolution through the Pleistocene (Fig. F9), and the bioevents of Okada and Bukry (1980) were considered for their biostratigraphic utility through the Cenozoic. An exception to this is the base of NN2, defined as the LO of *Discoaster druggii*; because of the species' rarity, the datum was not considered reliable enough to be used as a zonal marker. The calcareous nannofossil biostratigraphy of ODP Leg 181, off the east coast of New Zealand, showed that Pleistocene nannofossil assemblages had mid-latitude characteristics, and marker species that define standard biostratigraphic zones were recognized; however, standard zonal markers for the Pliocene and late Miocene (i.e., *Discoasters*, *Sphenoliths*, *Ceratoliths*, and *Amauroliths*)

were not always applicable, because these groups were either absent or occurred in such paucity as not to be useful (Shipboard Scientific Party, 1999). Calcareous nannofossil datums utilized during Expedition 317 were calibrated to the 2008 timescale (Ogg et al., 2008) and are given in Table T7. Taxonomic classification was based on Perch-Nielsen (1985) and Bown (1998, 2005). Samples were prepared as smear slides and analyzed using standard light microscope techniques under cross-polarized and plain light at 1000× magnification.

The total abundance of calcareous nannofossils was defined as follows:

VA = very abundant; >90% of sediment particles.

A = abundant; >50%–90% of sediment particles.

C = common; >10%–50% of sediment particles.

F = few; 1%–10% of sediment particles.

R = rare; <1% of sediment particles.

B = barren; no nannofossils.

The relative abundances of individual calcareous nannofossil taxa were recorded relative to the field of view (FOV) at 1000× magnification:

D = dominant; >100 specimens/FOV.

A = abundant; >10–100 specimens/FOV.

C = common; 1–10 specimens/FOV.

F = frequent; 1 specimen/1–10 FOVs.

R = rare; 1 specimen/10–100 FOVs.

P = present; 1 specimen/>100 FOVs.

Calcareous nannofossil preservation was categorized using the following criteria:

G = good; little or no evidence of dissolution and/or recrystallization; primary morphological characteristics only slightly altered; all specimens identifiable at the species level.

M = moderate; some etching and/or recrystallization; primary morphological characteristics partially altered; most specimens identifiable at the species level.

P = poor; specimens severely etched or overgrown; primary morphological characteristics largely destroyed; fragmentation evident; most specimens not identifiable at the species and/or generic level.

As time allowed, additional semiquantitative counts of calcareous nannofossils were made (where individual nannofossils were counted in five FOVs) in order to provide better insight into the cyclic nature of nannofossil abundance.

Diatoms

There have been numerous biostratigraphic and taxonomic studies of diatoms in Southern Ocean sediments (McCollum, 1975; Schrader, 1976; Fenner et al., 1976; Ciesielski, 1983; Gersonde and Burckle,

1990; Gersonde, 1990; Baldauf and Barron, 1991; Harwood and Maruyama, 1992; Censarek and Gersonde, 2002; Zielinski and Gersonde, 2002; Winter and Iwai, 2002). The adopted Neogene diatom zonal scheme used during Expedition 317 follows Cody et al. (2008), and the Paleogene zonal scheme follows Harwood and Maruyama (1992).

All diatom samples were prepared as smear slides using Pleurax as the mounting medium. Smear slides were set on a hot plate at 50°–60°C. Calcareous concretions were sieved with a 20 µm mesh after hydrochloric acid (HCl, 30%) was applied to dissolve the carbonate. This solution was kept in a 200 mL beaker for a few hours. The total abundance of diatoms and other biosiliceous components, together with assemblage composition, was recorded for all slides. For core catcher samples, wherever possible, 100 specimens (other than *Chaetoceros* resting spores) were counted. After counting, the slides were scanned to record the presence of other species missed in the original census. Between 100 and 1000 valves were observed in samples containing sufficient diatom remains. When <100 diatom valves were observed on a slide, all taxa were enumerated in a single count. Except for core catcher samples, the assessment of total diatom abundance was qualitative.

Diatom abundances were recorded as follows:

- A = abundant; >10 valves/FOV.
- C = common; 1–10 valves/FOV.
- F = few; ≥1 valve/10 FOVs and <1 valve/FOV.
- R = rare; ≥3 valves/traverse of coverslip and <1 valve/10 FOVs.
- X = present; <3 valves/traverse of coverslip, including fragments.
- B = barren; no valves.

Diatom preservation categories were described as follows:

- G = good; finely silicified and robust forms; no significant alteration of frustules other than moderate fragmentation.
- M = moderate; moderate concentration of heavily silicified forms and/or high degree of fragmentation of finely silicified forms.
- P = poor; finely silicified forms virtually absent; heavily silicified forms fragmented and/or corroded.

Paleomagnetism

Natural remanent magnetization

Natural remanent magnetization (NRM) was routinely measured on archive section halves using a 2G Enterprises superconducting rock magnetometer (SRM; model 760R) before and after alternating-field

(AF) demagnetization. The magnetometer includes three orthogonal direct-current superconducting quantum interference devices (DC SQUIDS) and is equipped with an in-line AF demagnetizer (2G Enterprises model 2G600) capable of producing peak fields of 80 mT at 200 Hz frequency. The magnetometer was run and data were acquired by a program called SRM (version 3.23), which was still in development. Two separate modules were used for continuous (section length) and discrete measurements, both reporting measurements in SI units. Previous expeditions had demonstrated that data could be acquired effectively using this software, but not all functions were available and persistent bugs slowed core flow. Testing during transit revealed that the module for discrete samples was particularly faulty and crashed often, in most instances because of communication problems with the degausser unit. The ramp up light on the front panel of the degausser unit sometimes did not light, which indicated that the magnetic field along the y -direction was not applied despite a normal display on the main personal computer (PC) screen. As a result, the discrete software module was not used during Expedition 317. Instead, discrete samples were measured on the SRM using the continuous software module. This software assumes a semicylindrical sample with an elongate z -axis when calculating magnetizations. Inclination, declination, and intensity must therefore be recalculated from the reported magnetic moments for discrete (cube) samples.

IODP orientation conventions were applied to the archive halves (+ x : vertically upward; + y : horizontally to the right when looking downcore; and + z : downcore). Core sections were measured at 5 cm intervals. In addition, NRM measurements were made at 5 cm intervals over 15 cm before the sample entered the SQUID sensors and again after the sample passed through. These measurements are referred to as header and trailer measurements, and they serve the dual functions of monitoring the background magnetic moment and allowing for future deconvolution analysis.

The noise levels of the SRM, established from empty core tray measurements taken both during transit and during drilling operations, were $\sim 4 \times 10^{-10}$ A/m² for the three SQUID sensors (the z -axis usually being the noisiest). For discrete samples with volumes of 6–10 cm³, this noise level equates to an intensity of 4×10^{-5} A/m. For split core samples with effective volumes of ~ 100 cm³, the tray noise level corresponds to an intensity of 4×10^{-6} A/m. In fact, the background resolution limit on remanence measurements of core samples in the SRM system was dictated by the magnetization of the core liner. Although measurements

of an unused, empty half liner had magnetizations on the order of 10^{-5} A/m (the same magnitude as the weakest section-half measurements), a used, empty half liner from Site U1352 had peak intensities on the order of 10^{-4} A/m. The remanence of the empty, used liner had consistently steep positive inclinations and declinations clustering to the north in the archive coordinate system. Measurements from several previous cruises indicate that accurate measurements are likely to be obtained only when split-core and discrete samples have intensities greater than 10^{-4} A/m and 10^{-3} A/m, respectively (Richter et al., 2007).

Two available calibration standards (an 8 cm³ cube standard with an intensity of 7.62 A/m and an 11.4 cm³ cylinder standard with an intensity of 5.98 A/m) were also measured during transit to the first site. Measured intensities were within 0.5 A/m of reported values. Flux jumps from the SQUIDS were sometimes encountered during the measurement of empty boats and of sections from Site U1354 but were seldom encountered during the measurement of sections from other sites. When a flux jump occurred, the measurement was repeated. Background tray measurements were taken when time allowed, usually once per shift.

Demagnetization of section-half NRM

The remanence of each section half was measured again after AF demagnetization was applied (using the 2G Enterprises AF demagnetization coils inline with the SRM). AF demagnetization was applied to remove both natural and drilling-induced viscous remanent magnetization overprints (see Richter et al., 2007). These overprints were observed as steep positive inclinations with declinations grouped around north in the archive section-half coordinates. This direction is the same as that observed in the used, empty liner. When time permitted (Site U1351), 10 mT and 20 mT demagnetization steps were applied and measured in turn. When time was short (Site U1352), only the 20 mT step was applied. Because only ~90 min was available to completely process each core, time was usually short and measurement spacing was altered to maintain core flow.

During the preceding Expedition 324, concerns that the demagnetizing coil on the SRM was malfunctioning at fields >20 mT were reported. No action was taken before the start of Expedition 317 because the nature and cause of the problems could not be determined. During transit to the first Expedition 317 site, an isothermal remanent magnetization (IRM) was imparted on a suite of discrete samples that were then demagnetized using the DTECH

Model D-2000 demagnetizer. This process was then repeated using the demagnetizing coils inline with the SRM. Note that the discrete specimens were demagnetized and measured using the SRM continuous core module software rather than the problematic discrete module software. No significant change in demagnetization behavior was observed up to 80 mT. No problems with the SRM demagnetizing coils were detected during Expedition 317. It may be that the apparent degausser coil malfunction reported during Expedition 324 (samples behaving as if they were acquiring an anhysteretic remanent magnetization during the course of AF demagnetization) arose from an unnoticed software communication problem with the degausser unit that led to an unsuccessful demagnetization protocol.

Paleomagnetism and rock magnetism of discrete samples

Oriented discrete samples were acquired from each section for onshore analyses. In lithified sediments, 8 cm³ cubes were cut with a rock saw, and an upward arrow was drawn on the split face of the working half. In soft sediments, samples were taken using the new IODP standard plastic boxes ("French cubes") having external dimensions of 2.2 cm × 2.2 cm × 2.3 cm (internal volume = ~6.9 cm³). These plastic cubes can be filled by pressing them directly into the split face of the working half of the core. Alternatively, an extruder can be used to extract sediment from the core and extrude it into the cube. These techniques, as described in Richter et al. (2007), result in azimuthally opposite orientations of the recovered cubes. For most soft-sediment cubes, we used a modified version of the extruder technique, which gave the same orientation as that given by pressing the cubes directly into the sediment. A long, open-topped extruder was used to cut through the sediment to the core liner. The column of sediment was then pushed from the bottom of the extruder out of the open top and into the cube. The use of the extruder resulted in a clean cut into the core, which made samples easy to extract. When sediment was very sticky, it was easier to press the cubes directly into the cut face of the core. By using the modified extruder technique most of the time, cubes could still be pressed into the sediment or cut with a rock saw when necessary and the orientation conventions of all cubes remained the same. In all cases, samples were extracted from the middle of the working half of the core with the arrow on the face of the cube pointing upcore, giving an orientation convention of +x (vertically downward normal to the face marked with the arrow), +y (horizontally to the right when looking along the arrow), and -z (along the arrow).

A pair of samples (one immediately above the other) was recovered from each core to compare demagnetization behavior. When time allowed, sets of discrete samples were measured in the SRM using foam blocks taped onto the core section tray at 15 cm intervals as sample holders. Paired, discrete samples were taken to allow for a fuller demagnetization of these samples in order to determine the complexity of the routinely measured NRM. One sample from each pair was demagnetized using AF demagnetization at 5 mT intervals up to 80 mT (the maximum demagnetization level of the SRM). Thermal demagnetization of the second sample was performed in the Schonstedt TSD-1 Thermal Demagnetizer. Richter et al. (2007) recommend that plastic cubes not be heated beyond 200°C; however, we found that cubes deformed at 140°C, and sediment had to be extracted from the cube and placed in a tinfoil container during heating if samples were to be demagnetized at higher temperatures.

After AF demagnetization, samples were used for rock magnetic experiments. Saturation IRM and coercivity of remanence were established by imparting a stepwise IRM up to 1 T using the ASC IM-10 impulse magnetizer. A backfield IRM was then imparted in the same manner, and magnetization was measured on the SRM after each step. An IRM was again imparted with a 1 T field, and this was stepwise demagnetized using alternating fields up to 80 mT on the SRM, allowing estimation of the mean destructive field of the samples.

Magnetic susceptibility

Three methods of measuring magnetic susceptibility were available on board. The physical properties group routinely measured the low-field susceptibility of whole cores with an 88 mm Bartington model MS2C loop sensor (MSL) at 2.5 or 5 cm intervals as part of the Whole-Round Multisensor Logger (WRMSL) (see “[Physical properties](#)”). A Bartington model MS2F point sensor (MSP) was also available on the SHMSL. Routine measurements were made at 5 cm intervals. Selected intervals were measured at 1–2 cm intervals. Bulk magnetic susceptibility of discrete samples was measured using a Kappabridge KLY 4S susceptibility meter, which was also used to monitor susceptibility changes during the thermal demagnetization of discrete samples.

Core orientation

APC cores were recovered using a nonmagnetic core barrel until overpull rendered this no longer feasible. Flexit orientation tools were used to orient APC cores when drilling conditions allowed.

The Flexit tool uses three orthogonally mounted fluxgate magnetometers to record orientation with respect to magnetic north of the double lines scribed on the core liner. The tool also has three orthogonally mounted accelerometers to monitor the movement of the drill assembly and help determine when the most stable, and thus most useful, core orientation data are gathered. Tool declination, inclination, total magnetic field, and temperature are recorded internally at regular intervals until the tool’s memory capacity is filled. For a measurement interval of 6 s, the tool can typically be run for ~24 h, although we aimed to switch tools at least every 8–12 h. Three Flexit tools (serial numbers 936, 937, and 938) were available.

The standard operating procedure involved synchronizing the instrument to a PC, running the Flexit software (version 3.5), and inserting the tool inside a pressure casing. The enclosed tool was then given to a core technician, who installed it on the sinker bars that reside above the core barrel. The double lines on the core liner were aligned relative to the tool. Prior to firing the APC, the core barrel was held stationary (along with the pipe and BHA) for several minutes while data to be used in constraining core orientation were recorded. When the APC fired, the core barrel was assumed to maintain the same orientation, although previous cruises have found evidence that the core barrel can rotate and/or the core liner can twist as it penetrates the sediments. Generally, the core barrel was pulled out after a few minutes, although it was left in the sediment for ~10 min for cores collected with the third-generation advanced piston corer temperature tool (APCT-3).

Once processed, data from the Flexit tool provided the azimuthal orientation of the double line of the core barrel (north in IODP coordinate systems). The azimuthal orientation was computed as follows. The magnetic toolface angle provided by the Flexit tool was corrected to true north by adding the present-day deviation of magnetic north from geographic north at the site location, as provided by the International Geomagnetic Reference Field (IGRF) (+25° at Site U1351). This corrected azimuthal orientation was then used to orient the cores by adding this value to the declination measured with the SRM.

Magnetostratigraphy

With drill sites at ~45°S, typical magnetic polarity zones could be identified by distinct changes in inclination of remanence. The present-day normal field in this region, as provided by the IGRF model, has a negative inclination (about –70°), so positive remanence inclinations indicate a reversed field.

When Flexit core orientation tools were used with nonmagnetic core barrels during APC coring, declination information could also be used to establish magnetic polarity.

The GPTS used during Expedition 317 is the same as that used during Expedition 320/321 and is constructed as follows.

1. Interval 0.000–23.030 Ma: the Neogene timescale of Lourens et al. (2004) was used. On this timescale, the Paleogene/Neogene boundary was placed at 23.030 Ma, based on an astronomically derived age for the base of Chron C6Cn.2n (Shackleton et al., 2000) updated to the new astronomical solution of Laskar et al. (2004) by Pälike et al. (2006a). Pälike et al. (2006b) estimated an age of 23.026 Ma for this reversal boundary (i.e., 4 k.y. younger than the estimate by Lourens et al., 2004).
2. Interval 23.278–41.510 Ma: the Pälike et al. (2006b; table S1) timescale was used from the top of Chron C6Cn.3n at 23.278 Ma to the base of Chron C19n at 41.510 Ma, which implies that the 248 k.y. long Chron C6Cn.2r is artificially shortened by 4 k.y. (1.6%) when shifting from the Miocene to the Oligocene timescale.
3. Interval 42.536–83.000 Ma: the Cande and Kent (1995) timescale was used from the top of Chron C20n to the top of Chron C34n, which implies that the 1.026 m.y. long Chron C19r is artificially lengthened by 11 k.y. (1.1%) when shifting from the Pälike et al. (2006b) timescale to the Cande and Kent (1995) timescale.

Physical properties

Shipboard physical property measurements were made during Expedition 317 to characterize lithologic units and aid in the following: correlating lithology with downhole geophysical logging data, assessing the lithologic dependence of porosity, assessing consolidation history, and interpreting seismic reflection profiles. The primary objectives of the Expedition 317 physical properties program were to collect medium-resolution data that would

1. Provide porosity information for the decompaction algorithms used in the backstripping calculations used to estimate eustatic magnitudes;
2. Facilitate hole-to-hole and site-to-site correlation and the construction of composite stratigraphic sections;
3. Provide a framework for possible postcruise climatic cyclostratigraphy studies;
4. Facilitate the construction of synthetic seismograms;

5. Investigate the characteristics of major seismic reflectors; and
6. Promote a better understanding of the strength of hemipelagic sediments in the context of sea level change, sequence stratigraphy, and possible changes of strength across unconformities.

Physical properties were measured on whole-round sections using the WRMSL. After cores were brought in from the catwalk, they were allowed to equilibrate to ambient room temperature (20°–22°C) to ensure thermal homogeneity in order to minimize temperature effects on physical property measurements and to protect the sensors from damage. The WRMSL incorporates a gamma ray attenuation (GRA) densitometer, an MSL, and a compressional *P*-wave velocity logger (PWL). NGR was also measured on whole-round sections using the NGRL. MSP measurements and color measurements (reflectance spectroscopy and colorimetry [RSC]) were taken on the archive halves of split cores using the SHMSL. High-resolution digital color images were captured using the Section Half Imaging Logger (SHIL). Moisture and density (MAD) measurements were made on discrete samples taken from section halves, often adjacent to samples used for XRD analyses. Bulk properties determined by MAD analyses include wet bulk density, dry bulk density, grain density, water content, and porosity. Shear strength was measured on working halves with the automated vane shear (AVS) system and with the fall cone penetrometer (FCP), which is a third-party tool provided by the Center for Marine Environmental Sciences (MARUM), University of Bremen, Germany.

To help illustrate key trends, the often noisy magnetic susceptibility, NGR, and color data were processed on board using the Igor Pro 5 software. An efficient approach was to use a built-in Gaussian filter. The binomial smoothing algorithm used (based on Pascal's triangle) is described by Marchand and Marmet (1983). The frequency response of the binomial smoothing algorithm is expressed as a percentage of the sampling frequency (= *n* passes). This method should be improved postcruise by cleaning the data from caved intervals of the uppermost and/or lowermost parts of the cores and by using more appropriate filtering methods. Processed data are available in `FILT_DATA` in "[Supplementary material](#)."

Whole-Round Multisensor Logger measurements

GRA bulk density, magnetic susceptibility, and compressional *P*-wave velocity were measured nondestructively with the WRMSL on all whole-round core sections. The quality of the WRMSL data is highly dependent on core condition. To optimize WRMSL

performance, sampling intervals and measurement residence times were the same for all sensors for any one core. Sampling intervals were initially set at 5 cm so that a 9.5 m long core would take ~1.2 h to pass through the WRMSL with a residence time of 3 s for each measurement and 14 s for all three measurements. During the course of the expedition, it became apparent that the sampling interval could be reduced without constraining the workflow. Therefore, the sampling resolution for all three measurements was increased to 2.5 cm to provide a more detailed record of the lowermost cores from Hole U1352C (Section 317-U1352C-87R-1 [1361.4 m; total depth]) and all cores from Sites U1353 and U1354. These sampling intervals are common denominators of the distances between the sensors installed on the WRMSL (30–50 cm), which allowed for a combination of sequential measurements that optimized total measurement time.

Section Half Multisensor Logger measurements

The SHMSL employs multiple sensors to measure bulk physical properties in a motorized and computer-controlled section-half logging machine. The SHMSL includes sensors for magnetic susceptibility, RSC, and a laser surface analyzer. The sampling interval was set at 5 cm for magnetic susceptibility and RSC. The SHIL captured continuous high-resolution images of the surface of the archive section halves.

Gamma ray attenuation bulk density

Bulk density reflects the combined effect of variations in porosity, grain density (dominant mineralogy), and coring disturbance. Porosity is controlled mainly by lithology and texture, compaction, and cementation (controlled by both mechanical and chemical processes).

The GRA densitometer on the WRMSL uses a 10 mCi ^{137}Cs capsule as the gamma ray source (principal energy peak = 0.662 MeV) and a scintillation detector. The narrow collimated peak is attenuated as it passes through the center of the core. Incident photons are scattered by the electrons of the sediment material by Compton scattering.

The attenuation of the incident intensity (I_0) is directly related to electron density in the sediment core of diameter (D), which can be related to bulk density given the average attenuation coefficient (in micrometers) of the sediment (Evans, 1965; Harms and Choquette, 1965). Because the attenuation coefficient is similar for most common minerals and aluminum, bulk density was obtained through a direct calibration of the densitometer using aluminum rods

of different diameters mounted in a core liner filled with distilled water. The GRA densitometer has a spatial resolution of <1 cm.

Magnetic susceptibility

Magnetic susceptibility is a measure of the degree to which a material can be magnetized by an external magnetic field. It provides information on the magnetic composition of the sediments, which can often be related to mineralogical composition (e.g., terrigenous versus biogenic materials) and diagenetic overprinting. Magnetite and a few other iron oxides with ferromagnetic characteristics have a specific magnetic susceptibility several orders of magnitude higher than clay, which has paramagnetic properties. Diamagnetic carbonate, silica, water, and plastics (core liner) have small negative values of magnetic susceptibility. Sediments rich in biogenic carbonate and opal therefore have generally low to negative magnetic susceptibility values because practically no clay or magnetite is present. In such cases, measured values approach the detection limit of the magnetic susceptibility sensors.

Magnetic susceptibility was measured using the non-contact pass-through “loop” sensor (MSL) on the WRMSL and the magnetic susceptibility “point” sensor (MSP) on the SHMSL. The MSL demands flush contact with the split core. A laser surface analyzer aids in the recognition of irregularities in the split-core surface (e.g., cracks and voids), and data from this tool were recorded to provide an independent check on the fidelity of SHMSL measurements.

The frequency at which the MSL operates is 621 Hz. The output of the magnetic susceptibility sensors can be set to centimeter-gram-second (cgs) units or SI units, which are the standard units used at IODP. However, to actually obtain dimensionless SI, volume-specific magnetic susceptibility values, the instrument units stored in the IODP database must be multiplied by a correction factor to compensate for instrument scaling and the geometric ratio, including core disturbance between core and loop dimensions. This correction was not undertaken during Expedition 317, and all magnetic susceptibility values are reported as instrument units.

Natural gamma radiation

The NGRL was designed and built at the Texas A&M University IODP-USIO facility from 2006 to 2008. The NGRL measures gamma rays emitted from whole-round core sections. Gamma rays arise primarily as a result of the decay of uranium, thorium, and potassium isotopes. Data generated from this instrument are used to augment geologic interpretations and fine-tune stratigraphic correlations.

The main NGR detector unit consists of 8 NaI scintillator detectors, 7 plastic scintillator detectors, 22 photomultipliers, and passive lead shielding. The NaI detectors are covered by at least 8 cm of lead shielding. In addition, lead separators (~7 cm of low-background lead) are positioned between the NaI detectors. In addition to this passive lead shielding, the NGR employs a plastic scintillator to suppress the high-energy gamma (γ) and muon (μ) components of cosmic radiation by producing a veto signal when charged particles from cosmic radiation pass through the plastic scintillator.

A measurement run consisted of counting two positions on each core section for at least 5 min each for a total of 16 measurements per section. Complete spectra for each measurement as well as computed total counts were uploaded to LIMS.

***P*-wave velocities**

P-wave velocity varies with a material's lithology, porosity, bulk density, state of stress, temperature, and fabric or degree of fracturing. In marine sediments and rocks, velocity is controlled by the degree of consolidation and lithification, fracturing, and the occurrence and abundance of free gas and gas hydrate. Microscopic and macroscopic fracturing may completely attenuate the signal to the point where it is not possible to obtain data. Together with bulk density, velocity data are used to calculate acoustic impedance and reflection coefficients that can be used to construct synthetic seismograms and estimate the depths of seismic horizons.

P-wave velocities were measured on whole-round sections with the *P*-wave logger (PWL) on the WRMSL and with the *P*-wave caliper (PWC) and *P*-wave bayonets (PWB) on split cores relative to a Cartesian coordinate system (x -, y -, and z -directions). The PWC measures *P*-wave velocity vertically to the sectional plane of the working half (x -axis), whereas the PWB measures the cross section (y -axis) and long axis (z -axis) of the core.

All tools transmit a 500 kHz *P*-wave pulse through the core section at a specified repetition rate. This signal is coupled to the sample by the plastic pole pieces of the transducers and by the pressure applied by the linear actuator. In contrast to the PWC and PWB, no water is used to improve coupling between the transducers of the PWL and the liner because the pressure applied by the actuator is known to be sufficient for reliable *P*-wave measurement. The transmitting and receiving ultrasonic transducers are aligned so that wave propagation is perpendicular to the section's long axis.

Traveltime is determined by signal processing software that automatically detects the first arrival of the

P-wave signal to a precision of 50 ns. It is challenging for an automated routine to pick the first arrival of a potentially weak signal with significant background noise. The search method skips the first positive amplitude and finds the second positive amplitude using a detection threshold limit, typically set to 30% of the maximum amplitude of the signal. It then finds the preceding zero crossing and subtracts one period to determine the first arrival. To avoid extremely weak signals, a minimum signal strength can be set (typically 0.02 V) and weaker signals will be ignored. To avoid cross-talk signals from the receiver at the beginning of the record, a delay (typically 0.01 ms) can be set to force the amplitude search to begin in the quiet interval preceding the first arrival. In addition, a trigger (typically 4 V) to initiate the arrival search process and the number of waveforms to be stacked (typically five) can also be set. A linear voltage differential transformer is used to measure the separation of the transducer to derive a travel path length for the signal (i.e., the slightly compressed core diameter). The ultrasonic *P*-wave velocity is then calculated after corrections have been made for system propagation delay, liner thickness, and liner material velocity.

Digital color imaging

The SHIL was used shortly after core splitting in an effort to avoid time-dependent color changes resulting from sediment drying and oxidation. The ship-board system uses a commercial line-scan camera lens (AF Micro Nikkor, 60 mm, 1:2.8 D) with illumination provided by a custom assembly of three pairs of light emitting diode (LED) strip lights that provide constant illumination over a range of surface elevations. Each pair of lights has a color temperature of 6500 K and emits 90,000 lux at 3 inches. The resolution of the line-scan camera was set at 10 pixels per millimeter. Users set a crop rectangle for each image to remove extraneous information. Images were saved in high-resolution TIFF format. Available files include the original high-resolution image with gray scale and ruler, as well as reduced JPEG images cropped to show only the section-half surface.

Spectrophotometry and colorimetry

Reflectance spectroscopy (spectrophotometry) was carried out using an Ocean Optics USB4000 spectrophotometer, which measures the reflectance spectra of the split core from the ultraviolet to near-infrared range. Colorimetric information from split cores was also recorded by this instrument in the $L^*a^*b^*$ color space system, which expresses color as a function of lightness (L^*) and color values a^* and b^* , where a^* reflects the balance between red (positive a^*) and green

(negative a^*) and b^* reflects the balance between yellow (positive b^*) and blue (negative b^*). When color values a^* and b^* are zero, there is no color and L^* determines gray scale.

Accurate spectrophotometry using the SHMSL demands flush contact between the instrument sensors and the split core. A built-in laser surface analyzer aids in the recognition of irregularities in the split-core surface (e.g., cracks and voids), and data from this tool were recorded in order to provide an independent check on the fidelity of SHMSL measurements.

Moisture and density

Wet and dry bulk density, grain density, water content, and porosity were determined from measurements of wet sediment mass and volume and/or dry sediment mass and volume. In soft sediments, $\sim 10 \text{ cm}^3$ samples were extracted, usually from the middle of each core section, and placed in pre-weighed 16 mL Wheaton beakers. Stiff sediments drilled with the XCB were sampled, where appropriate, by extracting $\sim 10 \text{ cm}^3$ blocks using a spatula and placing the blocks into a beaker, as above. Indurated sediments drilled with the RCB system were sampled by drilled cylinders $\sim 1.8 \text{ cm}$ in diameter and 2–2.5 cm in height. When the cylinders were regular in shape (no breakage, etc.) they were measured with an electronic digital caliper having a precision of 0.001 cm. Method C was applied to soft sediments and rock samples using the measurements of wet and dry mass and dry volume determined by gas pycnometry. In addition, Method D was applied to rock cylinder samples using wet volume determined with the caliper and dry mass and volume. One sample was routinely collected from each undisturbed section, and 3–4 samples per core were collected where recovery was good and sedimentation rates were high. Additional samples were taken where major changes in lithology were observed. Finally, for Holes U1353A and U1353B, one sample was taken by syringe on the catwalk during the initial core splitting in order to determine whether the WRMSL measurements and core-splitting procedures affected porosity results.

Sample mass was determined to a precision of 0.01 g using two Mettler Toledo electronic balances and a computer averaging system to compensate for the ship's motion. Dry sample volumes were determined using a hexapycnometer system consisting of six custom-configured Micromeritics AccuPyc 1330TC helium-displacement pycnometers with a precision of 1% of the nominal full-scale volume. Volume measurements were preceded by three purges of the sample chambers with helium warmed to $\sim 25^\circ\text{C}$.

Three acquisition cycles were used for each sample. A reference volume was included within each sample set and rotated sequentially among the cells to check for instrument drift and systematic error. Sample beakers used for discrete determination of moisture and density were calibrated before the cruise. Dry mass and volume were measured after samples were heated in an oven at $105^\circ \pm 5^\circ\text{C}$ for 24 h and allowed to cool in a desiccator. Procedures for the determination of these properties comply with the American Society for Testing and Materials (ASTM) designation (D) 2216 (ASTM International, 1990). Fundamental phase relationships and assumptions for the calculations of all physical property parameters are discussed by Blum (1997, Methods C and D in "Chapter 2: moisture and density") and summarized in "[Mass and volume calculation](#)" and "[Calculation of bulk properties](#)," below.

Mass and volume calculation

Method C (sediments and hard rock)

Wet mass (M_{wet}), dry mass (M_{dry}), and dry volume (V_{dry}) were measured in the laboratory. The mass ratio (r_m) is a computational constant of 0.965 (i.e., 0.965 g of freshwater per 1 g of seawater). Salt precipitated in sediment pores during the drying process is included in the M_{dry} and V_{dry} values. The mass of the evaporated water (M_{water}) and salt (M_{salt}) in the sample are given by

$$M_{\text{water}} = M_{\text{wet}} - M_{\text{dry}}$$

and

$$M_{\text{salt}} = M_{\text{water}} [s/(1 - s)],$$

where s is the assumed saltwater salinity (0.035) corresponding to a pore water density (ρ_{pw}) of 1.024 g/cm^3 (from experimental and empirical relations between salinity and density at laboratory conditions; Blum, 1997) and a salt density (ρ_{salt}) of 2.22 g/cm^3 . The corrected mass of pore water (M_{pw}), volume of pore water (V_{pw}), mass of solids excluding salt (M_{solid}), mass of salt (M_{salt}), volume of salt (V_{salt}), wet volume (V_{wet}), and volume of solids excluding salt (V_{solid}) are, respectively,

$$M_{\text{pw}} = (M_{\text{wet}} - M_{\text{dry}})/r_m,$$

$$V_{\text{pw}} = M_{\text{pw}}/\rho_{\text{pw}}$$

$$M_{\text{solid}} = M_{\text{wet}} - M_{\text{pw}}$$

$$M_{\text{salt}} = M_{\text{pw}} - (M_{\text{wet}} - M_{\text{dry}}),$$

$$V_{\text{salt}} = M_{\text{salt}}/\rho_{\text{salt}}$$

$$V_{\text{wet}} = V_{\text{dry}} - V_{\text{salt}} + V_{\text{pw}}$$

and

$$V_{\text{solid}} = V_{\text{wet}} - V_{\text{pw}}$$

Method D (hard rock and measured volume of soft sediment)

Wet (or total) volume (V_t), dry mass (M_{dry}), and dry volume (V_{dry}) were measured in the laboratory. Total mass, including freshwater in the pores, was calculated (using a density of water of 1 g/cm³) by

$$M_t = M_{\text{dry}} + (V_t - V_{\text{dry}}) \times \rho_w$$

Assuming a pore water density of 1.024, the volume of pore water is calculated by

$$V_{\text{pw}} = (V_t - V_{\text{dry}})/\rho_{\text{pw}}$$

Finally, the mass of pore water is

$$M_{\text{pw}} = V_{\text{pw}} \times \rho_{\text{pw}}$$

Calculation of bulk properties

For all sediment samples, water content (w) is expressed as the ratio of the mass of pore water to wet sediment (total) mass:

$$w = M_{\text{pw}}/M_{\text{wet}}$$

Wet bulk density (ρ_{wet}), dry bulk density (ρ_{dry}), sediment grain density (ρ_{solid}), porosity (ϕ), and void ratio (VR) are calculated from

$$\rho_{\text{wet}} = M_{\text{wet}}/V_{\text{wet}}$$

$$\rho_{\text{dry}} = M_{\text{solid}}/V_{\text{wet}}$$

$$\rho_{\text{solid}} = M_{\text{solid}}/V_{\text{solid}}$$

$$\phi = V_{\text{pw}}/V_{\text{wet}}$$

and

$$\text{VR} = V_{\text{pw}}/V_{\text{solid}}$$

Sediment strength

Shear strength describes the maximum strength of soil or sediment at which point a significant structural failure occurs in response to an applied shear stress. Sediment shear strength can be measured by various instruments in the laboratory, including

direct simple shear, triaxial shear, vane shear, and fall cone devices. Only fall cone and vane devices are suited for measuring the shear strength of very soft to stiff marine sediments. Fall cone and vane tests are useful for determining the undrained shear strength of undisturbed clay- or silt-rich samples. The FCP is a third-party tool used during Expedition 317 for the first time, whereas the vane shear device is routinely available. These shear strength tests are not suitable for coarser grained sediments or sediments containing silt or sand laminations. Because additional forces from the ship's motion add uncertainty to stress tests, both FCP and AVS tests were conducted so as to minimize the limitations of performing a single test. The sampling rate was one measurement per core section until the sediment became too firm for cone penetration or vane insertion.

Fall cone tests

The FCP test is a rapid, simple, accurate method for determining the undrained shear strength of fine-grained soils or sediments. Undrained shear strength is critical in evaluating sediment compaction as well as processes such as sliding, slope failure, and erosion.

FCP tests were conducted with a "Strassentest" apparatus Type 318H, which conforms to the British Standard BS 1377. The weight of the cone was 80 g with a 30° cone angle. The cone was carefully lowered to the surface of the sediment so that the tip of the cone touched but did not penetrate the sediment surface. The cone was then allowed to fall freely and penetrate the sediment under its own weight. After 5 s, a magnetic clamp stopped the free fall of the cone. The final cone penetration depth was measured with a dial gauge. This destructive measurement was done on the working halves of cores, with the fall direction parallel to the bedding plane.

Hansbo (1957) showed that (dynamic) undrained shear strength (s_u) is related to the final depth of penetration (h_f) of the cone and can be expressed as

$$s_u = (W \times K)/h_f^2,$$

where

W = cone weight (g),

K = fall cone factor (a constant), and

h_f = final penetration depth (mm).

Fall cone factor is a constant that is influenced by cone geometry, cone roughness, surrounding soil or sediment, and dynamic effects (Houlsby, 1982; Wood, 1985; Koumoto and Houlsby, 2001; Mahajan and Budhu, 2009). In empirical fall cone experi-

ments performed with cones of different angles, Wood (1985) showed that the average cone factor value for the 30° cone is $K = 0.85$. Koumoto and Houlby (2001) suggested that undrained shear strength in the fall cone test is dynamic shear strength, which is higher than static undrained shear strength because of the higher strain rates in the fall cone test. They proposed an empirically determined adjustment factor, K , to determine static undrained shear strength. For the British cone, the theoretically determined value of the constant is $K = 1.33$ (Dolinar and Trauner, 2005). In this study, we used Wood's factor to calculate undrained shear strength, yielding results in terms of Newtons (SI units) of kN/m^2 .

Vane shear tests

The AVS test was conducted using the "Giesa Automated Vane System." The Giesa system consists of a controller and a gantry for shear vane insertion. A four-bladed miniature vane (diameter = height = 12.7 mm) was pushed carefully into the sediment of the working halves until the top of the vane was level with the sediment surface. The vane was then rotated at a constant rate of 90°/min to determine the torque required to cause a cylindrical surface to be sheared by the vane. This destructive measurement was done with the rotation axis parallel to the bedding plane. The torque required to shear the sediment along the vertical and horizontal edges of the vane is a relatively direct measurement of shear strength. Undrained shear strength, s_u , is given as a function of pressure in SI units of Pascals ($\text{kPa} = \text{kN/m}^2$).

Both sediment strength tests were performed on working section halves at a resolution of one measurement per section. The tests were conducted in parallel to minimize the limitations of employing a single test. Samples were generally taken in undisturbed fine-grained sediments. XCB cores were sampled when core quality allowed, and measurements were made between "biscuits" and as far as possible from other drilling disturbances (e.g., cracks, gaps, or soupy core parts). Potential measurement failures in XCB cores due to low penetration depth of the fall cone and the formation of shear gaps during the insertion of the vane blades should be taken into consideration. No samples were taken from RCB cores because of the lithified nature of these sediments.

Geochemistry and microbiology

Organic geochemistry

Shipboard organic geochemistry for Expedition 317 included routine sets of analyses for (1) hydrocarbon gas in sediment cores, (2) inorganic carbon content

of sediment, (3) total carbon (TC), total nitrogen (TN), and total sulfur (TS) content of sediment, and (4) pyrolysis characterization of sedimentary organic matter using the source rock analyzer (SRA). Most of the procedures and instruments used during Expedition 317 were described by Pimmel and Claypool (2001) and generally are similar to those used during recent IODP expeditions. Comments on routine sampling and deviations from standard practice are noted below and in the individual site chapters.

Hydrocarbon gases

Sediment gas composition was typically determined at each interstitial water sampling point or at least once every core. Two sampling methods were employed: headspace (HS) sampling and gas void (VAC) sampling using a syringe. HS gas is given off after a known quantity of sediment is heated in a vial. VAC sampling is a direct extraction of gas from visible expansion voids within the core liner of the recovered core. Sediment plugs for HS analysis were taken directly after the core was brought onto the catwalk and were prepared for analysis using two methods (Fig. F10):

1. The first sediment plug (code HS), consisting of 5 cm^3 of sediment, was usually sampled using a cork borer, put into an HS vial, and crimp-sealed for standard IODP hydrocarbon safety monitoring. When the sediment became too lithified to extract using a cork borer, fragments of core were chiseled out of the core and placed in the vial. HS samples for onboard analyses were heated at 70°C for 30 min before being injected into the gas chromatograph (GC).
2. The second sediment plug (code LIPP1), consisting of 3–5 cm^3 of sediment, was sampled as above and put into a vial containing 5 mL of a 1M sodium hydroxide solution, capped with a pre-cleaned butyl stopper (heated with 1M KOH and rinsed three times with nanopure water), and frozen upside down for shore-based analyses of stable carbon isotopes.

Gases obtained by either HS or VAC sampling were analyzed by one of two GC systems: an Agilent/HP 6890 Series II (GC3) or an Agilent/HP 6890A natural gas analyzer (NGA). Gases were introduced by injection from a 5 mL syringe directly connected to the GC system via a 1 cm^3 sample loop; helium was used as the carrier gas.

The GC3 system determines concentrations of methane (C_1), ethane (C_2), ethene ($\text{C}_2=$), propane (C_3), and propene ($\text{C}_3=$) with a flame ionization detector (FID) using a 2.4 m × 3.2 mm internal diameter (ID) stainless steel column packed with 100/120 mesh

HayeSep R. Helium was used as the carrier gas, and the GC oven temperature was programmed to hold for 0.5 min at 90°C, ramp at 30°C/min to 100°C, ramp at 15°C/min to 110°C, remain at 110°C for 4.5 min, and then ramp at 50°C/min to 150°C with a final holding time of 1.8 min. The FID temperature was 250°C.

The NGA system measures concentrations of C₁–C₇ hydrocarbons with an FID as well as concentrations of N₂, O₂, and CO₂ with a thermal conductivity detector (TCD). TCD separation used three columns: a 6 ft × 2.0 mm ID stainless steel column (Poropak T [50/80 mesh]), a 3 ft × 2.0 mm ID stainless steel molecular sieve column (13X; 60/80 mesh), and a 2.4 m × 3.2 mm ID stainless steel column packed with 80/100 mesh HayeSep R (Restek). FID separation was performed on a DB1 capillary column (60 m × 0.32 mm) with 1.5 μm phase thickness. FID separation used helium as the carrier gas, and the GC oven temperature was programmed to hold for 2 min at 50°C, ramp at 8°C/min to 70°C, and then ramp at 25°C/min to 200°C with a final holding time of 5 min. The FID temperature was 250°C.

Data were collected and evaluated with an Agilent ChemStation data-handling program. For both systems, chromatographic response was calibrated to nine different gas standards with variable quantities of low molecular weight hydrocarbons, N₂, O₂, CO₂, Ar, and He and checked on a daily basis. Gas components are reported as parts per million by volume (ppmv) of the injected sample. Methane in the uppermost HS samples is also expressed as millimoles per liter of pore volume (mM), assuming a porosity of 0.45, a sample volume of 5 cm³, and a vial volume of 21.5 cm³:

$$C_1 \text{ (mM)} = \text{ppmv } C_1 \times ([21.5 - 5]/5)/(23,400 \times 0.45) \\ = \text{ppmv } C_1 \times 0.0003.$$

Sampling for carbonate and organic matter analyses

Sediment samples collected for shipboard analysis (nominally 10 cm³ wet volume; typically ~3 g dry mass) were selected from the working half of the core on the sampling table in collaboration with sedimentologists. Samples were selected based on (1) major lithology, so that questions regarding carbonate content could be answered, and (2) any darker, more organic-rich lithologies, based on visual differences. Samples were freeze-dried for at least 12 h. Dried samples were crushed to a fine powder and carefully homogenized with a mortar and pestle in preparation for carbonate and organic matter analyses.

Inorganic carbon and carbonate

The inorganic carbon (IC) content of sediment samples was determined by coulometry using a UIC 5011 CO₂ coulometer in which samples of ~10 mg of freeze-dried, ground sediment were reacted with 1N HCl. The liberated CO₂ was back-titrated to a colorimetric end-point. The carbonate content of sediment (in weight percent) was calculated from IC content by assuming that all carbonate occurs as calcium carbonate:

$$\text{CaCO}_3 = \text{IC} \times 8.33.$$

Accuracy was ensured during analysis batches by running a carbonate standard (100 wt% CaCO₃) every 10 samples and continuing analysis only if values were between 99 and 101 wt%. Typical precision was assessed using 11 replicate analyses of a carbonate sample (Table T8), which gave a standard deviation of 1.2 for a sample with a mean carbonate content of 66.4 wt% and a coefficient of variation of 0.018.

Elemental analyses

TC, TN, and TS contents of sediment samples were determined with a ThermoElectron FlashEA elemental analyzer 1112 equipped with a ThermoElectron packed column (CHNS/NCS) and a thermal conductivity detector (TCD). An aliquot of 8–12 mg of freeze-dried, ground sediment was weighed into tin cups, one small spatula of vanadium pentoxide catalyst was added, and the sample was combusted in a stream of oxygen at 900°C. The reaction gases were passed through a reduction chamber to reduce nitrogen oxides to nitrogen; they were then separated by the GC before detection by the TCD.

All measurements were calibrated to a sulfanilamide standard (N = 16.27 wt%, C = 41.84 wt%, and S = 18.62 wt%) that was run every 10 samples. Analyses were only continued if standard data varied by <1% from these values for N and C. Based on the drift of N, C, and S in the sulfanilamide standard in typical batches, S content varies more than that of N and C. Analyses were only continued if standard data for S varied by <10%.

Typical precision was assessed using 10 replicate analyses of a rock standard from Weatherford Laboratories (99986; PWDR5) (Table T9) having a nominal total organic carbon (TOC) content of 3.11 wt% and an IC content of 0.43 ± 0.02 wt% based on coulometry (TC = 3.54 wt%). These replicate analyses show standard deviations of 0.032, 0.046, and 0.032 wt% for N, C, and S, respectively. The coefficients of variation are 0.055, 0.013, and 0.020 wt% for N, C, and S, respectively.

TOC_{DIFF} content was calculated as the difference between TC and IC from coulometry:

$$\text{TOC}_{\text{DIFF}} = \text{TC} - \text{IC}.$$

Organic matter characterization

The type and quantity of organic matter in sediments were evaluated by pyrolysis assay using the SRA (Weatherford Laboratories). Between 60 and 150 mg of freeze-dried, ground sediment was weighed into SRA crucibles. Volatile hydrocarbon (HC) content was released when the sample was heated at 340°C for 3 min as the S₁ peak (mg HC/g rock). Hydrocarbons were released during the pyrolysis of kerogen as the temperature was increased from 340° to 640°C at 25°C/min as the S₂ peak (mg HC/g rock). The nominal temperature of the maximum rate of hydrocarbon yield during S₂ analysis is T_{max} . CO₂ (as mg C/g rock) released during pyrolysis between 340° and 390°C is the S₃ peak. CO₂ (as mg C/g rock) produced by oxidizing the pyrolysis residue at 580°C is the S₄ peak, but this is not directly reported. TOC_{SRA} was calculated from S₁, S₂, and S₄, assuming that S₁ and S₂ are 83% carbon:

$$\text{TOC}_{\text{SRA}} (\%) = (0.83 \times [S_1 + S_2] + S_4)/10.$$

The carbon-normalized hydrogen index (HI) (mg HC/g C) and the oxygen index (OI) (mg CO₂/g C) were calculated from pyrolysis values:

$$\text{HI} = (100 \times S_2)/\text{TOC}$$

and

$$\text{OI} = (100 \times S_3)/\text{TOC}.$$

All measurements were preceded by a blank and then calibrated to a rock standard from Weatherford Laboratories (99986; PWDR5); the same standard was used for quality control (QC) every 10 samples. Analysis was only continued if QC data fell within the permitted range for this standard, as defined by Weatherford Laboratories (Table T10). Typical precision was assessed using eight replicate analyses of the rock standard. Coefficients of variation for this data set fell between 0.005 (T_{max}) and 0.1 (OI) (Table T10). In practice, S₃ and OI were occasionally more variable than permitted for the 99986 standard when used as a QC standard in batches of samples; the range of error was as high as ±50%.

Total organic carbon measurement

TOC was measured using two completely independent methods during Expedition 317. In the first

method, TOC_{SRA} was derived directly from the SRA as the sum of pyrolysis carbon ($0.83 \times [S_1 + S_2]/10$) and residual carbon ($S_4/10$). The S₄ parameter is the oxidizable (at 580°C) residual carbon remaining after pyrolysis. This technique has the advantage of being derived directly during an analytical run on one instrument.

In the second method, TOC_{DIFF} was derived from the difference between TC (measured on the elemental analyzer) and IC (measured by coulometry). This technique has the advantage of being derived partly from the traditional elemental analysis approach but the disadvantage of relying on two separate instruments, because carbon associated with carbonate content must be subtracted from TC.

To provide constraints on the difference between these methods and advise IODP of the best approach for shipboard TOC measurements, a small batch of 10 samples from Hole U1351A was selected for offline decarbonation. This was achieved by reacting the rock powder with gently warmed 2M HCl in a beaker to remove the carbonates, after which the samples were washed, filtered, freeze-dried, and re-crushed. The decarbonated fractions were then analyzed by both the elemental analyzer and the SRA (Table T11).

The 10 selected samples have variable carbonate contents (2.4–31.4 wt%) and thus variable original IC contents (0.29–3.76 wt%; Fig. F11). Like the main data set, the subset has considerably higher TOC_{SRA} than TOC_{DIFF} (Fig. F11A). TOC measured on the decarbonated samples (TOC_{decarbonated TC}) does not equal TOC_{DIFF} but is variable, expressed as a difference of –1.0 to 0.1 (Table T11). This difference does not correlate with the original IC contents (Fig. F11B), meaning that the variability is not related to carbonate content. Furthermore, no correlation exists between carbonate content and the original difference between TOC_{DIFF} and TOC_{SRA}. A good correlation is present between TOC_{SRA} and TOC_{decarbonated TC} (Fig. F11C), having almost the same offset as TOC_{DIFF} versus TOC_{SRA}. TOC_{decarbonated TC} is more closely correlated with the measurement of TOC by the SRA on decarbonated samples (TOC_{SRA [decarbonated]}), but an offset remains whereby the SRA gives higher TOC values than the elemental analyzer (Fig. F11D).

TOC_{SRA (decarbonated)}} is considerably reduced (20%–70%) compared to original TOC_{SRA} (Table T11). Removing carbonate should lead to an increase in TOC in the residue, not a decrease, so bulk removal of carbonate using the technique described above clearly alters and removes a portion of organic matter. This means that the technique commonly used to measure TOC

(bulk offline removal of carbonates by acid digestion followed by TC measurement) may be invalid. It may be better to remove carbonates using acid treatment in the tin cups to avoid the partial removal of organic matter.

In conclusion, the different TOC measurements reflect inherent differences in the way the two instruments (CHNS elemental analyzer and SRA) measure organic carbon content. The temperature of combustion is higher for the elemental analyzer (900°C) than for the SRA (580°C), and the two instruments are calibrated in quite different ways. The difference does not relate to carbonate content. We recommend that bulk carbonate removal not take place prior to TOC measurement. In order to determine the correct TOC profile for Site U1351 (Fig. F11C–F11D), low TOC% standards must be measured. At the time of measurement of Expedition 317 samples, the only TOC standard available in the laboratory was the rock standard from Weatherford Laboratories (99986; PWDR5), which has a TOC of 3.11%.

Inorganic geochemistry: interstitial water analyses

Sampling

Interstitial water was extracted from 10–15 cm long whole-round samples (labeled red/orange for interstitial water in Fig. F10). Whole-round interstitial water samples were collected at a rate of 3–6 per core where recovery permitted in the shallow (~25–85 m deep) hole at each site dedicated to geochemistry, microbiology, and geotechnical whole-round sampling. The depth of each dedicated hole was intended to cover sediments from the seafloor to the sulfate/methane interface and an approximately equal distance below. In the main deep hole at each site, one whole-round interstitial water sample was taken per core until geochemical profiles stabilized. Thereafter, whole-round samples were collected once every other core until total depth was reached or until the cores became too lithified (Site U1352). These whole-round samples were cut on the catwalk, capped, and taken to the laboratory for immediate processing. This high-resolution sampling technique enabled the creation of high-resolution chemical profiles for the interstitial waters at each site.

In the dedicated hole, one 30 cm long whole-round sample was taken per core in order to provide sufficient interstitial water for shore-based analysis (LIPP4; Fig. F10). In addition, a separate 10 cm whole-round sample (code ISHI) was taken from the same sections (Fig. F10) to meet a shore-based sample request for more interstitial water.

When too many samples needed to be processed immediately during high-resolution sampling, capped whole-round core sections were stored in the cold room until they were squeezed (no longer than 12 h after core retrieval). Gloves were used during sample processing. After extrusion from the core liner, the surface of each whole-round sample was carefully scraped with a clean spatula to remove potential contamination from seawater and sediment smearing in the borehole. For APC cores, 1 cm was removed from the outer diameter and from the top and bottom faces of the samples. For XCB cores, where borehole contamination is higher, as much as 30% of the sediment was removed from each whole-round sample.

The remaining sediment (~50–300 cm³) was placed in a titanium squeezer modified after the stainless steel squeezer of Manheim and Sayles (1974). In most cases, gauge pressures as high as 20 MPa were applied using a laboratory hydraulic press to extract interstitial water. Interstitial water was passed through a prewashed Whatman Number 1 filter fitted above a titanium screen, filtered through a 0.45 µM polysulfone disposable filter (Whatman Puradisc PES), and subsequently extruded into a prewashed (10% HCl) 50 mL plastic syringe attached to the bottom of the squeezer assembly. In most cases, 20–40 cm³ of pore water was collected from each sample, which required squeezing the sediment for 20–40 min. Interstitial water subsamples collected from the syringe were immediately analyzed for salinity, pH, alkalinity, and sulfate. The remaining interstitial water was divided into aliquots and stored in several vials in a freezer for other shipboard and shore-based analyses. Any filter cake that remained after whole rounds were squeezed for interstitial water was divided into subsamples for shore-based analyses.

Salinity, pH, and alkalinity analyses

Interstitial water analyses followed the procedures outlined by Gieskes et al. (1991), Murray et al. (2000), and user manuals for new shipboard instrumentation, with modifications as indicated. Interstitial water was routinely analyzed for salinity with a Reichert temperature-compensated manual refractometer, previously calibrated using the International Association for the Physical Sciences of the Oceans (IAPSO) seawater standard. Alkalinity and pH were measured immediately after squeezing by Gran titration with a Metrohm autotitrator. The IAPSO seawater standard was used for the standardization of alkalinity. Variation for alkalinity was 2%–3% based on the IAPSO standard run after every fifth sample.

Ion chromatograph anion and cation analyses

Sulfate, chloride, magnesium, calcium, sodium, and potassium concentrations in interstitial water were determined with a Dionex ICS-3000 ion chromatograph on 1:200 diluted aliquots in 18 M Ω water. The IAPSO seawater standard was used to standardize measurements made on the ion chromatograph by running it after every fifth sample. The coefficient of variation based on seven repeat analyses of an interstitial water sample for anions and cations measured on the ion chromatograph was 0.002% (Table T12). Any batches of samples with >2% drift for the IAPSO standard were rerun. Acceptable 2% limits for the IAPSO seawater standard are given in Table T13.

Spectrophotometry analyses

Phosphate, ammonium, and silica concentrations in interstitial water were determined using an OI analytical discrete analyzer (DA3500) spectrophotometer unit, which is an automated system that controls sample analysis and reagent aspiration, dispensing, heating, and mixing.

In the phosphate method, orthophosphate reacts with Mo(VI) and Sb(III) in an acidic solution to form an antimony-phosphomolybdate complex. Ascorbic acid reduces this complex to form a blue color, measured at 880 nm. Potassium phosphate monobasic (KH₂PO₄) was used to produce a calibration curve and as an internal standard.

In the ammonium method, phenol undergoes diazotization, and the subsequent diazo compound is oxidized by sodium hypochlorite to yield a blue color, measured spectrophotometrically at 640 nm. Ammonium chloride (NH₄Cl) was used to produce a calibration curve and as an internal standard.

In the silica method, silica in solution as silicic acid or silicate is reacted with a molybdate reagent in acid media to form the β -molybdosilicic acid. The complex is reduced by ascorbic acid to form molybdenum blue, measured at 420 nm. Synthetic seawater containing sodium silicofluoride (Na₂SiF₆) was used to produce a calibration curve and as an internal standard.

The reproducibility for phosphate and silica concentrations in interstitial water is ~5% and that for ammonium is ~20%.

Minor element analyses by inductively coupled plasma–atomic emission spectroscopy

Minor elements in interstitial water were determined by inductively coupled plasma–atomic emission spectroscopy (ICP-AES) with a Teledyne Prodigy

high-dispersion ICP-AES. Minor elements (Mn, Fe, B, Sr, Ba, Si, and Li) were analyzed as described by Murray et al. (2000) by preparing calibration standards in an acidified (2% HNO₃, by volume) sodium chloride matrix (25 g NaCl/L). Samples and standards were diluted 1:10 using the 2% HNO₃. To control for instrumental drift and improve precision, an internal standard (10 ppm yttrium) was added to the solution before digestion by 2% HNO₃. Drift correction was made when necessary using the factor from a drift monitor solution (middle value standard solution), which was analyzed after every seventh sample. The coefficient of variation based on duplicate samples is typically <5% (Table T14).

Microbiology

The Canterbury Basin is a promising place in which to expand our knowledge of the deep biosphere because it is in a complex setting representing the history of life under a variety of environmental constraints. The Canterbury Basin is heavily influenced by the input of terrestrial organic matter and is therefore an excellent end-member environment to complement the marine settings that have been studied during previous drilling expeditions. The microbiology program during Expedition 317 sought to determine the following:

1. Depth profiles of total prokaryotic and viral cell counts (SYBR Green cell counting) and intact polar lipid (IPL) concentrations to quantify living biomass;
2. The identities and distribution of microbial and unicellular eukaryotic groups present at each site using 16S/18S ribosomal deoxyribonucleic acid (rDNA)/ribosomal ribonucleic acid (rRNA) (small subunit ribosomal RNA/DNA) clone libraries or tags 454 pyrosequencing (or alternatively, using catalyzed reporter deposition–fluorescence in situ hybridization [CARD-FISH] with probes specific to domain, phylum, and family regions), quantitative polymerase chain reaction (Q-PCR), and IPL chemotaxonomy; and
3. The activity of dominant groups, functional gene clone libraries, enrichment-isolations of strains under diverse nutritional (with diverse carbon and energy sources) and physiological (notably under high pressure) conditions, stable isotope probing (SIP), determination of main carbon turnover processes by $\delta^{13}\text{C}$ analysis of IPLs and correlation to major carbon pools, and analysis of changes in dissolved organic matter pore water constituents by Fourier transform–ion cyclotron resonance–mass spectrometry during incubation with various substrates.

Core handling and sampling

To ensure the preservation of microbial communities, a special sampling strategy was required. This sample strategy was well described for ODP Leg 201 (Shipboard Scientific Party, 2003a).

Generally, when a core arrived on the core deck it was immediately sectioned into 1.5 m sections (Fig. F10). In Sections 1, 3, and 5 of every core from the hole dedicated for whole-round sampling and in Section 3 of every 5–6 cores from the main hole(s), two neighboring whole-round (code WRND) core samples, each 10 cm long, were sliced using sterilized spatulas for microbial analysis: one for IPL analysis (code LIPP5) and one for microbial characterization (code ALA) (Fig. F10). The LIPP5 whole round was capped without further treatment at both ends, sealed in a plastic bag, labeled, and immediately frozen in a -80°C freezer until shipment on dry ice to the shore-based laboratory. The ALA whole round was capped at both ends using sterilized end-caps and transferred to the cold chamber (set to $<8^{\circ}\text{C}$) for further subsampling. The end of the section adjacent to the ALA whole round (top of Sections 2, 4, and 6 of cores from the dedicated hole; top of Section 4 of cores from the main hole[s]) (Fig. F10) was sampled for perfluorocarbon contamination checks. In the hole dedicated to whole-round sampling, one additional whole-round sample (LIPP6) was taken per core (Fig. F10) under sterile conditions and transferred into an anaerobic chamber in the cold room ($<8^{\circ}\text{C}$) for subsampling. After the seawater-contaminated outer layer of sediment was removed, 30 cm^3 of the LIPP6 sample was transferred to a sterile 30 mL plastic tube (Sarstedt, Germany) and immediately frozen at -80°C for determination of the microbial community composition; the remaining sample was transferred into a sterile 1 L Schott bottle sealed with a butyl stopper for storage at 4°C under a nitrogen atmosphere until shipment at 4°C (incubation sample). The standard ODP/IODP bags previously used for transporting samples under a nitrogen atmosphere at 4°C were not used because they were found to leak (Lipp et al., 2010).

The ALA whole-round samples for microbiological characterization were subsampled under sterile conditions in the anaerobic chamber in the cold room ($<8^{\circ}\text{C}$) as follows:

Samples for molecular analysis ($100\text{--}150\text{ cm}^3$; DNA extraction) were taken from the inner part of the ALA whole-round cores with a sterile 30 mL cut-off syringe, transferred into three 50 mL polypropylene tubes (Sarstedt, Germany), and directly frozen at -80°C for onshore analysis. In order to limit RNA degradation, five 2 cm^3 samples for RNA extraction were taken as previously described and immediately frozen at -80°C .

Samples for CARD-FISH analysis (1 cm^3) were taken with a sterile 2 mL cut-off syringe as previously described by Pernthaler et al. (2001) and stored in a -20°C freezer until shipment. The cell walls of the microorganisms have to be permeabilized to the point that the oligonucleotide probes pass through the cell walls and the cellular ribosomal RNA content is preserved. This was done by fixing cells in buffered formaldehyde solution (1 cm^3 of sediment fixed in 9 mL of sterile 3% formalin/3% NaCl solution at room temperature for $\sim 4\text{ h}$), followed by two washing steps with phosphate buffered saline (PBS) $1\times$ and the addition of 4 mL of a PBS:ethanol (1:1) solution. Samples were then frozen at -20°C until processing in onshore laboratories.

Samples for cultures ($6\text{--}10\text{ cm}^3$) were taken from the inner part of the core with a 5 mL cut-off sterile syringe and placed into 100 mL Schott vials before storage at 4°C . The samples were flushed with nitrogen for several minutes to eliminate any biogas from the anaerobic chamber that would facilitate the growth of methanogenic or acetogenic microorganisms.

Samples for cell counts (1 cm^3) were taken with a sterile 2 mL cut-off syringe and placed in 15 mL polypropylene tubes (Sarstedt, Germany) containing 9 mL of 3% formalin/3% NaCl solution and stored at 4°C until analysis. This slurry represented a 1:10 dilution of the original sample.

Additional samples (1 cm^3) for monitoring the infiltration of the $0.5\text{ }\mu\text{m}$ fluorescent microsphere beads were taken on the ALA whole rounds with a sterile 2 mL cut-off syringe from the outer and inner parts of the core and placed in 15 mL polypropylene tubes (Sarstedt, Germany) containing 9 mL of 3% NaCl solution and stored at 4°C until bead counting (Fig. F10).

Rock sampling

Sometimes the bottoms of the deepest holes were characterized by hard or cemented intervals that required a different sampling strategy. After core retrieval on the catwalk, LIPP5 and ALA whole-round rock samples were immediately taken into the cold room. The LIPP5 whole round sample was directly frozen at -80°C , and the ALA whole round was subsampled under a laminar flow fume hood. The rock samples were carefully cleaned under ultraviolet (UV) light by scraping off the outside sediment layers using sterile spatulas before being washed with a sterile 3% NaCl solution. Afterward, the cleaned samples were exposed to UV radiation for 15 min on sterile aluminum foil. The scraping of the outside surfaces, combined with washing and exposure to UV light, removed surface contamination. Rocks

were then crushed into several pieces by wrapping them in sterile aluminum foil and breaking them into pieces with several forceful hammer strokes. The rock samples were subsequently subdivided for DNA/RNA extractions, cell counts, CARD-FISH, and cultures, as described above. Rock samples for contamination testing using both chemical and particulate tracers were taken from the outer and inner parts of the whole round. This sampling strategy did not allow preservation of the samples in an anaerobic atmosphere. Consequently, the samples used for enrichment cultures were immediately gassed with pure sterile nitrogen for ~30 min. All materials used for sampling (spatulas, tweezers, hammer, etc.) were sterilized for 45 min in an autoclave at 135°C.

Contamination tests

The amount of sample contamination during drilling and handling was evaluated by running two types of tests as previously described for ODP Legs 185 (Smith et al., 2000) and 201 (Shipboard Scientific Party, 2003a), and for IODP Expedition 301 (Expedition 301 Scientists, 2005).

Perfluorocarbon tracers

Perfluorocarbon tracer (PFT; perfluoromethylcyclohexane, C₆F₁₁CF₃; Oakwood Products, 003295) has a molecular weight of 350.06 g/mol and a density of 1.78 g/mL. Its solubility is ~2 mg/L in water and 104 mg/L in methanol. During drilling, the rate of the tracer injection was adjusted to maintain a final concentration of ~1 mg/L in the drilling fluid using shipboard rig instrumentation software to control pumping rates. Using sterile cut-off 3 mL syringes, ~3 cm³ subcores were taken from the center of the sediment cores and from the periphery of the sediment cores at the core liner. In this way, parallel data sets were collected to determine the extent of contamination at the periphery of the sediment core, along the core liner, and in the center of the core (Smith et al., 2000). PFT concentration was analyzed using the GC (HP6890). The column used on the GC was an HP-PLOT/AL₂O₃ (15 m length × 0.25 mm ID × 5 μm film thickness). The inlet temperature was 170°C, and the inlet pressure was 16.23 psi. The detector temperature was 275°C. The column oven temperature was held at 100°C for 3.5 min and then ramped at 50°C/min to 200°C. At this time, 500 μL of headspace was injected, resulting in a PFT peak eluting at ~8.5–9.2 min. For GC calibration, standard solutions were made by diluting the perfluoromethylcyclohexane in methanol to 10⁻³, 10⁻⁵, 10⁻⁷, 10⁻⁹, and 10⁻¹¹. Attempts were made to construct a standard curve by plotting the peak area versus the amount of perfluoromethylcyclohexane injected.

Particulate tracer: fluorescent microspheres

A plastic bag containing a suspension of submicron-sized fluorescent microspheres (2 × 10¹¹ microspheres/20 mL bags; Carboxylate YG 0.50 μm microspheres; Polyscience, USA) was introduced into the core catchers of all core barrels from which microbiological samples would be taken (Smith et al., 2000). During drilling, the beads were released inside the core barrel as the sediment entered and were dispersed onto the outer surface of the core. When the core was retrieved, 1 cm³ samples for particulate tracer analysis were taken at the periphery of the core, adjacent to the outer PFT samples, and placed in 15 mL polypropylene tubes (Sarstedt, Germany) containing 9 mL of sterile 3% NaCl solution before storage at 4°C. The infiltration of fluorescent microspheres into the inner part of the core was checked on the samples taken near the samples taken for cell counts. The total number of microspheres was determined by epifluorescence microscopy using a Zeiss Axio-plan 2 imaging microscope (Germany) equipped with a blue filter (17 FITC, 460/402 nm) at 1000× magnification.

Cell counts

IODP provides an outstanding opportunity to explore the deep biosphere. Microbiological data collected from 25 ODP and IODP expeditions worldwide mostly comprise total cell counts performed by cell staining with 4',6-diamidino-2-phenylindole (DAPI), acridine orange (AO; Daley and Hobbie, 1975), and SYBR Green (Noble and Fuhrman, 1998). However, the enumeration of total cell numbers in marine sediment samples still represents a major challenge because the nonspecific binding of fluorescent dye and/or autofluorescence from sediment particles strongly hampers the recognition of cell-derived signals. Lately, new cell extraction procedures have been developed (Lunau et al., 2005; Kallmeyer et al., 2008), but these can be time consuming on board ship.

Recently, Morono et al. (2009) developed a highly efficient and discriminating detection and enumeration technique for microbial cells in sediments using dilute (1%) hydrofluoric acid (HF). This weak acid reduces nonbiological fluorescent signals, such as that from amorphous silica, and enhances the efficiency of cell detachment from particles.

Procedure

Under an aspirant hood, 50 μL of sediment slurry (described above) was mixed with 450 μL of an HF solution (1.0% [wt/v] HF and 3% [wt/v] NaCl) in a plastic test tube and then incubated for 20 min at room temperature. The HF reaction was stopped by

adding 2 mL of stop solution (1M tris-hydrochloric acid [HCl; pH 8.0], 0.125M CaCl₂, and 25% methanol). Subsequently, the mixture was sonicated at 20 W for 5 min using an ultrasonic bath (Fisher, FS14H).

A volume of 50–750 µL of sonicate was mixed with 2.5 mL of 3% NaCl and directly filtered through a 0.22 mm pore size black polycarbonate membrane without centrifugation. In order to eliminate potential carbonate particles and/or precipitates, the membrane was treated with 1 mL of 0.1M HCl for 5 min on the filtration device. The membrane was then washed with 5 mL of TE buffer (10 mM tris-HCl and 1.0 mM ethylenediaminetetraacetic acid [EDTA]; pH 8.0) and air dried.

A volume of 80 µL of SYBR Green (25×) was added to the filtered cells, and the sample was incubated at room temperature for 15 min, followed by air drying. Subsequently, the filter was mounted on the slide with 40–50 µL of a mounting solution containing an antifade agent ([50% glycerol, 50% PBS 1×, 0.05M Na₂HPO₄, and 0.85% NaCl; pH 7.5] and 0.1% *p*-phenylenediamine [in a 1:2 mixture] made daily from a 10% aqueous stock). The cells were counted using epifluorescence microscopy with a blue filter set as described above. Two hundred FOVs were usually counted per sample.

Enrichment cultures

The deep marine subsurface biosphere is a natural habitat characterized by complex conditions that are often difficult to reproduce in the laboratory. In addition, the mean generation times of the populations have been estimated to be very long. This explains why there are only a few reports of successful cultivation and isolation in pure cultures (D'Hondt et al., 2002; Batzke et al., 2007). However, cultivation is the easiest way to access a microorganism's physiology, and we have a lot to learn from microbial isolates originating from the deep biosphere. For this reason, during this expedition we enriched various types of microorganisms likely to grow in this environment. Several enrichment media were prepared on board, based on an artificial salt solution detailed in Table T15. Different substrates were added according to the requirements of the physiological type of the targeted prokaryotes. The enrichment cultures were 1% inoculated from 25% sediment slurries prepared by adding a sterile 3% (w/v) NaCl solution to the samples collected for culturing. The enrichments were prepared under a laminar flow hood located in the cold room and flushed with pure N₂. The growth of cells was observed by microscopy, and successful enrichments were shipped at 4°C.

We targeted different groups of prokaryotes: methanogens, acetogens, sulfate-reducers, and fermenters. We used several substrates and incubated the cultures at near the in situ temperature (Table T16). The turbidity of the culture, together with photonic and fluorescence microscopy, were used to detect positive growth within the cultures. In addition, methanogens were recognized by the autofluorescence of their F420 cofactor when exposed to UV light.

Heat flow

Heat flow reflects the tectonic evolution of oceanic and continental plates, which may be accompanied by volcanism or hotspot activity. In addition to plate evolution, sedimentary processes associated with fluid circulation can also influence heat flow. Determination of heat flow requires measurement of thermal conductivity and geothermal gradient. Thermal conductivity is an intrinsic physical property of material and is dependent on pressure and temperature. It commonly varies with depth in accordance with the variation of other index properties such as porosity and bulk density. The Bullard method (Bullard, 1939) uses a linear relationship of thermal resistance versus temperature to determine heat flow over a depth interval with an established geothermal gradient. Thermal conductivity is routinely measured during IODP expeditions as part of the physical properties suite of measurements. Geothermal gradient can be calculated if successful temperature measurements are taken at several depths.

Geothermal gradient

In situ temperature data were obtained using two types of downhole tools: (1) the APCT-3, for use in soft-sediment formations, and (2) the Sediment Temperature (SET) tool, for use in more indurated sediment formations. The APCT-3 is deployed in the APC cutting shoe, and the temperature measurement is taken shortly after the core barrel is fired into pristine sediment. The results are associated with the bottom of the cored interval for that APC deployment. The SET tool is deployed in a separate wireline run, during which the ~1 m long probe is pushed into the bottom of the hole ahead of the bit. The results are associated with the interval 1 m below the top of the next advancement (cored or drilled interval). Both tools record time–temperature data in their onboard data loggers. After tool retrieval, the data are downloaded to a computer and the asymptotic temperature is estimated using the TFIT software (version 1.0). The tools are capable of measuring temperature in the range of –20° to 100°C with an accuracy of ±0.02°C.

Thermal conductivity

Thermal conductivity measurements were conducted on whole-round sections after the cores had passed through the WRMSL and the NGRL. Prior to measurements, the sections were equilibrated to ambient laboratory temperature (19°C) for at least 4 h to ensure thermal homogeneity.

Thermal conductivity was measured with the TK04 (Teka Berlin) system using the needle probe method (Von Herzen and Maxwell, 1959) in two configurations: (1) the full-space needle probe (VLQ) for soft sediments and (2) the half-space needle probe (HLQ) for rocks (“puck probe”). The needle probe contains a heater wire and a calibrated thermistor. The probe is assumed to be a perfect conductor because it is much more conductive than sediment. Under this assumption, the temperature of the superconductive probe has a linear relationship to the natural logarithm of time after initiation of heating:

$$T(t) = (q/4\pi k) \times \ln(t) + C,$$

where

- T = temperature (K),
- q = heat input per unit length per unit time (J/m/s),
- k = thermal conductivity (W/[m·K]),
- t = time after initiation of heating (s), and
- C = a constant.

One measuring cycle consists of three steps: (1) temperature drift self-test, (2) thermal conductivity measurement, and (3) 10 min break. Several measuring cycles can be performed automatically at each sampling location and used to calculate average conductivity. A self-test, which included a drift study, was conducted at the beginning of each measurement cycle. Once the samples were equilibrated, the heater circuit was closed and the temperature rise in the probes was recorded. Thermal conductivities were calculated from the rate of temperature rise while the heater current was flowing. Temperatures measured during the first 80 s of the heating cycle were fit to an approximate solution of a constantly heated line source (for details, see Blum, 1997).

Thermal conductivity measurements were taken once per section (~7 per full core), and one measuring cycle was performed for each measurement in soft sediments into which the TK04 needle could be inserted without risk of damage. When core material was too hard to use the full-space needle probe, the puck probe method was used instead. The puck probe method uses the same theory as the full-space needle probe method except that a flat circular puck is used as the probe and the working half of the split

core is used instead of the whole-round core. Due to the limited time available, hard rock measurements were limited to one measurement with five measuring cycles per core because puck probe data showed large scatter. Heating power was adjusted to keep the power control value within a range of 2–3 W, as suggested by the TK04 manual. Drift control was set at 40 s for quick measurement. Based on repeated tests, this setting does not greatly affect the accuracy of measured values.

When the full-space needle probe method was used, the needle was inserted into unconsolidated sediment through a small 2 mm hole drilled into the core liner perpendicular to what would become the split-core surface. Thermal transfer compound was used during previous expeditions to improve the coupling between the needle and the sediment. However, it was not used during Expedition 317 to eliminate the possibility that the compound would contaminate the split-core surface and affect core description. Additionally, testing of the thermal transfer compound using sediments that were provided as test samples prior to drilling revealed no improvement in thermal coupling.

When the puck probe method was used, the probe was attached to the split-core surface with rubber rings in a seawater tube. Although at least 5 bar of pressure is recommended by the manufacturer to connect the puck probe thermally to the split-core surface, we used several rubber rings because our rock samples were too weak to bear the ~300 kg weight (corresponding to 5 bar) over the probe. Results obtained using the rubber rings with the puck probe are similar to those obtained with the full-space needle probe inserted into a drilled hole within hard rock. A Styrofoam box filled with seawater was used to achieve thermal coupling between the puck probe and the core and to minimize thermal disturbance. The water depth in the box was high enough to cover the contact surface between the puck probe and the core. Accordingly, it was important to get rid of air bubbles at the contact surface before taking measurements.

Thermal conductivity data were discarded when (1) contact between the probe and sediment was poor, as evidenced by a logarithm of extreme time (LET) of <50 s and/or <100 solutions in the software; (2) thermal conductivity was close to that of water (0.6 W/[m·K]), resulting from dilution of sediments during coring; and (3) measurements were taken in caved-in layers such as shell hash. In most cases, the first two criteria are controlling parameters for monitoring measurement quality. Measurement error was considered to be 5%–10% (Blum, 1997).

At sites where in situ temperatures were measured, thermal conductivity was corrected for in situ temperature and pressure prior to the calculation of heat flow. Laboratory values were corrected to in situ conditions following Hyndman et al. (1974):

$$\lambda_{\text{in situ}}(z) = \lambda_{\text{lab}} \times \left[1 + \frac{(z_w + \rho_{\text{sed}} \times z)}{182,900} + \frac{T(z) - T_{\text{lab}}}{400} \right],$$

where

$$\begin{aligned} \lambda_{\text{in situ}}(z) &= \text{in situ thermal conductivity at depth } z \text{ (m)}, \\ \lambda_{\text{lab}} &= \text{laboratory-measured thermal conductivity}, \\ z_w &= \text{water depth (m)}, \\ \rho_{\text{sed}} &= \text{bulk density of sediment (g/cm}^3\text{)}, \\ T(z) &= \text{in situ temperature at depth } z \text{ (m), and} \\ T_{\text{lab}} &= \text{laboratory temperature.} \end{aligned}$$

CSF-A was the standard depth scale used for temperature and thermal conductivity measurements. The correction process typically adjusted thermal conductivity by up to $\pm 5\%$ for 2000 m CSF-A and 500 m water depth.

Thermal conductivity values are commonly averaged across a depth interval using a geometric mean because heat is assumed to flow vertically through the sediment layers. Averaged thermal conductivity (λ_{avg}) is calculated as follows:

$$\frac{1}{\lambda_{\text{avg}}} = \frac{1}{Z} \sum_{i=1}^n \frac{z_i}{\lambda_i},$$

where

$$\begin{aligned} \lambda_i &= \text{thermal conductivity at the } i\text{th layer with} \\ &\quad \text{thickness } z_i \text{ and} \\ Z &= \text{total thickness of all layers,} \end{aligned}$$

that is,

$$Z = \sum_{i=1}^n z_i.$$

In practice, z_i is the measurement frequency interval used (e.g., section or core). The length of the core catcher and/or of unrecovered sections that were not measured is added to the closest measured section.

Heat flow calculation

To estimate heat flow we use the Bullard method (Bullard, 1939), which is useful when thermal conductivity varies over a depth interval where geothermal gradient is established (e.g., Pribnow et al., 2000). It assumes a linear relationship between temperature and thermal resistance of the sediment:

$$T(z) = T_0 + q \times \Omega(z),$$

where

$$z = \text{depth (m CSF-A),}$$

T_0 = temperature at $z = 0$, and

q = heat flow.

Thermal resistance ($\Omega[z]$) is defined as

$$\Omega(z) = \int_0^z \frac{dz}{\lambda(z)} \approx \sum_{i=1}^I \frac{z_i - z_{i-1}}{\lambda_i},$$

where

$$\begin{aligned} z_i &= \text{bottom depth of the } i\text{th horizontal layer,} \\ z_{i-1} &= \text{top depth of the } i\text{th horizontal layer,} \\ \lambda_i &= \text{thermal conductivity, and} \\ I &= \text{the number of horizontal layers between} \\ &\quad \text{the seafloor (} z = 0 \text{) and depth } z. \end{aligned}$$

A plot of temperature versus thermal resistance (a Bullard plot) allows estimation of (1) surface temperature (T_0) from the intercept with $z = 0$ and (2) heat flow from the slope of a line fitted to the data. Data in a Bullard plot fall in a line when conditions between the seafloor and depth z include (1) conductive cooling, (2) steady state, and (3) no heat source/sink.

If thermal conductivity increases linearly with depth, thermal conductivity is represented as

$$\lambda(z) = \lambda_0 + \Gamma \times z,$$

where

$$\begin{aligned} \lambda_0 &= \text{estimated surface thermal conductivity and} \\ \Gamma &= \text{the slope.} \end{aligned}$$

When establishing the fitting line, we used thermal conductivity corrected to in situ pressure and temperature conditions as described above.

Then, thermal resistance is solved as

$$\Omega_i = [\ln(\lambda_0 + \Gamma \times z_i) - \ln(\lambda_0)]/\Gamma,$$

where Ω_i is the thermal resistance of the i th horizontal layer.

Downhole logging

Downhole logs are used to determine the physical, chemical, and structural properties of the formation penetrated by a borehole. Data are rapidly collected, continuous with depth, and measured in situ; they can be interpreted in terms of the stratigraphy, lithology, mineralogy, and geochemical composition of the penetrated formation. Where core recovery is incomplete or disturbed, log data may provide the only way to characterize the borehole section. Where core recovery is good, log and core data complement one another and may be interpreted jointly.

Downhole logs measure formation properties on a scale that is intermediate between those obtained from laboratory measurements on core samples and those from geophysical surveys. They are useful in calibrating the interpretation of geophysical survey data (e.g., through the use of synthetic seismograms) and provide a necessary link for the integrated understanding of physical properties on all scales.

Wireline logging

Logs are recorded during wireline logging operations with a variety of Schlumberger logging tools, which are combined into several tool strings and run down the hole after coring operations are completed. During Expedition 317, the following three tool strings were planned for deployment (Fig. F12; Table T17):

1. The triple combination (triple combo) tool string, which consists of the Hostile Environment Natural Gamma Ray Sonde (HNGS), Hostile Environment Litho-Density Sonde (HLDS), Phasor Dual Induction–Spherically Focused Resistivity Tool (DIT), and Accelerator Porosity Sonde (APS). During Expedition 317, the General Purpose Inclinerometry Tool (GPIT) was also included in the tool string;
2. The Formation MicroScanner (FMS)-sonic tool string, which consists of the FMS, GPIT, HNGS, and Dipole Sonic Imager (DSI); and
3. The Versatile Seismic Imager (VSI) with the Scintillation Gamma Ray Tool (SGT).

Each tool string also contains a telemetry cartridge for communicating through the wireline to the Schlumberger data acquisition system (the MAXIS unit) on the drillship. Because of difficult hole conditions, some of these tool strings had to be reduced or reconfigured. See individual site chapters for details.

In preparation for logging, the boreholes were flushed of debris by circulating viscous drilling fluid. In most cases, the boreholes were then filled with a seawater-based logging gel (sepiolite mud mixed with seawater; approximate density = 8.8 lb/gal, or 1.055 g/cm³) to help stabilize the borehole walls. The limited supply of logging gel available during Expedition 317 required that the appropriateness of its use be evaluated at some sites. The BHA was pulled up to 60–100 m wireline log depth below seafloor (WSF). The tool strings were then lowered downhole by a seven-conductor wireline cable during sequential runs before being pulled up at constant speed, typically 250–400 m/h, to provide continuous measurements of several properties simultaneously. A wireline heave compensator (WHC) was used when necessary to minimize the effect of ship heave on the tool position in the borehole (see “[Wireline heave](#)

[compensator](#)”). During each logging run, incoming data were recorded and monitored in real time on the Schlumberger MAXIS 500 system.

Logged sediment properties and tool measurement principles

The logged properties, and the principles used by the tools to measure them, are briefly described below. Tool name acronyms, the parameters measured by each tool, the sampling interval, and the vertical resolution are summarized in Table T18. More detailed information on individual tools and their geological applications may be found in Ellis and Singer (2007), Goldberg (1997), Lovell et al. (1998), Rider (1996), Schlumberger (1989, 1994), and Serra (1984, 1986, 1989). A complete online list of acronyms for Schlumberger tools and measurement curves is available at www.apps.slb.com/cmd/index.aspx.

Natural radioactivity

The HNGS was used in the triple combo and the FMS-sonic tool strings to measure and classify natural radioactivity in the formation. The HNGS uses two bismuth germanate scintillation detectors and five-window spectroscopy to determine concentrations of K, Th, and U. The radioactive isotopes of these three elements dominate the natural radiation spectrum. The HNGS filters out gamma ray energies below 500 keV, eliminating sensitivity to bentonite or KCl in the drilling mud and improving measurement accuracy.

The SGT uses a sodium iodide scintillation detector to measure total natural gamma ray emissions, combining the spectral contributions of K, U, and Th concentrations in the formation. The SGT is not a spectral tool but provides high-resolution total gamma ray.

The inclusion of a gamma ray sonde in every tool string allows the use of gamma ray data for depth correlation between multiple logging strings and passes.

Density

Formation density was measured with the HLDS. The sonde contains a radioactive cesium (¹³⁷Cs) gamma ray source (622 keV) and far and near gamma ray detectors mounted on a shielded skid, which is pressed against the borehole wall by a hydraulically activated eccentricizing arm. Gamma rays emitted by the source experience both Compton scattering and photoelectric absorption. Compton scattering involves the ricochet of gamma rays off electrons in the formation via elastic collision, transferring energy to the electron in the process. The

number of scattered gamma rays that reach the detectors is proportional to the density of electrons in the formation, which is in turn related to bulk density. Porosity may also be derived from this bulk density if the matrix (grain) density is known.

The HLDS also measures photoelectric absorption as the photoelectric effect (PEF). Photoelectric absorption of gamma rays occurs when their energy is reduced below 150 keV after being repeatedly scattered by electrons in the formation. Because PEF depends on the atomic number of the elements in the formation, it also varies according to the chemical composition of the minerals present and can be used for the identification of some minerals. For example, the PEF of calcite = 5.08 barns per electron (b/e^-), illite = 3.03 b/e^- , quartz = 1.81 b/e^- , hornblende = 10.49 b/e^- , and plagioclase (albite) = 1.68 b/e^- .

Good coupling between the tool and borehole wall is essential for good HLDS logs. Poor contact results in the underestimation of density values. Both density correction and caliper measurement of the hole are used to check the contact quality.

Porosity

Formation porosity was measured with the APS, which includes a minitron neutron generator that produces fast (14.4 MeV) neutrons and five neutron detectors (four epithermal and one thermal) positioned at different spacing from the minitron. The tool's detectors count neutrons that arrive at the detectors after being scattered and slowed by collisions with atomic nuclei in the formation.

The highest energy loss occurs when neutrons collide with hydrogen nuclei, which have practically the same mass as the neutron (the neutrons simply bounce off heavier elements without losing much energy). If the hydrogen (i.e., water) concentration is low, as in low-porosity formations, neutrons can travel farther before being captured, and count rates increase at the detector. The opposite effect occurs in high-porosity formations where water content is high. However, because hydrogen bound in minerals such as clays or in hydrocarbons also contributes to the measurement, the raw porosity value is often an overestimate.

Upon reaching thermal energies (0.025 eV), the neutrons are captured by the nuclei of Cl, Si, B, and other elements, resulting in a gamma ray emission. This neutron capture cross section (Σ_f) is also measured by the tool.

Electrical resistivity

The DIT provides three measures of electrical resistivity, each with a different depth of investigation into

the formation. Two induction devices (deep and medium depths of penetration) transmit high-frequency alternating currents through transmitter coils, creating magnetic fields that induce secondary currents in the formation. These currents produce a new inductive signal, proportional to the conductivity of the formation, which is measured by the receiving coils. The measured conductivities are then converted to resistivity (in units of ohmmeters). A third device, a spherically focused resistivity instrument with higher vertical resolution than the induction devices, sends a current into the formation while trying to maintain a constant voltage drop. The amount of current necessary to maintain the voltage gives a direct measure of resistivity. This device uses several electrodes to focus the current flow into the formation so that equipotential surfaces are spherical. Calcite, silica, and hydrocarbons are electrical insulators, whereas ionic solutions like pore water are conductors. Electrical resistivity, therefore, can be used to evaluate porosity for a given salinity and resistivity of pore water.

Acoustic velocity

The DSI measures transit times between sonic transmitters and an array of eight receivers. It combines replicate measurements, thus providing a measurement of compressional velocity through sediments that is relatively free from the effects of formation damage and of an enlarged borehole (Schlumberger, 1989). Along with the monopole transmitters found on most sonic tools, the DSI also has two cross-dipole transmitters, which allows for an additional measurement of shear wave velocity. Dipole measurements are necessary to measure shear velocities in slow formations whose shear velocity is less than the velocity of sound in the borehole fluid. Such slow formations are typically encountered in deep ocean drilling.

Formation MicroScanner

The FMS provides high-resolution images of borehole wall microresistivity. The tool has four orthogonal arms and pads, each containing 16 button electrodes that are pressed against the borehole wall during recording. The electrodes are arranged in two diagonally offset rows of eight electrodes each. A focused current is emitted from the button electrodes into the formation, with a return electrode near the top of the tool. The resistivity of the formation at the button electrodes is derived from the intensity of current passing through the button electrodes. Processing transforms these measurements into oriented high-resolution images that reveal the geologic structure of the borehole wall. Features such as bedding,

stratification, fracturing, slump folding, and bioturbation can be resolved. The images are oriented to magnetic north so that fabric analysis can be carried out and the dip and direction (azimuth) of planar features in the formation can be measured.

The maximum extension of the FMS caliper arms is 15 inches. In holes with a diameter >15 inches, pad contact will be inconsistent and the FMS images may appear out of focus and too conductive. Irregular borehole walls will also adversely affect the images if contact with the wall is poor.

Accelerometry and magnetic field measurement

Three-component acceleration and magnetic field measurements are made with the GPIT. The primary purpose of this tool, which incorporates a three-component accelerometer and a three-component magnetometer, is to determine the acceleration and orientation of the FMS-sonic tool string during logging. Thus, the FMS images can be corrected for irregular tool motion, and the dip and direction (azimuth) of features in the FMS images can be determined. During Expedition 317, the GPIT was also used to record downhole tool motion and evaluate the performance of the new WHC in real time.

Vertical seismic profile

In a vertical seismic profile (VSP) experiment, a borehole seismic tool is anchored against the borehole wall at regularly spaced intervals to record the full waveform of elastic waves generated by a seismic source positioned just below the sea surface. These “check shot” measurements relate depth in the hole to traveltime in reflection seismic lines. The VSI is usually composed of multiple shuttles separated by acoustically isolating spacers, each containing a three-axis geophone, but only one shuttle was to be used during Expedition 317. The plan for Expedition 317 was to anchor the VSI against the borehole wall at 20 m intervals, and to take 5–10 recordings at each station. The recorded waveforms could then be stacked and a one-way traveltime determined from the median of the first breaks for each station. The seismic source to be used was a Sercel G. Gun Parallel Cluster, composed of two 250 in³ air guns separated by 1 m. The cluster is generally positioned on the port side of the *JOIDES Resolution* at a water depth of ~7 m with a borehole offset of ~30 m. However, no VSP experiments were carried out during Expedition 317 because of poor hole conditions.

Log data quality

The principal influence on log data quality is the condition of the borehole wall. If the borehole diam-

eter varies over short intervals because of washouts or ledges of harder material, the logs from tools that require good contact with the borehole wall (i.e., the FMS and density tools) may be degraded. Deep investigation measurements that do not require contact with the borehole wall (i.e., gamma ray, resistivity, and sonic velocity) are generally less sensitive to borehole conditions. Very narrow (bridged) sections also cause irregular log results. The quality of the borehole can be improved by minimizing the circulation of drilling fluid while drilling, flushing the borehole to remove debris, and logging as soon as possible after drilling and conditioning are completed.

The quality of the logging depth determination depends on several factors. The depth of the logging measurements is determined from the length of the cable played out from the winch on the ship. The seafloor (mudline) is identified on the natural gamma log by the abrupt reduction in gamma ray count at the water/sediment boundary. Discrepancies between drilling depth and wireline log depth occur because of core expansion, incomplete core recovery, or incomplete heave compensation for drillers depth. In the case of log depth, discrepancies between successive runs occur because of incomplete heave compensation, insufficient correction for cable stretch, and cable slip. In the case of very fine sediments in suspension, the mudline can be an elusive datum. Tidal changes in sea level also have an effect. To minimize wireline tool motion caused by ship heave, a WHC was used to adjust the wireline length for rig motion during wireline logging operations (Goldberg, 1990).

Wireline heave compensator

Evaluation of a new hydraulic WHC system continued during Expedition 317. This system is designed to compensate for the vertical motion of the ship and maintain a steady motion of the logging tools. It uses vertical acceleration measurements made by a motion reference unit (MRU), which is located under the rig floor near the center of gravity of the ship, to calculate the ship's vertical motion. It then adjusts the length of the wireline by varying the distance between two sets of pulleys through which the cable passes. Real-time measurements of uphole (surface) and downhole acceleration are made simultaneously by the MRU and by the GPIT, respectively. A Lamont-Doherty Earth Observatory (LDEO)-developed software package allows these data to be analyzed and compared in real time, displaying the actual motion of the logging tool string and enabling evaluation of the compensator's efficiency. In addition to the WHC's improved design and smaller footprint

compared to the previous system, its location with the winch unit on the starboard side of the derrick contributes to a significant reduction in the time needed to prepare for logging operations.

Logging data flow and log depth scales

Data for each wireline logging run were monitored in real time and recorded using the Schlumberger MAXIS 500 system. The initial logging data were referenced to the rig floor (WRF). After logging was completed, the data were shifted to a seafloor reference (WSF) based on the step in gamma radiation at the sediment/water interface. These data were made available to the science party.

The downhole log data were also transferred onshore to LDEO for standardized data processing. The main processing task was depth matching to remove depth offsets between different logging runs, which resulted in a new depth scale: wireline log matched depth below seafloor (WMSF). Also, corrections were made to certain tools and logs, documentation for the logs was prepared (with an assessment of log quality), and the data were converted to ASCII for the conventional logs and GIF for the FMS images. Schlumberger GeoQuest's GeoFrame software package was used for most of the data processing. The data were transferred back to the ship within a few days of logging and made available (in ASCII and DLIS formats) through the shipboard IODP logging database.

Core-log-seismic integration

A depth–traveltime relationship must be determined at each site to correlate core and log data acquired in depth with seismic reflection measurements, which are a function of traveltime. For example, a direct measurement of the depth–traveltime relationship is given by the first arrival times in the VSP (see above).

The depth–traveltime relationship can also be estimated by constructing synthetic seismograms, which are computed from reflection coefficients obtained from contrasts in *P*-wave velocity and density, to match the seismic traces closest to the borehole. When the quality of the shipboard sonic logs was sufficient, synthetic seismograms were calculated from the density and V_p logs using the IESX seismic interpretation package (part of the Schlumberger GeoFrame software suite), which allows for interactive adjustments of the depth–traveltime relationship until a good match is achieved between features in the synthetic seismogram and the measured seismic data. A calibrated depth–traveltime relationship allows for correlation of borehole stratigraphy with seismic reflection features (e.g., assignment of ages

to prominent seismic reflectors that can then be correlated away from the drill site).

Stratigraphic correlation

As part of standard IODP shipboard procedure when coring multiple holes at individual drill sites, stratigraphic correlation was carried out on board to correlate adjacent holes using Correlator software. This software allows depth adjustment of individual or multiple cores to enable ties to be made between cores in separate holes based on the expression of onboard core logging data. In accordance with standard IODP protocol, onboard correlation did not involve depth adjustment of individual core sections, nor were individual core/section depth scales stretched or compressed to force the correlation of intracore tie points. Rather, this first-order approach to stratigraphic correlation established a framework from which more detailed correlation can be carried out postcruise.

Depth adjustment of individual cores is often necessary for a variety of reasons, such as differences in seafloor topography between holes or inconsistent mudline definition. Equally, stratigraphic variation may occur between holes because of slight differences in sedimentation rates and erosion histories. Further complication in the correlation procedure may stem from a lack of unambiguous correlation tie points between holes. Ambiguities may arise from differences in the physical properties of contemporaneous strata, the occurrence of noncontemporaneous strata at similar depths (e.g., incised channel fills), inaccuracies/imprecision in physical property data, and drilling disturbances that affect the fidelity of the data.

The first-order objective of correlation across holes at Expedition 317 sites was to establish a common CCSF depth scale for cores from multiple holes. Furthermore, the possession of two or more overlapping records from adjacent holes provided an opportunity to construct a spliced stratigraphic record against a CCSF scale. This spliced record has the potential to optimize both the completeness of the site's stratigraphic record and the fidelity of the associated stratigraphic data. For the four sites drilled during Expedition 317, the key physical property data used to aid correlation were shipboard NGR, magnetic susceptibility, color, and GRA bulk density. In general, NGR and magnetic susceptibility typically provided the best data for correlation.

References

ASTM International, 1990. Standard method for laboratory determination of water (moisture) content of soil and

- rock (Standard D2216–90). In *Annual Book of ASTM Standards for Soil and Rock* (Vol. 04.08): Philadelphia (Am. Soc. Testing Mater.). [revision of D2216-63, D2216-80]
- Agnini, C., Muttoni, G., Kent, D.V., and Rio, D., 2006. Eocene biostratigraphy and magnetic stratigraphy from Possagno, Italy: the calcareous nannofossil response to climate variability. *Earth Planet Sci. Lett.*, 241(3–4):815–830. doi:10.1016/j.epsl.2005.11.005
- Backman, J., 1986. Late Paleocene to middle Eocene calcareous nannofossil biochronology from the Shatsky Rise, Walvis Ridge and Italy. *Palaeogeogr., Palaeoclimatol., Palaeoecol.*, 57(1):43–59. doi:10.1016/0031-0182(86)90005-2
- Backman, J., 1987. Quantitative calcareous nannofossil biochronology of middle Eocene through early Oligocene sediment from DSDP Sites 522 and 523. *Abh. Geol. Bundesanst. (Austria)*, 39:21–31.
- Baldauf, J.G., and Barron, J.A., 1991. Diatom biostratigraphy: Kerguelen Plateau and Prydz Bay regions of the Southern Ocean. In Barron, J., Larsen, B., et al., *Proc. ODP, Sci. Results*, 119: College Station, TX (Ocean Drilling Program), 547–598. doi:10.2973/odp.proc.sr.119.135.1991
- Batzke, A., Engelen, B., Sass, H., and Cypionka, H., 2007. Phylogenetic and physiological diversity of cultured deep-biosphere bacteria from equatorial Pacific Ocean and Peru margin sediments. *Geomicrobiol. J.*, 24(3–4):261–273. doi:10.1080/01490450701456453
- Berggren, F.C., Kent, D.V., Swisher, C.C., III, and Aubry, M.-P., 1995. A revised Cenozoic geochronology and chronostratigraphy. In Berggren, W.A., Kent, D.V., Aubry, M.-P., and Hardenbol, J. (Eds.), *Geochronology, Time Scales and Global Stratigraphic Correlation*. Spec. Publ.—SEPM (Soc. Sediment. Geol.), 54:129–212.
- Blaj, T., Backman, J., and Raffi, I., 2009. Late Eocene to Oligocene preservation history and biochronology of calcareous nannofossils from paleo-equatorial Pacific Ocean sediments. *Riv. Ital. Paleontol. Stratigr.*, 115(1):67–84.
- Blum, P., 1997. Physical properties handbook: a guide to the shipboard measurement of physical properties of deep-sea cores. *ODP Tech. Note*, 26. doi:10.2973/odp.tn.26.1997
- Bown, P.R. (Ed.), 1998. *Calcareous Nannofossil Biostratigraphy*: Dordrecht, The Netherlands (Kluwer Academic Publ.).
- Bown, P.R., 2005. Paleogene calcareous nannofossils from the Kilwa and Lindi areas of coastal Tanzania: Tanzania Drilling Project Sites 1 to 10. *J. Nannoplankton Res.*, 27(1):21–95.
- Bullard, E.C., 1939. Heat flow in South Africa. *Proc. R. Soc. London, Ser. A*, 173(955):474–502. doi:10.1098/rspa.1939.0159
- Burton, J.D., 1996. The ocean: a global geochemical system. In Summerhayes, C.P., and Thorpe, S.A. (Eds.), *Oceanography: An Illustrated Guide*: London (Manson Publishing Ltd.), 165–181.
- Cande, S.C., and Kent, D.V., 1995. Revised calibration of the geomagnetic polarity timescale for the Late Cretaceous and Cenozoic. *J. Geophys. Res., [Solid Earth]*, 100(B4):6093–6095. doi:10.1029/94JB03098
- Censarek, B., and Gersonde, R., 2002. Miocene diatom biostratigraphy at ODP Sites 689, 690, 1088, 1092 (Atlantic sector of the Southern Ocean). *Mar. Micropaleontol.*, 45(3–4):309–356. doi:10.1016/S0377-8398(02)00034-8
- Ciesielski, P.F., 1983. The Neogene and Quaternary diatom biostratigraphy of subantarctic sediments, Deep Sea Drilling Project Leg 71. In Ludwig, W.J., Krasheninnikov, V.A., et al., *Init. Repts. DSDP, 71*: Washington, DC (U.S. Govt. Printing Office), 635–666. doi:10.2973/dsdp.proc.71.125.1983
- Cody, R.D., Levy, R.H., Harwood, D.M., and Sadler, P.M., 2008. Thinking outside the zone: high-resolution quantitative diatom biochronology for the Antarctic Neogene. *Palaeogeogr., Palaeoclimatol., Palaeoecol.*, 260(1–2):92–121. doi:10.1016/j.palaeo.2007.08.020
- Cooper, R.A., 2004. *The New Zealand Geological Timescale*. Inst. Geol. Nucl. Sci. Monogr., 22.
- Crundwell, M.P., 2004. New Zealand late Miocene biostratigraphy and biochronology: studies of planktic foraminifers and bolboforms at oceanic Sites 593 and 1123 and selected onland sections [Ph.D. thesis]. Univ. Waikato, New Zealand.
- Crundwell, M.P., Cooke, P.J., Nelson, C.S., and Spiegler, D., 2005. Intraspecific morphological variation in late Miocene *Bolboforma*, and implications for their classification, ecology, and biostratigraphic utility. *Mar. Micropaleontol.*, 56(3–4):161–176. doi:10.1016/j.marmicro.2005.05.003
- Crundwell, M.P., and Nelson, C.S., 2007. A magnetostratigraphically constrained chronology for late Miocene bolboformids and planktic foraminifers in the temperate Southwest Pacific. *Stratigraphy*, 4(1):1–34. http://www.micropress.org/micropen2/articles/1/5/71902_articles_article_file_1502.pdf
- Crundwell, M.P., Scott, G.H., and Thrasher, G.P., 1994. Calibration of paleobathymetry indicators by integrated seismic and paleontological analysis of forest sequences, Taranaki Basin, New Zealand. In *The Post Maui Challenge: Investment and Development Opportunities*. N. Z. Pet. Conf. Proc., 169–178.
- Daley, R.J., and Hobbie, J.E., 1975. Direct counts of aquatic bacteria by a modified epifluorescence technique. *Limnol. Oceanogr.*, 20(5):875–882. doi:10.4319/lo.1975.20.5.0875
- de Kaenel, E., Siesser, W.G., and Murat, A., 1999. Pleistocene calcareous nannofossil biostratigraphy and the western Mediterranean sapropels, Sites 974 to 977 and 979. In Zahn, R., Comas, M.C., and Klaus, A. (Eds.), *Proc. ODP, Sci. Results*, 161: College Station, TX (Ocean Drilling Program), 159–183. doi:10.2973/odp.proc.sr.161.250.1999
- D'Hondt, S., Rutherford, S., and Spivack, A.J., 2002. Metabolic activity of the subsurface life in deep-sea sediments. *Science*, 295(5562):2067–2070. doi:10.1126/science.1064878
- Dolinar, B., and Trauner, L., 2005. Impact of soil composition on fall cone test results. *J. Geotechnol. Geoenviron.*

- Eng.*, 131(1):126–130. doi:10.1061/(ASCE)1090-0241(2005)131:1(126)
- Droser, M.L., and Bottjer, D.J., 1986. A semiquantitative field classification of ichnofabric. *J. Sediment. Res.*, 56(4):558–559. <http://jseires.sepmonline.org/cgi/content/abstract/56/4/558/>
- Ellis, D.V., and Singer, J.M., 2007. *Well Logging for Earth Scientists*, (2nd ed.): Dordrecht, The Netherlands (Springer).
- Evans, H.B., 1965. GRAPE—a device for continuous determination of material density and porosity. *Trans. SPWLA Annu. Logging Symp.*: 6(2):B1–B25.
- Expedition 301 Scientists, 2005. Methods. In Fisher, A.T., Urabe, T., Klaus, A., and the Expedition 301 Scientists, *Proc. IODP*, 301: College Station, TX (Integrated Ocean Drilling Program Management International, Inc.). doi:10.2204/iodp.proc.301.105.2005
- Fenner, J., Schrader, H.-J., and Wienigk, H., 1976. Diatom phytoplankton studies in the southern Pacific Ocean: composition and correlation to the Antarctic Convergence and its paleoecological significance. In Hollister, C.D., Craddock, C., et al., *Init. Repts. DSDP*, 35: Washington, DC (U.S. Govt. Printing Office), 757–813. doi:10.2973/dsdp.proc.35.app3.1976
- Gartner, S., 1977. Calcareous nannofossil biostratigraphy and revised zonation of the Pleistocene. *Mar. Micropaleontol.*, 2:1–25. doi:10.1016/0377-8398(77)90002-0
- Gersonde, R., 1990. Taxonomy and morphostructure of Neogene diatoms from the Southern Ocean, ODP Leg 113. In Barker, P.F., Kennett, J.P., et al., *Proc. ODP, Sci. Results*, 113: College Station, TX (Ocean Drilling Program), 791–802. doi:10.2973/odp.proc.sr.113.128.1990
- Gersonde, R., and Burckle, L.H., 1990. Neogene diatom biostratigraphy of ODP Leg 113, Weddell Sea (Antarctic Ocean). In Barker, P.F., Kennett, J.P., et al., *Proc. ODP, Sci. Results*, 113: College Station, TX (Ocean Drilling Program), 761–789. doi:10.2973/odp.proc.sr.113.126.1990
- Gieskes, J.M., Gamo, T., and Brumsack, H., 1991. Chemical methods for interstitial water analysis aboard JOIDES Resolution. *ODP Tech. Note*, 15. doi:10.2973/odp.tn.15.1991
- Goldberg, D., 1990. Test performance of the Ocean Drilling Program wireline heave motion compensator. *Sci. Drill.*, 1:206–209.
- Goldberg, D., 1997. The role of downhole measurements in marine geology and geophysics. *Rev. Geophys.*, 35(3):315–342. doi:10.1029/97RG00221
- Hansbo, S., 1957. A new approach to the determination of the shear strength of clay by the fall-cone test. *R. Swed. Geotech. Inst., Proc.*, 14.
- Harms, J.C., and Choquette, P.W., 1965. Geologic evaluation of a gamma-ray porosity device. *Trans. SPWLA Annu. Logging Symp.*: 6(2):C1–C37.
- Harwood, D.M., and Maruyama, T., 1992. Middle Eocene to Pleistocene diatom biostratigraphy of Southern Ocean sediments from the Kerguelen Plateau, Leg 120. In Wise, S.W., Jr., Schlich, R., et al., *Proc. ODP, Sci. Results*, 120: College Station, TX (Ocean Drilling Program), 683–733. doi:10.2973/odp.proc.sr.120.160.1992
- Hayward, B.W., Grenfell, H.R., Reid, C.M., and Hayward, K.A., 1999. Recent New Zealand benthic foraminifera: taxonomy, ecologic distribution, biogeography, and use in paleoenvironmental assessment. *N. Z. Geol. Surv. Bull.*, 75:1–258.
- Hornibrook, N. de B., 1961. Tertiary foraminifera from Oamaru District (N. Z.), Part 1. Systematics and distribution. *Paleontol. Bull.*, 34.
- Hornibrook, N. de B., 1981. *Globorotalia* (planktic Foraminifera) in the late Pliocene and early Pleistocene of New Zealand. *N. Z. J. Geol. Geophys.*, 24(2):263–292.
- Hornibrook, N. de B., 1982. Late Miocene to Pleistocene *Globorotalia* (Foraminifera) from DSDP Leg 29, Site 284, southwest Pacific. *N. Z. J. Geol. Geophys.*, 25(1):83–99.
- Hornibrook, N. de B., Brazier, R.C., and Strong, C.P., 1989. Manual of New Zealand Permian to Pleistocene foraminiferal biostratigraphy. *Paleontol. Bull.*, 56.
- Hornibrook, N. de B., and Jenkins, D.G., 1994. DSDP 594, Chatham Rise, New Zealand—Late Neogene planktonic foraminiferal biostratigraphy revisited. *J. Micropalaeontol.*, 13:93–101.
- Houlsby, G.T., 1982. Theoretical analysis of the fall cone test. *Géotechnique*, 32(2):111–118. doi:10.1680/geot.1982.32.2.111
- Hyndman, R.D., Erickson, A.J., and Von Herzen, R.P., 1974. Geothermal measurements on DSDP Leg 26. In Davies, T.A., Luyendyk, B.P., et al., *Init. Repts. DSDP*, 26: Washington, DC (U.S. Govt. Printing Office), 451–463. doi:10.2973/dsdp.proc.26.113.1974
- Jovane, L., Florindo, F., Coccioni, R., Dinarès-Turell, J., Marsili, A., Monechi, S., Roberts, A.P., and Sprovieri, M., 2007. The middle Eocene climatic optimum event in the Contessa Highway section, Umbrian Apennines, Italy. *Geol. Soc. Am. Bull.*, 119(3–4):413–427. doi:10.1130/B25917.1
- Kallmeyer, J., Smith, D.C., Spivack, A.J., and D'Hondt, S., 2008. New cell extraction procedure applied to deep subsurface sediments. *Limnol. Oceanogr.: Methods*, 6:236–245. <http://www.aslo.org/lomethods/free/2008/0236.pdf>
- Kameo, K., and Bralower, T.J., 2000. Neogene calcareous nannofossil biostratigraphy of Sites 998, 999, and 1000, Caribbean Sea. In Leckie, R.M., Sigurdsson, H., Acton, G.D., and Draper, G. (Eds.), *Proc. ODP, Sci. Results*, 165: College Station, TX (Ocean Drilling Program), 3–17. doi:10.2973/odp.proc.sr.165.012.2000
- Kennett, J.P., and Srinivasan, M.S., 1983. *Neogene Planktonic Foraminifera: A Phylogenetic Atlas*: Stroudsburg, PA (Hutchinson Ross).
- Koumoto, T., and Houlsby, G.T., 2001. Theory and practice of the fall cone test. *Géotechnique*, 51(8):701–712. doi:10.1680/geot.2001.51.8.701
- Laskar, J., Robutel, P., Joutel, F., Gastineau, M., Correia, A.C.M., and Levrard, B., 2004. A long-term numerical solution for the insolation quantities of the Earth. *Astron. Astrophys.*, 428(1):261–285. doi:10.1051/0004-6361:20041335

- Lipp, J.S., Orcutt, B.N., Holler, T., Teske, A., and Hinrichs, K.-U., 2010. Effect of storage conditions on archaeal and bacterial communities in subsurface marine sediments. *Geomicrobiol. J.*, 27(3):261–272. doi:10.1080/01490450903410423
- Lourens, L.J., Hilgen, F.J., Laskar, J., Shackleton, N.J., and Wilson, D., 2004. The Neogene period. In Gradstein, F.M., Ogg, J., et al. (Eds.), *A Geologic Time Scale 2004*: Cambridge (Cambridge Univ. Press), 409–440.
- Lovell, M.A., Harvey, P.K., Brewer, T.S., Williams, C., Jackson, P.D., and Williamson, G., 1998. Application of FMS images in the Ocean Drilling Program: an overview. In Cramp, A., MacLeod, C.J., Lee, S.V., and Jones, E.J.W. (Eds.), *Geological Evolution of Ocean Basins: Results from the Ocean Drilling Program*. Geol. Soc. Spec. Publ., 131(1):287–303. doi:10.1144/GSL.SP.1998.131.01.18
- Lunau, M., Lemke, A., Walther, K., Martens-Habben, W., and Simon, M., 2005. An improved method for counting bacteria from sediments and turbid environments by epifluorescence microscopy. *Environ. Microbiol.*, 7(7):961–968. doi:10.1111/j.1462-2920.2005.00767.x
- Mahajan, S.P., and Budhu, M., 2009. Shear viscosity of clays using the fall cone test. *Géotechnique*, 59(6):539–543. doi:10.1680/geot.7.00114
- Manheim, F.T., and Sayles, F.L., 1974. Composition and origin of interstitial waters of marine sediments, based on deep sea drill cores. In Goldberg, E.D. (Ed.), *The Sea* (Vol. 5): *Marine Chemistry: The Sedimentary Cycle*: New York (Wiley), 527–568.
- Marchand, P., and Marmet, L., 1983. Binomial smoothing filter: a way to avoid some pitfalls of least-squares polynomial smoothing. *Rev. Sci. Instrum.*, 54(8):1034–1041. doi:10.1063/1.1137498
- Martini, E., 1971. Standard Tertiary and Quaternary calcareous nannoplankton zonation. *Proc. Int. Conf. Planktonic Microfossils*, 2:739–785.
- Mazzullo, J.M., Meyer, A., and Kidd, R.B., 1988. New sediment classification scheme for the Ocean Drilling Program. In Mazzullo, J.M., and Graham, A.G. (Eds.), *Handbook for shipboard sedimentologists*. ODP Tech. Note, 8:45–67. doi:10.2973/odp.tn.8.1988
- McCollum, D.W., 1975. Diatom stratigraphy of the Southern Ocean. In Hayes, D.E., Frakes, L.A., et al., *Init. Repts. DSDP*, 28: Washington, DC (U.S. Govt. Printing Office), 515–571. doi:10.2973/dsdp.proc.28.112.1975
- McKee, E.D., and Weir, G.W., 1953. Terminology for stratification and cross-stratification in sedimentary rocks. *Geol. Soc. Am. Bull.*, 64(4):381–390. doi:10.1130/0016-7606(1953)64[381:TFSACI]2.0.CO;2
- Morono, Y., Terada, T., Masui, N., and Inagaki, F., 2009. Discriminative detection and enumeration of microbial life in marine subsurface sediments. *ISME J.*, 3(5):503–511. doi:10.1038/ismej.2009.1
- Munsell Color Company, Inc., 2000. *Munsell Soil Color Chart*: New York (Gretag-Macbeth).
- Murray, R.W., Miller, D.J., and Kryc, K.A., 2000. Analysis of major and trace elements in rocks, sediments, and interstitial waters by inductively coupled plasma-atomic emission spectrometry (ICP-AES). *ODP Tech. Note*, 29. doi:10.2973/odp.tn.29.2000
- Noble, R.T., and Fuhrman, J.A., 1998. Use of SYBR Green I for rapid epifluorescence counts of marine viruses and bacteria. *Aquat. Microb. Ecol.*, 14:113–118. doi:10.3354/ame014113
- Okada, H., and Bukry, D., 1980. Supplementary modification and introduction of code numbers to the low-latitude coccolith biostratigraphic zonation (Bukry, 1973; 1975). *Mar. Micropaleontol.*, 5:321–325. doi:10.1016/0377-8398(80)90016-X
- Ogg, J.G., Ogg, G., and Gradstein, F.M., 2008. *The Concise Geologic Time Scale*: Cambridge (Cambridge Univ. Press). <http://www.cambridge.org/catalogue/catalogue.asp?isbn=9780521898492>
- Pälike, H., Frazier, J., and Zachos, J.C., 2006a. Extended orbitally forced palaeoclimatic records from the equatorial Atlantic Ceara Rise. *Quat. Sci. Rev.*, 25(23–24):3138–3149. doi:10.1016/j.quascirev.2006.02.011
- Pälike, H., Norris, R.D., Herrle, J.O., Wilson, P.A., Coxall, H.K., Lear, C.H., Shackleton, N.J., Tripathi, A.K., and Wade, B.S., 2006b. The heartbeat of the Oligocene climate system. *Science*, 314(5807):1894–1898. doi:10.1126/science.1133822
- Perch-Nielsen, K., 1985. Cenozoic calcareous nannofossils. In Bolli, H.M., Saunders, J.B., and Perch-Nielsen, K. (Eds.), *Plankton Stratigraphy*: Cambridge (Cambridge Univ. Press), 427–554.
- Perntaler, J., Glöckner, F.O., Schönhuber, W., and Amann, R., 2001. Fluorescence in situ hybridization with rRNA-targeted oligonucleotide probes. *Meth. Enzymol.*, 30:207–226.
- Pimmel, A., and Claypool, G., 2001. Introduction to shipboard organic geochemistry on the *JOIDES Resolution*. *ODP Tech. Note*, 30. doi:10.2973/odp.tn.30.2001
- Poag, C.W., and Karowe, A.L., 1986. Stratigraphic potential of *Bolboforma* significantly increased by new finds in the North Atlantic and South Pacific. *Palaios*, 1(2):162–171. doi:10.2307/3514510
- Pribnow, D.F.C., Kinoshita, M., and Stein, C.A., 2000. *Thermal Data Collection and Heat Flow Recalculations for ODP Legs 101–180*: Hanover, Germany (Inst. Joint Geosci. Res., Inst. Geowiss. Gemeinschaftsauf. [GGA]). <http://www-odp.tamu.edu/publications/heatflow/ODPReprt.pdf>
- Raffi, I., Backman, J., Fornaciari, E., Pälike, H., Rio, D., Lourens, L., and Hilgen, F., 2006. A review of calcareous nannofossil astrobiochronology encompassing the past 25 million years. *Quat. Sci. Rev.*, 25(23–24):3113–3137. doi:10.1016/j.quascirev.2006.07.007
- Richter, C., Acton, G., Endris, C., and Radsted, M., 2007. Handbook for shipboard paleomagnetists. *ODP Tech. Note*, 34. doi:10.2973/odp.tn.34.2007
- Rider, M.H., 1996. *The Geological Interpretation of Well Logs* (2nd ed.): Caithness (Whittles Publ.).
- Savrdra, C.E., Krawinkel, H., McCarthy, F.M.G., McHugh, C.M.G., Olson, H.C., and Mountain, G., 2001. Ichnofabrics of a Pleistocene slope succession, New Jersey margin: relations to climate and sea-level dynamics. *Palaeogeogr., Palaeoclimatol., Palaeoecol.*, 171(1–2):41–61. doi:10.1016/S0031-0182(01)00266-8

- Schlumberger, 1989. *Log Interpretation Principles/Applications*: Houston (Schlumberger Educ. Serv.), SMP-7017.
- Schlumberger, 1994. *IPL Integrated Porosity Lithology*: Houston (Schlumberger Wireline Testing), SMP-9270.
- Schrader, H.-J., 1976. Cenozoic planktonic diatom biostratigraphy of the southern Pacific Ocean. In Hollister, C.D., Craddock, C., et al., *Init. Repts. DSDP*, 35: Washington, DC (U.S. Govt. Printing Office), 605–671. [doi:10.2973/dsdp.proc.35.136.1976](https://doi.org/10.2973/dsdp.proc.35.136.1976)
- Scott, G.H., Bishop, S., and Burt, B.J., 1990. Guide to some Neogene Globotalids (Foraminiferida) from New Zealand. *N. Z. Geol. Surv. Paleontol. Bull.*, 61:1–135.
- Serra, O., 1984. *Fundamentals of Well-Log Interpretation* (Vol. 1): *The Acquisition of Logging Data*: Amsterdam (Elsevier).
- Serra, O., 1986. *Fundamentals of Well-Log Interpretation* (Vol. 2): *The Interpretation of Logging Data*. Amsterdam (Elsevier).
- Serra, O., 1989. *Formation MicroScanner Image Interpretation*: Houston (Schlumberger Educ. Serv.), SMP-7028.
- Shackleton, N.J., Hall, M.A., Raffi, I., Tauxe, L., and Zachos, J., 2000. Astronomical calibration age for the Oligocene–Miocene boundary. *Geology*, 28(5):447–450. [doi:10.1130/0091-7613\(2000\)28<447:ACAFTO>2.0.CO;2](https://doi.org/10.1130/0091-7613(2000)28<447:ACAFTO>2.0.CO;2)
- Shepard, F.P., 1954. Nomenclature based on sand-silt-clay ratios. *J. Sediment. Res.*, 24(3):151–158.
- Shipboard Scientific Party, 1999. Explanatory notes. In Carter, R.M., McCave, I.N., Richter, C., Carter, L., et al., *Proc. ODP, Init. Repts.*, 181: College Station, TX (Ocean Drilling Program), 1–65. [doi:10.2973/odp.proc.ir.181.102.2000](https://doi.org/10.2973/odp.proc.ir.181.102.2000)
- Shipboard Scientific Party, 2003a. Explanatory notes. In D'Hondt, S.L., Jørgensen, B.B., Miller, D.J., et al., *Proc. ODP, Init. Repts.*, 201: College Station, TX (Ocean Drilling Program), 1–103. [doi:10.2973/odp.proc.ir.201.105.2003](https://doi.org/10.2973/odp.proc.ir.201.105.2003)
- Shipboard Scientific Party, 2003b. Explanatory notes. In Mix, A.C., Tiedemann, R., Blum, P., et al., *Proc. ODP, Init. Repts.*, 202: College Station, TX (Ocean Drilling Program), 1–76. [doi:10.2973/odp.proc.ir.202.102.2003](https://doi.org/10.2973/odp.proc.ir.202.102.2003)
- Shipboard Scientific Party, 2004. Explanatory notes. In Tucholke, B.E., Sibuet, J.-C., Klaus, A., et al., *Proc. ODP, Init. Repts.*, 210: College Station, TX (Ocean Drilling Program), 1–69. [doi:10.2973/odp.proc.ir.210.102.2004](https://doi.org/10.2973/odp.proc.ir.210.102.2004)
- Smith, D.C., Spivack, A.J., Fisk, M.R., Haveman, S.A., Staudigel, H., and the Leg 185 Shipboard Scientific Party, 2000. Methods for quantifying potential microbial contamination during deep ocean coring. *ODP Tech. Note*, 28. [doi:10.2973/odp.tn.28.2000](https://doi.org/10.2973/odp.tn.28.2000)
- Spiegler, D., 1999. *Bolboforma* biostratigraphy from the Hatton-Rockall Basin (North Atlantic). In Raymo, M.E., Jansen, E., Blum, P., and Herbert, T.D. (Eds.), 1999. *Proc. ODP, Sci. Results*, 162: College Station, TX (Ocean Drilling Program), 35–49. [doi:10.2973/odp.proc.sr.162.013.1999](https://doi.org/10.2973/odp.proc.sr.162.013.1999)
- Spiegler, D., and Erlenkeuser, H., 2001. O- und C-Isotope im Biogenkarbonat von Foraminiferen und *Bolboformen* aus dem Miozän der Forschungsbohrung Nieder Ochtenhausen (Niedersachsen, Nord-Deutschland). *Geol. Jahrb. Reihe A*, 152:461–494.
- Spiegler, D., and Müller, C., 1992. Correlation of *Bolboforma* zonation and nannoplankton stratigraphy in the Neogene of the North Atlantic: DSDP Sites 12-116, 49-408, 81-555 and 94-608. *Mar. Micropaleontol.*, 20(1):45–58. [doi:10.1016/0377-8398\(92\)90008-8](https://doi.org/10.1016/0377-8398(92)90008-8)
- Spiegler, D., and von Daniels, C.H., 1991. A stratigraphic and taxonomic atlas of *Bolboforma* (Protozoa, incertae sedis, Tertiary). *J. Foraminiferal Res.*, 21:126–158. [doi:10.2113/gsjfr.21.2.126](https://doi.org/10.2113/gsjfr.21.2.126)
- Vella, P., 1957. Studies in New Zealand foraminifera, Part I. Foraminifera from Cook Strait; Part II. Upper Miocene to Recent species of the genus *Notorotalia*. *Paleontol. Bull.*, 28.
- Villa, G., Fioroni, C., Pea, L., Bohaty, S., and Persico, D., 2008. Middle Eocene–late Oligocene climate variability: calcareous nannofossil response at Kerguelen Plateau, Site 748. *Mar. Micropaleontol.*, 69(2):173–192. [doi:10.1016/j.marmicro.2008.07.006](https://doi.org/10.1016/j.marmicro.2008.07.006)
- Von Herzen, R., and Maxwell, A.E., 1959. The measurement of thermal conductivity of deep-sea sediments by a needle-probe method. *J. Geophys. Res.*, 64(10):1557–1563. [doi:10.1029/JZ064i010p01557](https://doi.org/10.1029/JZ064i010p01557)
- Wentworth, C.K., 1922. A scale of grade and class terms for clastic sediments. *J. Geol.*, 30(5):377–392. [doi:10.1086/622910](https://doi.org/10.1086/622910)
- Widdel, F., Kohring, G.-W., and Mayer, F., 1983. Studies on dissimilatory sulfate-reducing bacteria that decompose fatty acids. *Arch. Microbiol.*, 134(4):286–294. [doi:10.1007/BF00407804](https://doi.org/10.1007/BF00407804)
- Winter, D., and Iwai, M., 2002. Data report: neogene diatom biostratigraphy, Antarctic Peninsula Pacific margin, ODP Leg 178 rise sites. In Barker, P.F., Camerlenghi, A., Acton, G.D., and Ramsay, A.T.S. (Eds.), *Proc. ODP, Sci. Results*, 178: College Station, TX (Ocean Drilling Program), 1–25. [doi:10.2973/odp.proc.sr.178.230.2001](https://doi.org/10.2973/odp.proc.sr.178.230.2001)
- Wood, D.M., 1985. Some fall-cone tests. *Géotechnique*, 35(1):64–68. [doi:10.1680/geot.1985.35.1.64](https://doi.org/10.1680/geot.1985.35.1.64)
- Zielinski, U., and Gersonde, R., 2002. Plio–Pleistocene diatom biostratigraphy from ODP Leg 177, Atlantic sector of the Southern Ocean. *Mar. Micropaleontol.*, 45:225–268. [doi:10.1016/S0377-8398\(02\)00031-2](https://doi.org/10.1016/S0377-8398(02)00031-2)

Publication: 4 January 2011
MS 317-102

Figure F1. Core section description form, Expedition 317.

Expedition 317 Canterbury Basin:

Site: _____ Hole: _____ Core: _____ Section: _____ Top Depth: _____

Major Lithology: _____

Minor Lithology: _____

Offset (cm)	Lithology (graphic) Sed. Structures	Color	Drilling disturb.	Trace F. Bioturb.	Accessories: Mineral, fossils Misc structures Glauconite %	Samples	Core Description, comments, boundary type, other	Logged by:	Date:
0									
10									
20									
30									
40									
50									
60									
70									
80									
90									
100									
110									
120									
130									
140									
150									



Figure F2. Ternary plots of lithology naming scheme, Expedition 317. Modified from Shipboard Scientific Party (2004). Lower ternary plot follows Shepard (1954).

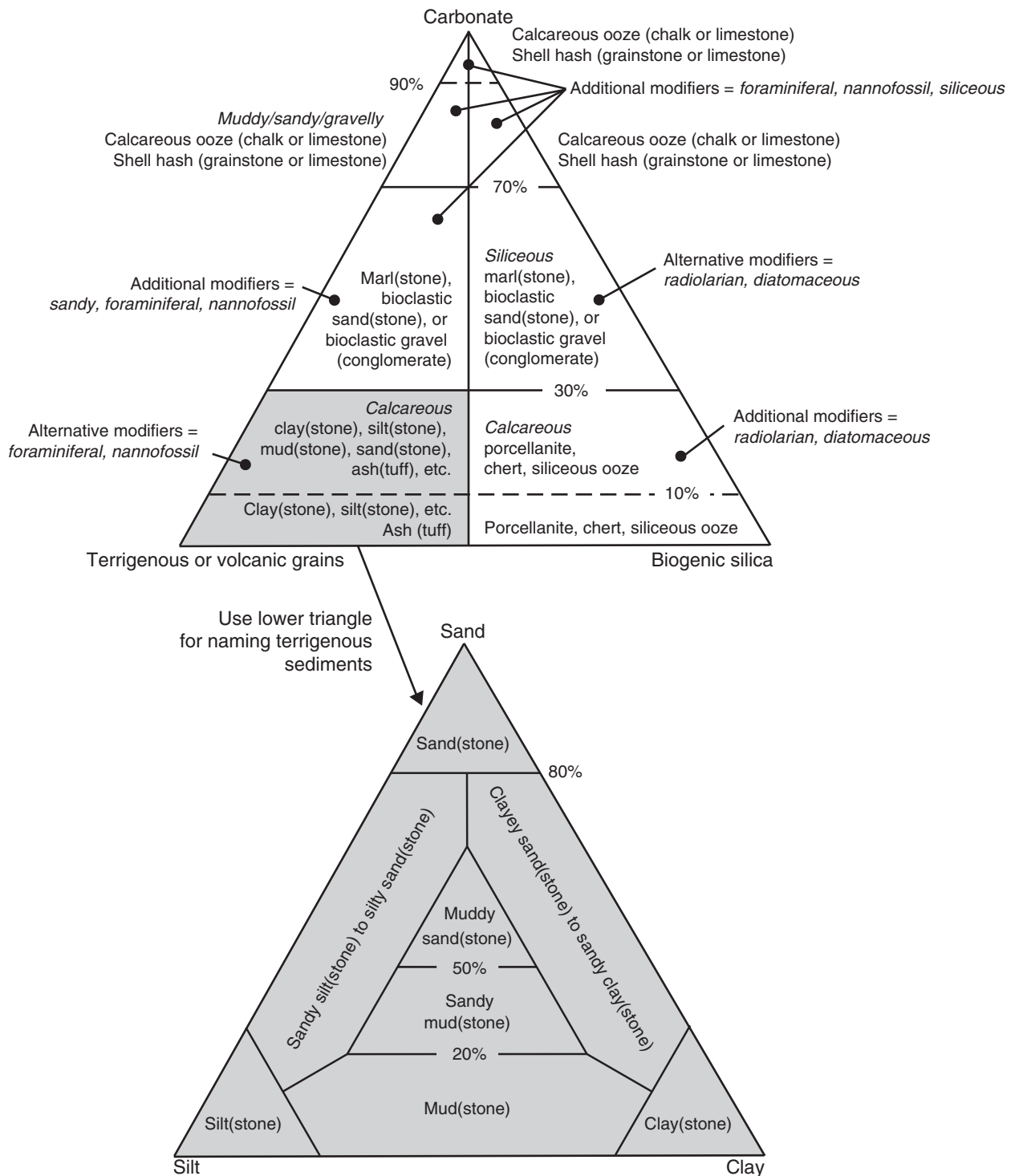


Figure F3. Core standard graphic report (“barrel sheet”) legend, including drilling disturbance, lithology, sedimentary and tectonic structures, and sample types, Expedition 317.

Lithology

Siliciclastics:

	Clay(stone)		Muddy gravel (conglomerate)
	Mud(stone)		Sandy gravel (conglomerate)
	Silt(stone)		Gravel (conglomerate)
	Sandy mud(stone)		Interbedded clay(stone) and mud(stone)
	Muddy sand(stone)		Interbedded silt(stone) and mud(stone)
	Very fine - fine sand(stone)		Interbedded sand(stone) and mud(stone)
	Medium - very coarse sand(stone)		

Calcareous:

	Chalk/limestone
	Muddy chalk/limestone
	Marl(stone)
	Shell hash

Mixed calcareous and siliceous:

	Siliceous mud(stone)
	Siliceous marl(stone)
	Siliceous chalk/limestone

Additional symbols:

	Lost core
	Void

Volcaniclastic:

	Ash/tuff
--	----------

Sedimentary structures

Contacts:

	Gradational
	Sharp
	Wavy
	Scoured
	Bioturbated
	Firmground
	Hardground
	Faulted boundary

Bedding features:

	Horizontal stratification		Herringbone stratification
	Low-angle cross bedding		Lens/pod
	High-angle cross bedding		Mud drape
	Current ripples		Imbricated
	Climbing ripples		Fluid escape structures
	Wave ripples		Color banding
	Interference ripples		Fining upward
	Wavy bedding/laminae		Coarsening upward

Other:

	Tilted bedding		Ball and pillow
	Normal fault		Flame structures
	Reverse fault		Chaotic strata
	Laminated		Convolute
	Thinly bedded		Mottled
	Thickly bedded		Desiccation cracks
	Graded bedding		Sole marks
	Uniform texture		

Ichnofabric and trace fossils

1 None	2 Slight	3 Moderate	4 Heavy	5 Complete
<i>Ophiomorpha</i>	<i>Thalassinoides</i>	<i>Planolites</i>	<i>Skolithos</i>	<i>Chondrites</i>
<i>Zoophycus</i>	Burrow			

Lithologic accessories

	Vein		Rare shell fragments		Common shell fragments		Worm tube		Black organic laminae
	Ash layer (<2 cm)		Rare plant fragments		Common plant fragments		Nodule		Isolated pebble
	Calcareous concretion		Silica concretion		Rootlets		Glauconitic		Pyritic
	Pyrite concretion		Siderite		Paleosols		Micaceous		Benthic foraminifer
	Bivalve		Gastropod		Brachiopod		Bryozoa		Echinoderm

Drilling disturbances

	Biscuit		Gas expansion		Fractured/cracked		Flow-in	Intensity of disturbance:	
	Brecciated		Soupy		Deformed strata		Cave-in		Slightly disturbed
									Heavily disturbed

Shipboard sampling

S	Smear slide	B	Microbiology	P	Micropaleontology	T	Thin section	M	Moisture/density
C	Carbonate	I	Interstitial water	X	X-ray diffraction	H	Headspace		



Figure F4. Ichnofabric index legend, Expedition 317. Modified from Droser and Bottjer (1986) and Savrda et al. (2001).

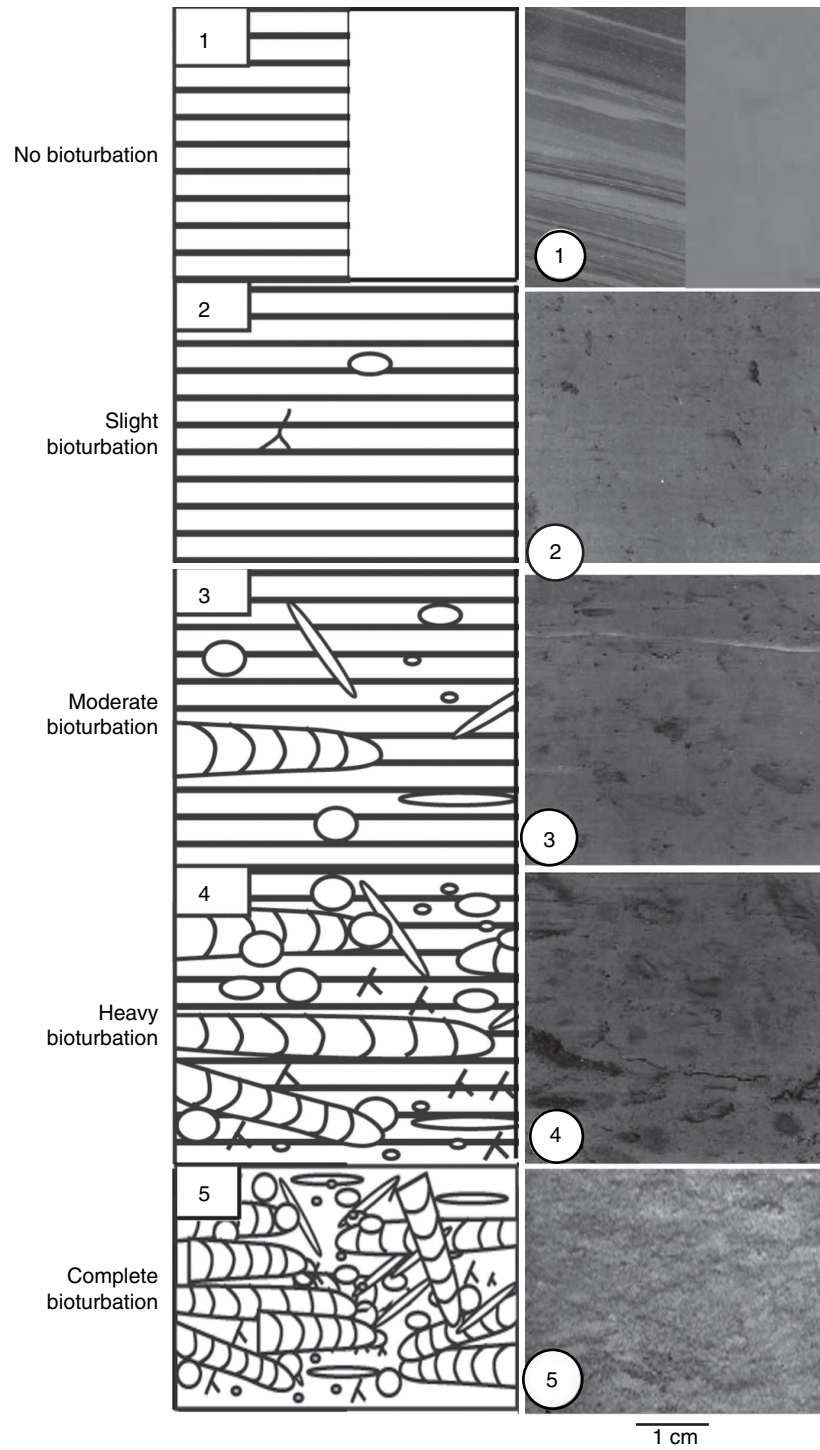


Figure F5. Holocene to late Paleogene geochronologic units (0–40 Ma) and geomagnetic polarity timescale correlated with calcareous nannofossil zones (modified after Martini, 1971), New Zealand stages (Cooper, 2004), and bolboformid zones (Crundwell and Nelson, 2007). The geological timescale of Ogg et al. (2008) was adopted for Expedition 317. Black bars = normal polarity, white bars = reversed polarity. **A.** 0–10 Ma. (**Continued on next two pages.**)

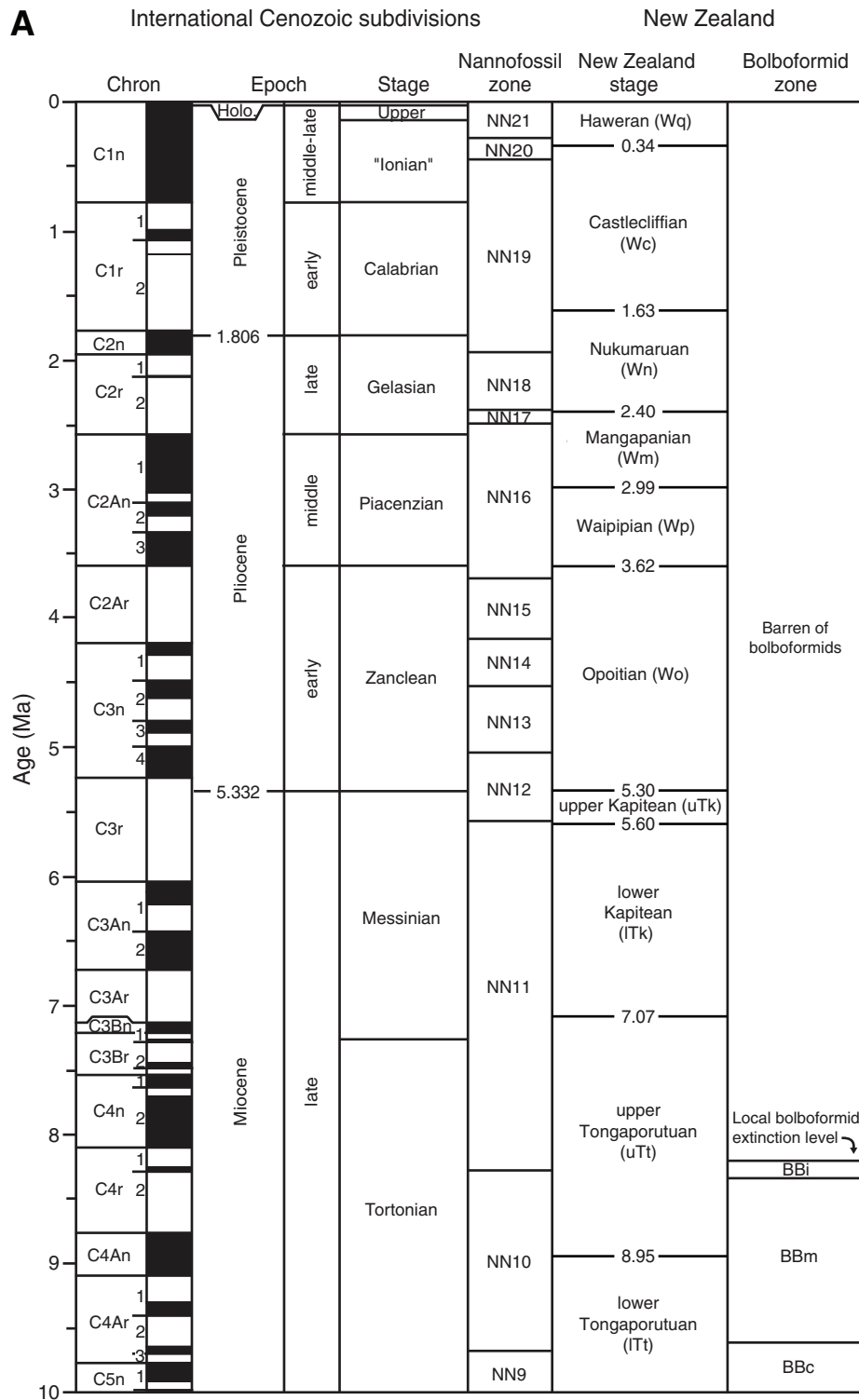


Figure F5 (continued). B. 10–20 Ma. (Continued on next page.)

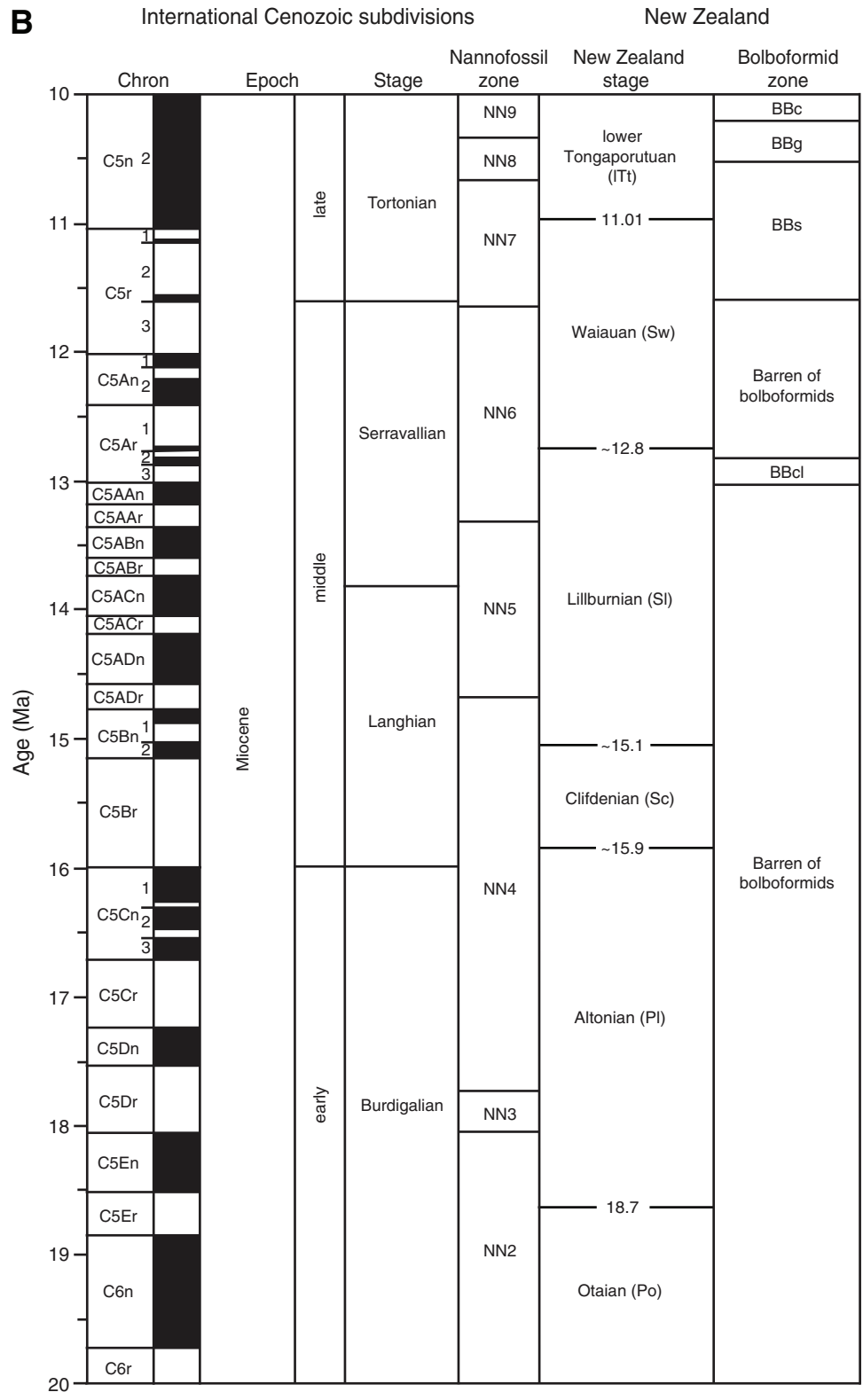


Figure F5 (continued). C. 20–40 Ma.

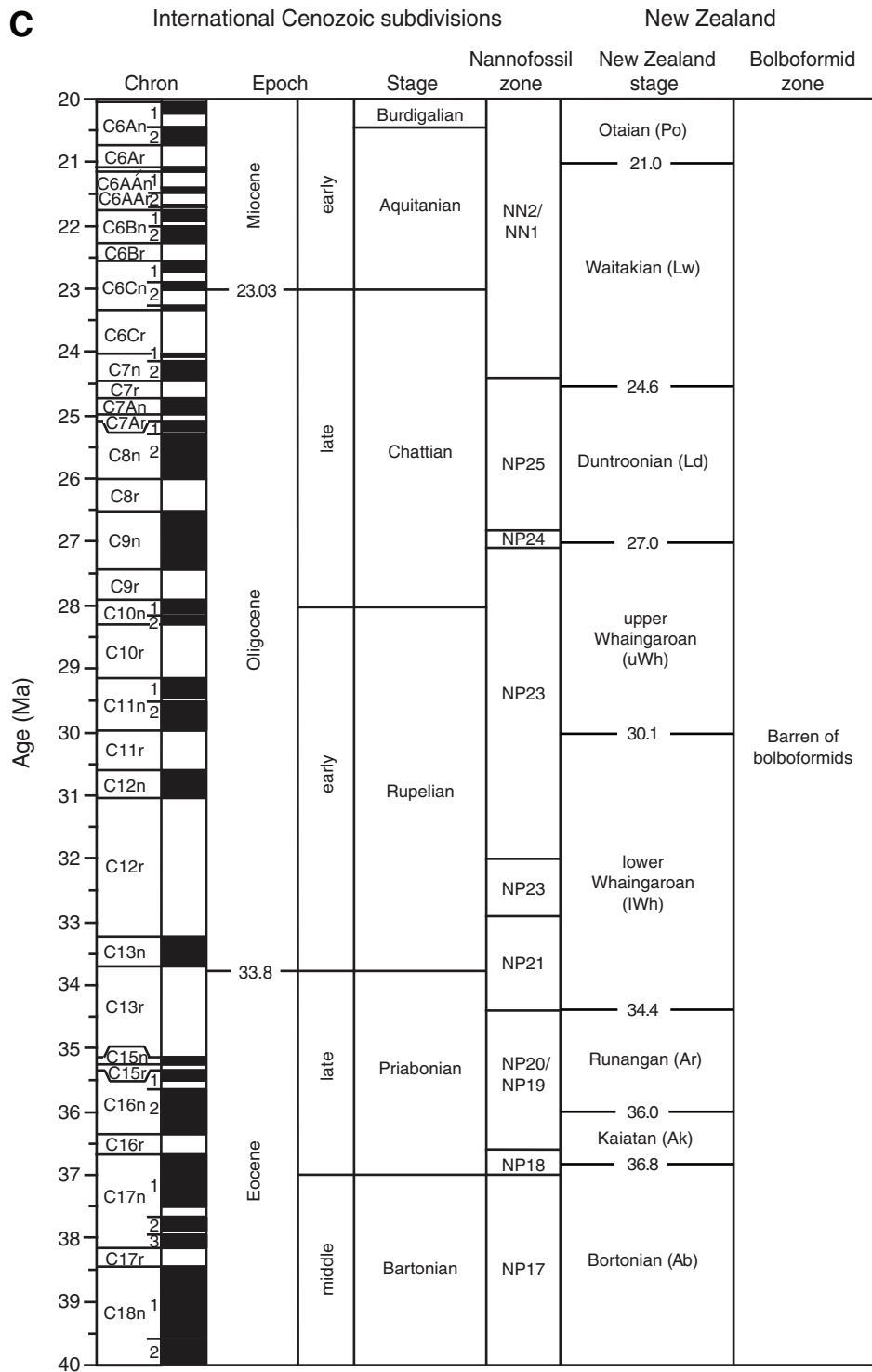


Figure F6. Ranges of the most stratigraphically useful planktonic and benthic foraminifers and bolboformids used for correlation of Neogene and Quaternary Kapitean to Haweran Stages in New Zealand for Expedition 317, after Cooper (2004) and recalibrated to Ogg et al. (2008). GPTS = geomagnetic polarity timescale. S-D = sinistral-dextral coiling directions, CCZ = Challenger coiling zone, PCZ = Palliser coiling zone, TCZ = Tuke-mokihi Coiling Zone, GCZ = Glomar coiling zone, MCZ = Mapiiri Coiling Zone, KCZ = Kaiti Coiling Zone, S = most specimens sinistrally coiled, R = most specimens randomly coiled. A. 0–6 Ma. (Continued on next three pages.)

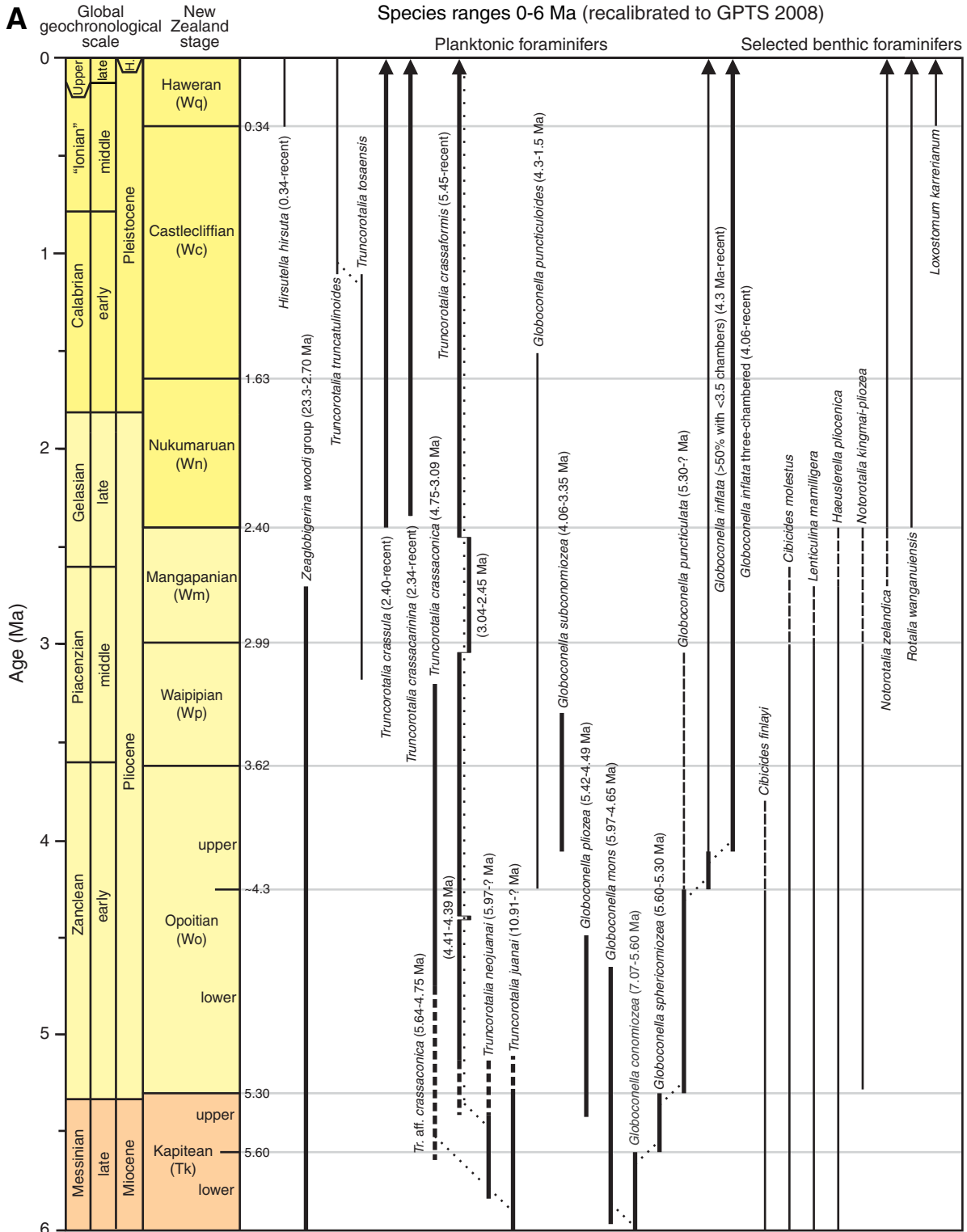


Figure F6 (continued). B. 4–12 Ma. (Continued on next page.)

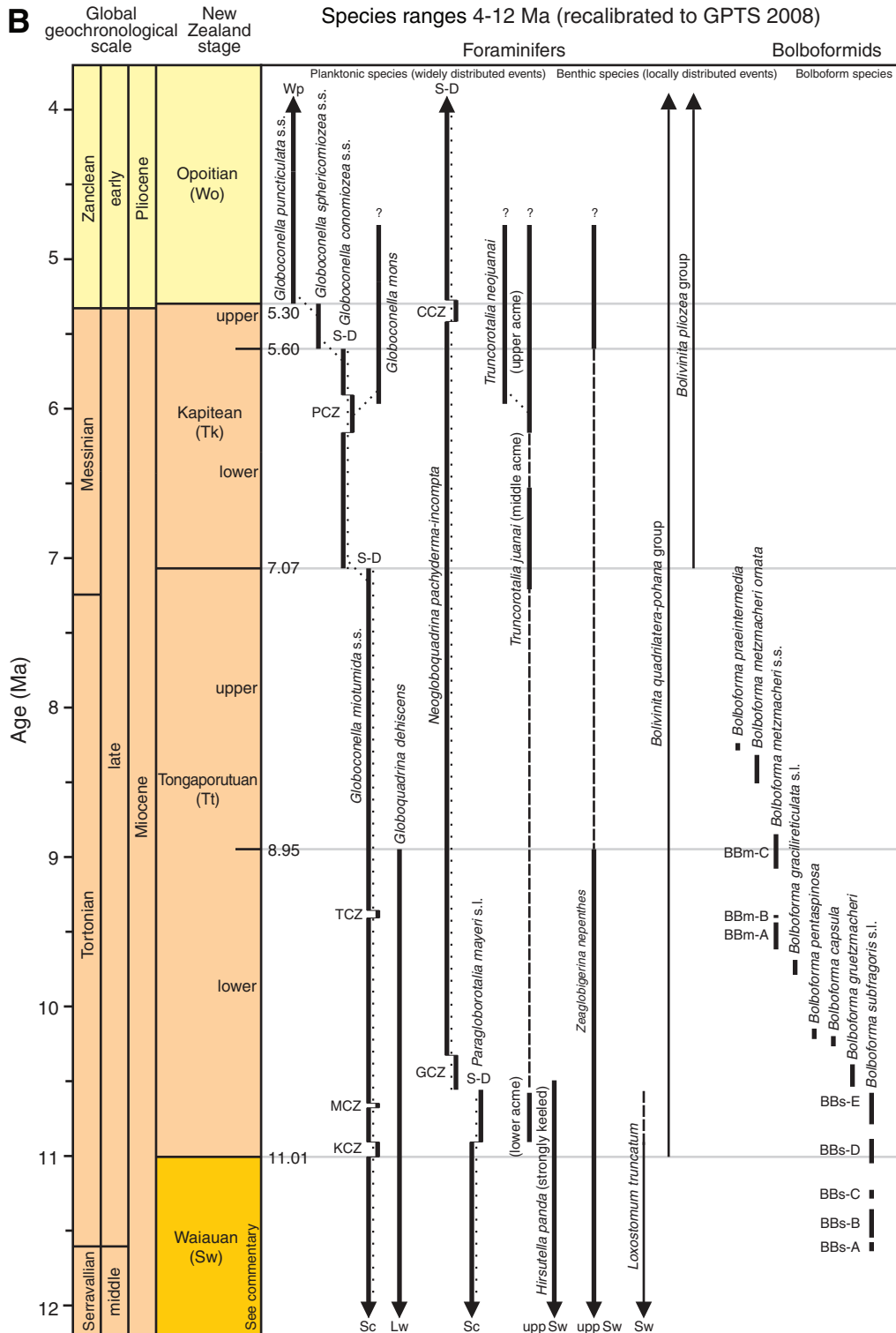


Figure F6 (continued). C. 10–18 Ma. (Continued on next page.)

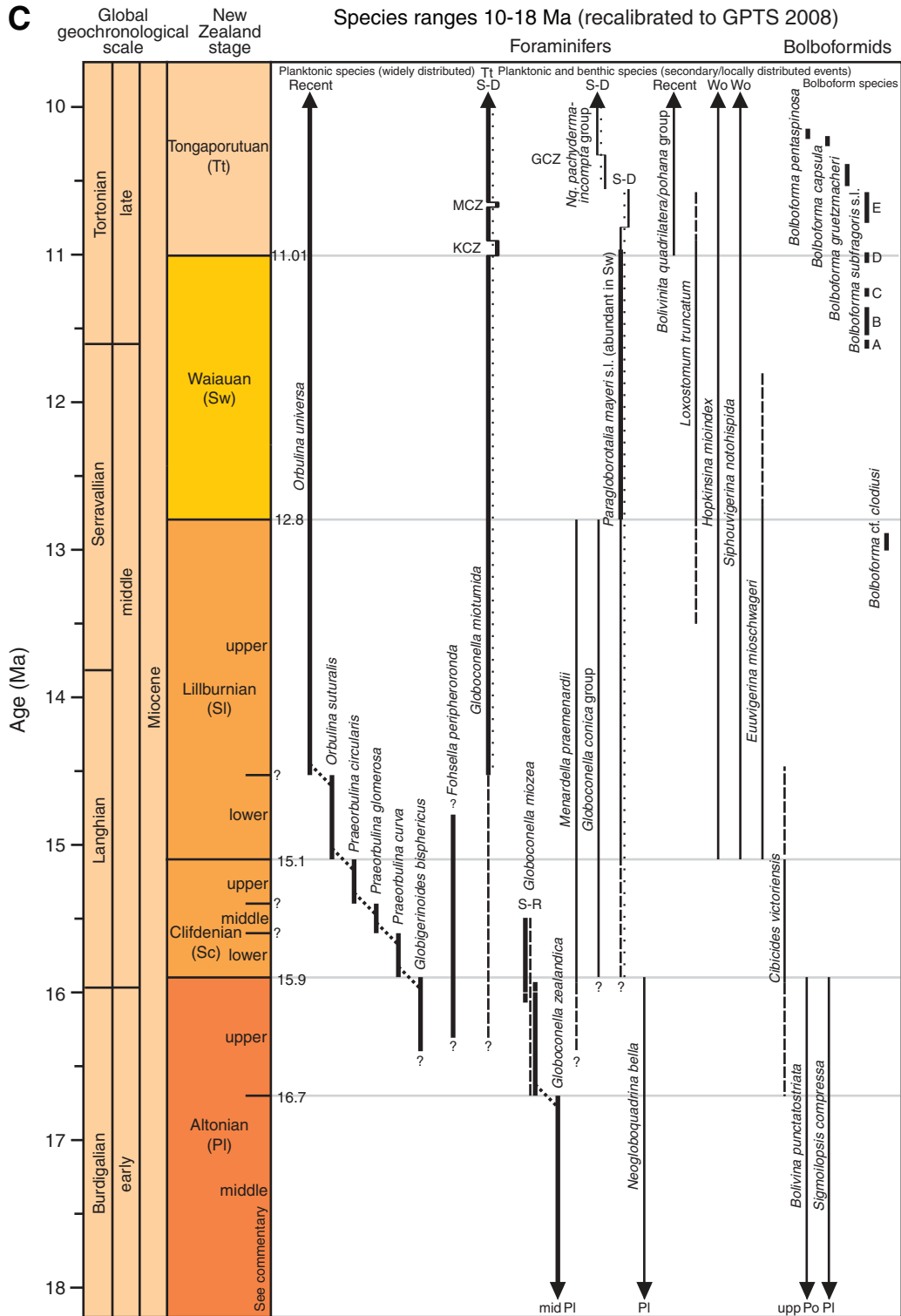


Figure F6 (continued). D. 16–24 Ma.

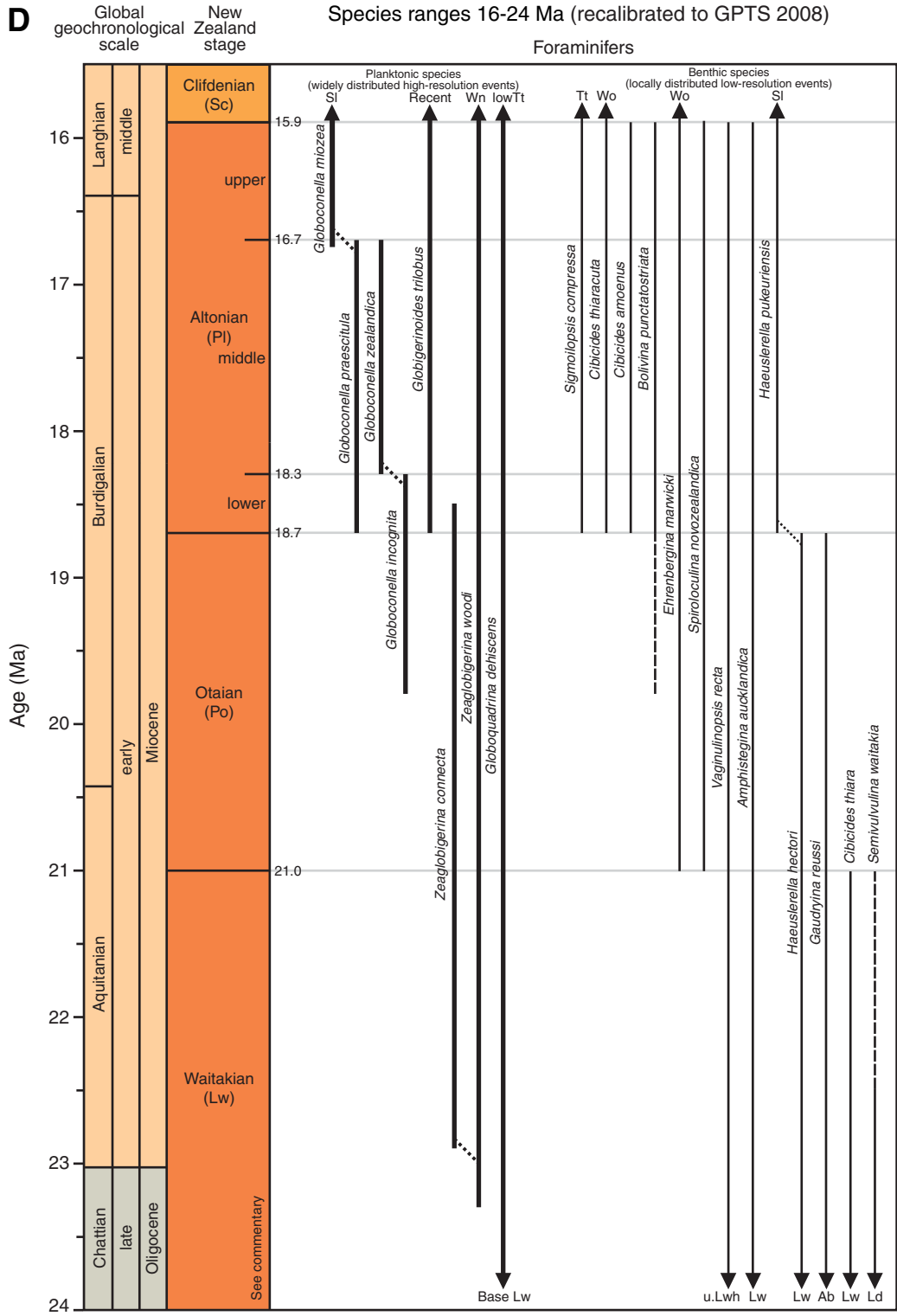


Figure F7. Adopted marine paleoenvironmental classification (after Hayward et al., 1999). Oceanicity assignments are based on planktonic foraminifer abundances relative to total foraminifers (planktonic %). Planktonic abundances <5% = sheltered or restricted inner neritic; abundances >95% = open oceanic. Paleodepth assignments during Expedition 317 were primarily based on benthic foraminiferal assemblages. Calibration of bathyal subenvironments follows Hayward et al. (1999) and Crundwell et al. (1994). Note that oceanicity determinations are partially independent of water depth.

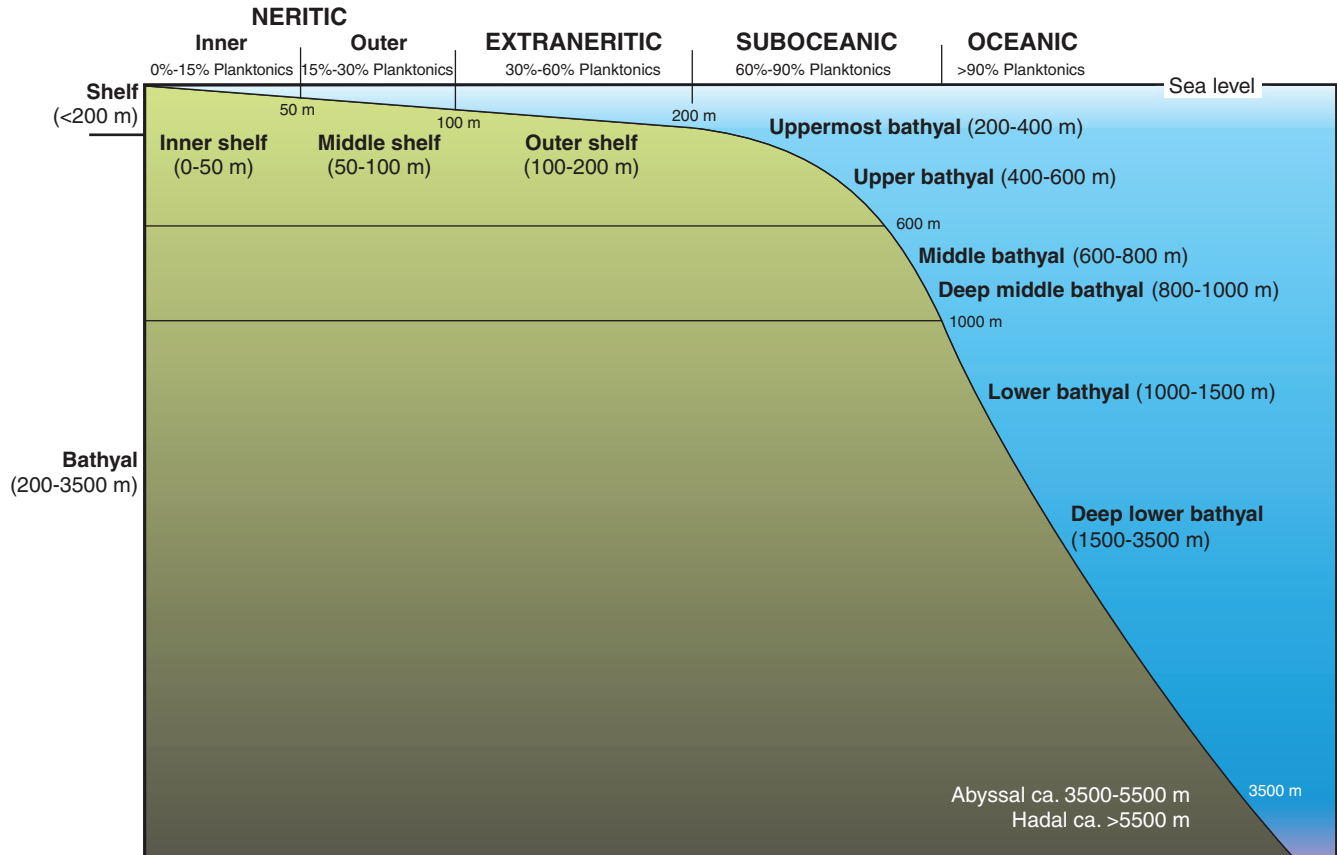


Figure F8. Eocene–Holocene calcareous nannofossil zones and datums, Expedition 317, modified after Martini (1971) and the geomagnetic polarity timescale of Ogg et al. (2008). Black bars = normal polarity, white bars = reversed polarity. LO = last occurrence, HO = highest occurrence, HCO = highest common occurrence, LRO = lowest regular occurrence, LCO = lowest common occurrence, X = crossover event (i.e., the co-occurrence of two marker species), AE = acme end. A. 0–20 Ma. (Continued on next page.)

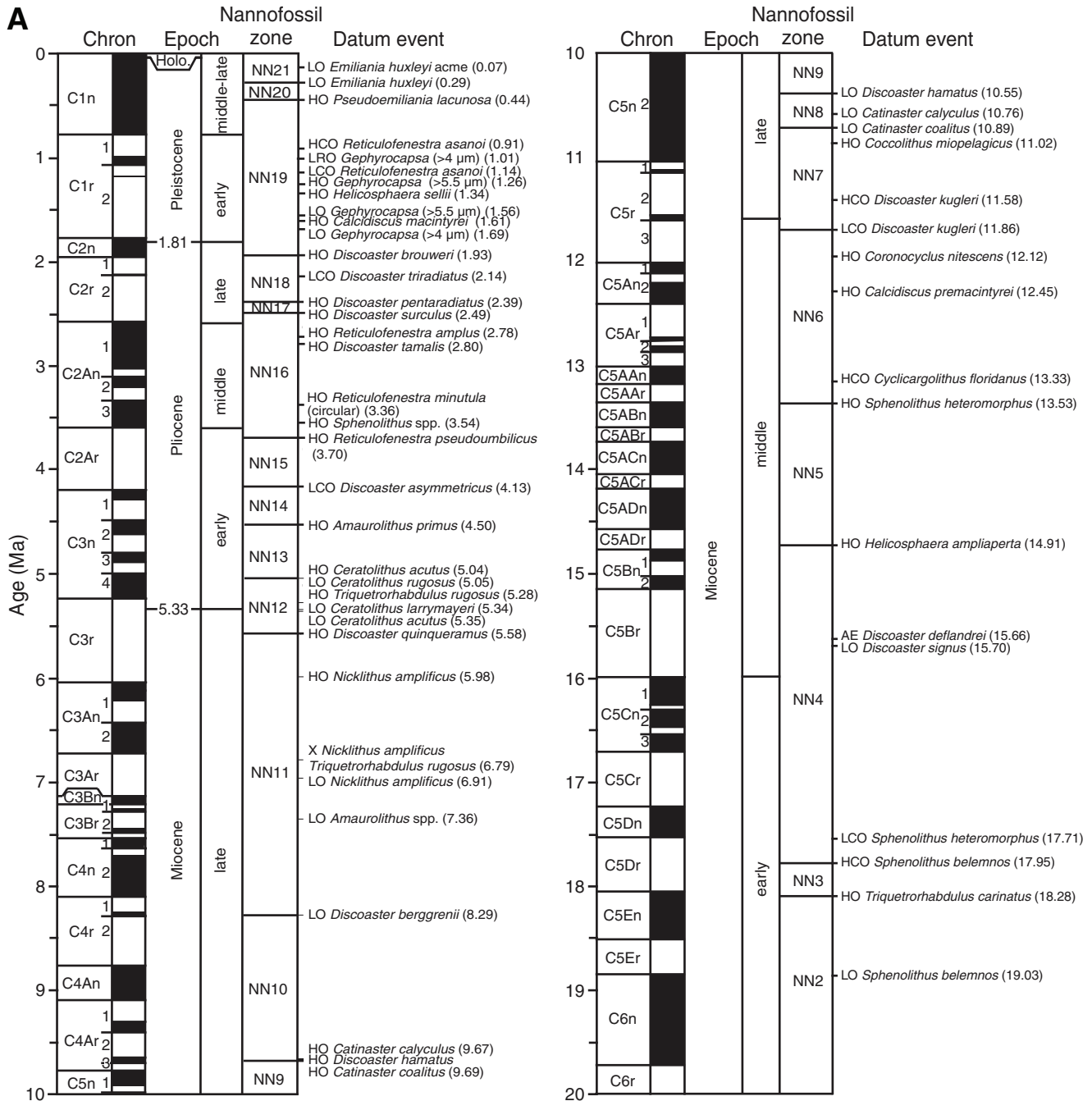


Figure F8 (continued). B. 20–40 Ma.

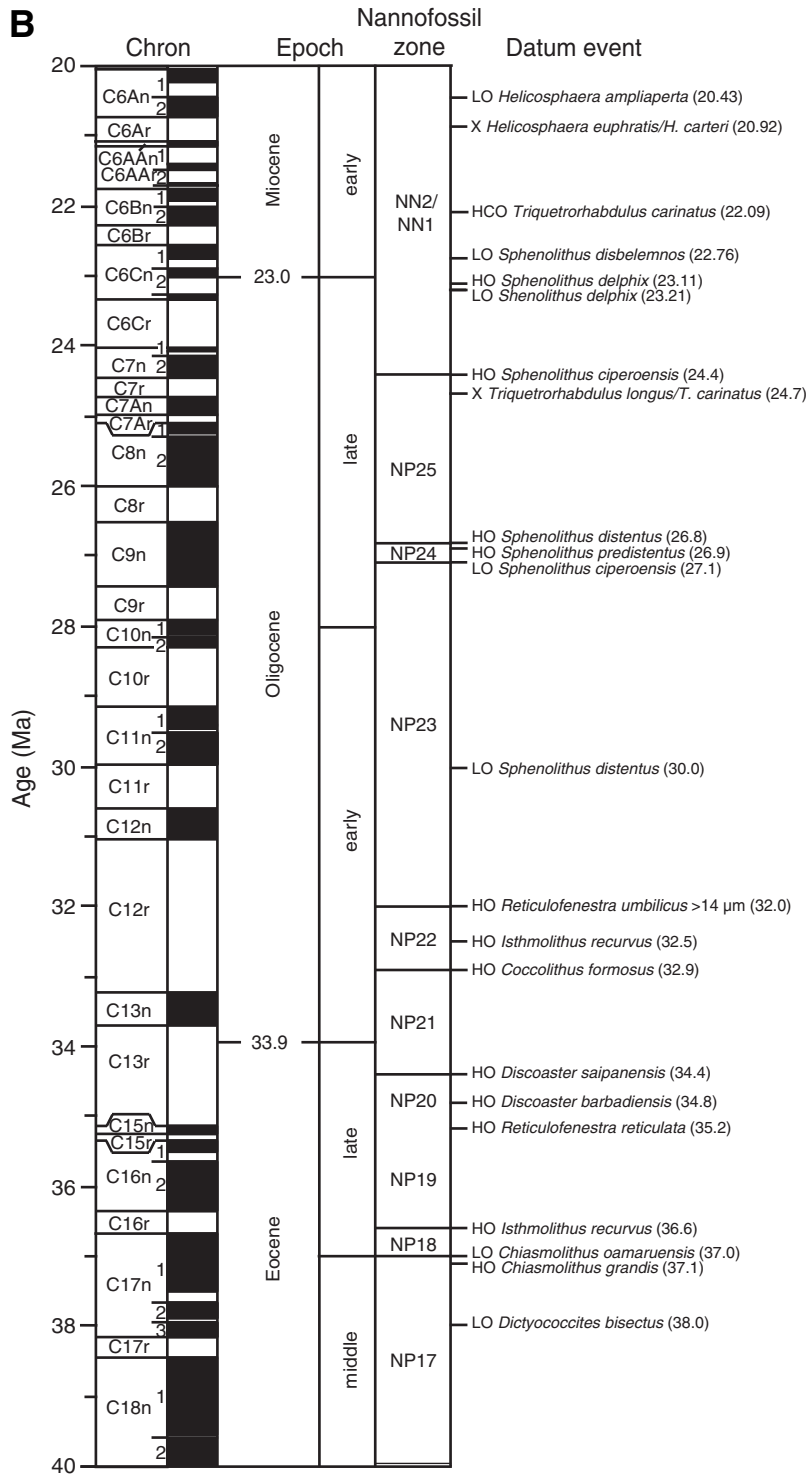


Figure F9. Quaternary (Pleistocene–Holocene) calcareous nannofossil scheme, Expedition 317, after Gartner (1977). LO = lowest occurrence, HO = highest occurrence, AB = acme beginning. Zonal codes modified after Martini (1971).

Zonal code	Zones (after Gartner, 1977)	
NN21b	<i>Emiliana huxleyi</i> acme Zone	
		AB <i>Emiliana huxleyi</i> (0.07 Ma)
NN21a	<i>Emiliana huxleyi</i> Zone	
		HO <i>Emiliana huxleyi</i> (0.29 Ma)
NN20	<i>Gephyrocapsa oceanica</i> Zone	
		LO <i>Pseudoemiliana lacunosa</i> (0.44 Ma)
NN19	small <i>Gephyrocapsa</i> Zone	LO small <i>Gephyrocapsa</i>
	<i>Helicosphaera sellii</i> Zone	LO <i>Helicosphaera sellii</i> (1.34 Ma)
	<i>Calcidiscus macintyreii</i> Zone	LO <i>Calcidiscus macintyreii</i> (1.61 Ma)
	<i>Discoaster brouweri</i> Zone	LO <i>Discoaster brouweri</i> (1.93 Ma)

Figure F10. Expedition 317 sampling strategy for (A) the shallow (~25–85 m) hole at each site dedicated to whole-round sampling for geochemistry, microbiology, and geotechnical studies and (B) the main, deep hole(s) at each site, usually implemented every fifth core below the maximum depth of the dedicated hole. Section numbers, sample codes, and whole-round dimensions are shown.

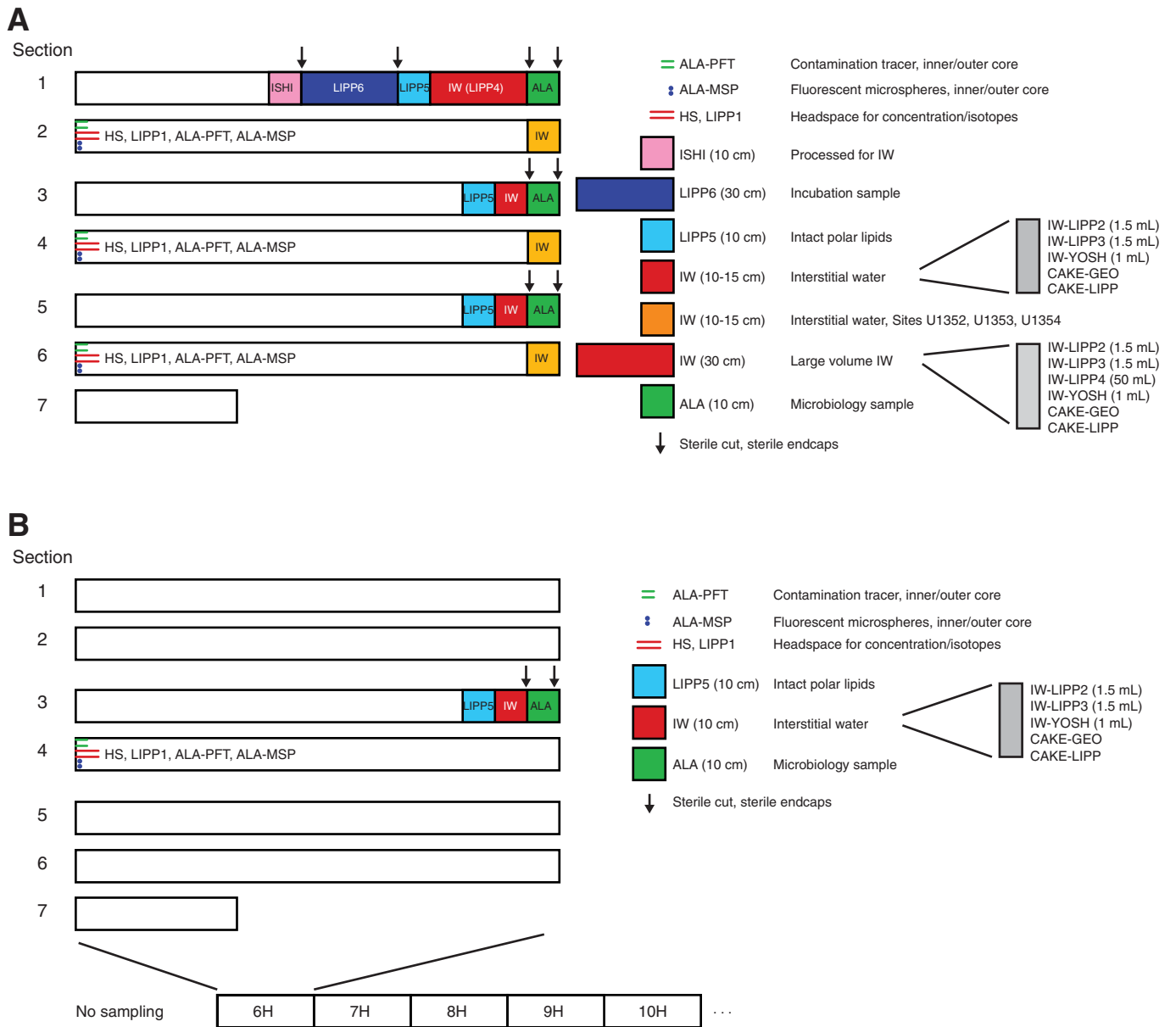


Figure F11. Diagrams showing results of decarbonation experiments on 10 sediment samples from Site U1351. TOC = total organic carbon, TC = total carbon. **A.** TOC_{DIFF} vs. TOC_{SRA} . **B.** Difference of TOC_{DIFF} and decarbonated TC vs. original inorganic carbon. **C.** $\text{TOC}_{\text{decarbonated TC}}$ vs. TOC_{SRA} . **D.** $\text{TOC}_{\text{decarbonated TC}}$ vs. $\text{TOC}_{\text{SRA (decarbonated)}}$.

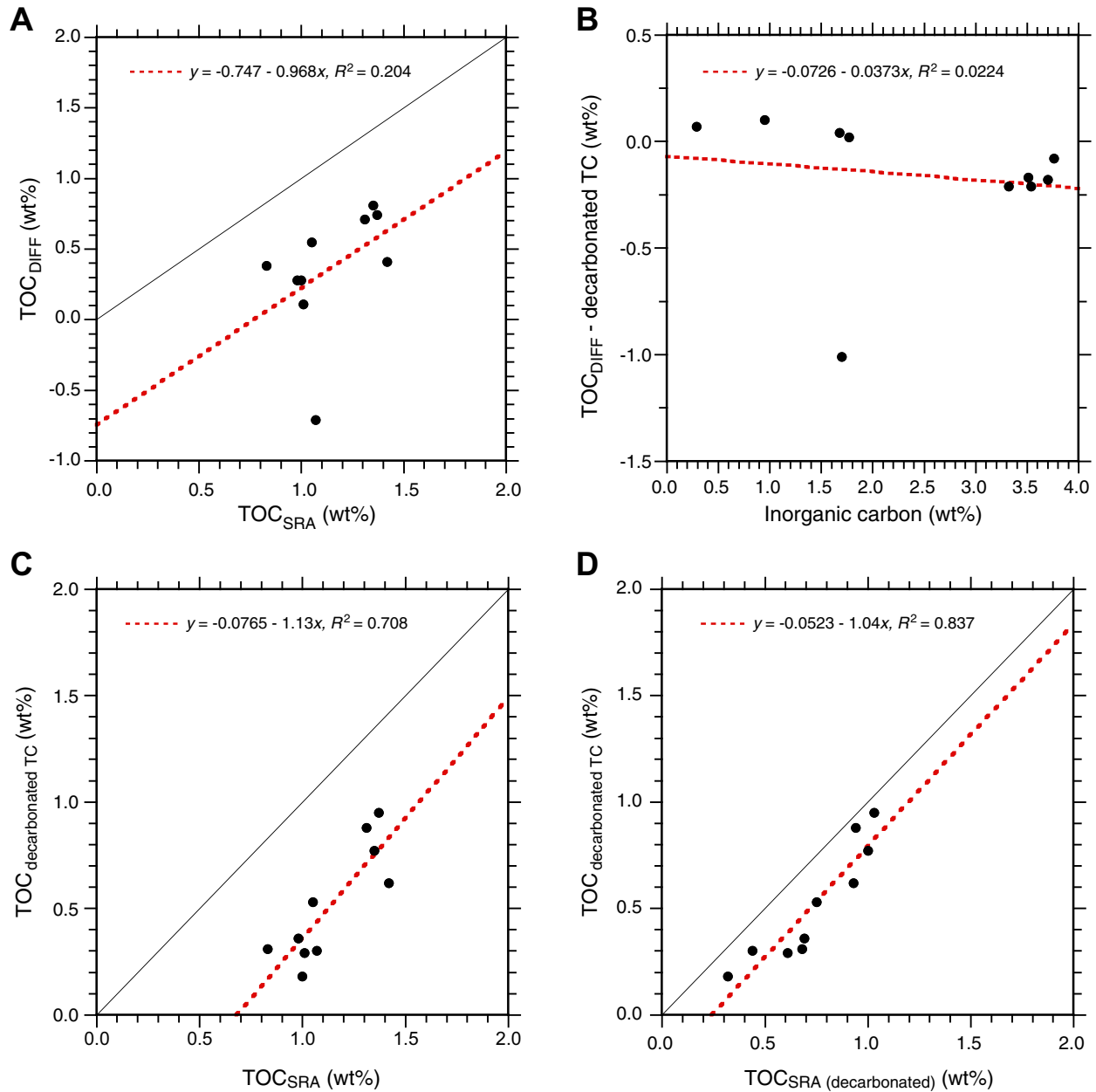


Figure F12. Wireline tool strings planned for deployment during Expedition 317. See site chapters for tool strings deployed at each site.

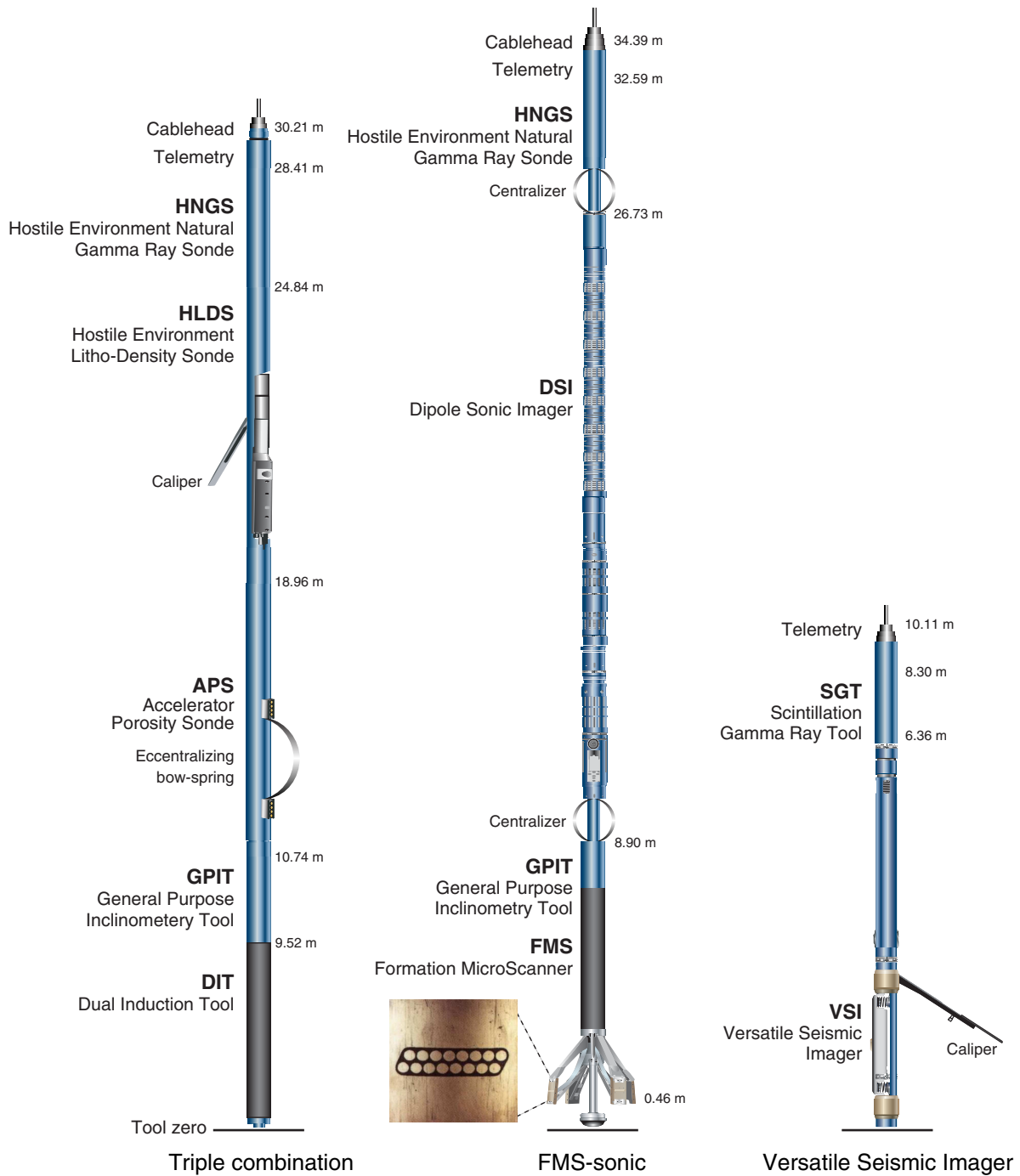


Table T1. IODP depth scale terminology, Expedition 317.

Depth scale name	Acronym	Origin	Method description	Submethod	Unit	Previous name	Previous unit
Drillers depth scale Drilling depth below rig floor	DRF	Drill floor	Add the lengths of all drill string components deployed beneath the rig floor, from bit to the point on the rig floor where the length of the deployed portion of the last string is measured.	Describe submethod of measuring drill string component length and length deployed at rig floor	m	Depth	mbrf
Drilling depth below seafloor	DSF	Seafloor	Subtract the distance between rig floor and seafloor, estimated by one of several submethods, from the drilling depth below rig floor (DRF)	A. Tag seafloor B. Mudline core C. Visual control D. Inherit depth E. Other	m	Depth	mbsf
Core depth scale Core depth below seafloor	CSF	Seafloor	Measure core sample or measurement offset below the core top and add it to the core top's drilling depth below seafloor; apply one of the submethods.	A. Let overlap if long B. Scale if long C. Other	m	Depth	mbsf
Core composite depth	CCSF	Seafloor	Align cores from one hole or multiple adjacent holes based on one of the submethods. The result is a newly constructed depth scale.	A. Append if long B. Scale by factor C. Correlate features D. Splice E. Other	m	Depth	mcd
Wireline depth scale Wireline log depth below rig floor	WRF	Drill floor	Measure length of wireline extended beneath the rig floor.	Describe submethod	m	Depth	mbrf
Wireline log depth below seafloor	WSF	Seafloor	Subtract the distance between rig floor and seafloor, estimated by one of several submethods, from the wireline log depth below rig floor (WRF)	A. Seafloor signal B. Drilling depth C. Inherit depth D. Other	m	Depth	mbsf
Wireline log speed-corrected depth below seafloor	WSSF	Seafloor	Correction for irregular motion of the tool during logging using accelerometer data; used for high-resolution logs such as microresistivity (FMS).	Describe submethod if applicable	m	Depth	mbsf
Wireline log matched depth below seafloor	WMSF	Seafloor	Pick log data from one run as a reference and map other run data using several tie points.	Describe reference log and number/type of tie points used	m	Depth	mbsf

Table T2. Locations of peaks used for mineral recognition in X-ray diffraction analyses, Expedition 317.

Mineral	Peak	
	2 θ	Å
Mica	8.567–9.054	10.321–9.767
Hornblende	10.342–10.638	8.554–8.316
Chlorite	12.291–12.656	7.201–6.994
Total clays	19.529–19.981	4.546–4.444
Quartz	20.677–21.025	4.296–4.225
Plagioclase	27.707–28.159	3.220–3.169
Calcite	28.908–29.882	3.089–2.990
Siderite	32.005–32.092	2.796–2.789
Pyrite	32.962–33.240	2.717–2.695
Dolomite	41.140–41.401	2.194–2.181
K-feldspar	50.501–51.006	1.807–1.791

Table T3. Calibrated planktonic foraminifer and bolboformid datums, Expedition 317. (See table notes.) (Continued on next two pages.)

Planktonic foraminifer datum/New Zealand stage boundary	Age (Ma)		Reference
	Berggren et al. (1995)	GPTS (2008)	
LO <i>Hirsutella hirsuta</i>	0.34	0.34	Cooper (2004)
Base Haweran (Wq) Stage	0.34	0.34	Cooper (2004)
LO <i>Truncorotalia truncatulinoides</i>	~1.1	~1.1	Cooper (2004)
HO <i>Truncorotalia tosaensis</i>	~1.1	~1.1	Scott (pers. comm., ODP Site 1123)
HO <i>Globoconella puncticuloides</i>	~1.5	~1.5	Cooper (2004)
Base Castlecliffian (Wc) Stage	1.63	1.63	Cooper (2004)
LO <i>Truncorotalia crassacarinina</i>	2.34	2.34	Cooper (2004)
LO <i>Truncorotalia crassula</i>	2.40	2.40	Cooper (2004)
Base Nukumaruan (Wn) Stage	2.40	2.40	Cooper (2004)
Top upper <i>Truncorotalia crassaformis</i> dextral coiling zone	2.45	2.45	Cooper (2004)
HO <i>Zeaglobigerina woodi</i> group	~2.7	~2.7	Crundwell (pers. obs., ODP Site 1123)
Base Mangapanian (Wm) Stage	3.00	2.99	Cooper (2004)
Base upper <i>Truncorotalia crassaformis</i> dextral coiling zone	3.05	3.04	Cooper (2004)
LO <i>Truncorotalia tosaensis</i>	3.09	3.09	Cooper (2004)
HO <i>Truncorotalia crassaconica</i>	3.09	3.09	Cooper (2004)
HO <i>Globoconella subconomiozea</i>	3.35	3.35	Cooper (2004)
Base Waipipian (Wp) Stage	3.60	3.62	Cooper (2004)
LO <i>Globoconella subconomiozea</i>	4.05	4.06	Cooper (2004)
LO <i>Globoconella puncticuloides</i>	~4.3	~4.3	Cooper (2004)
LO <i>Globoconella inflata</i> s.s. (populations >50% with <3.5 chambers)	~4.3	~4.3	Cooper (2004)
HO <i>Globoconella puncticulata</i> s.s. (populations <50% with >3.5 chambers)	~4.3	~4.3	Cooper (2004)
Top lower <i>Truncorotalia crassaformis</i> dextral coiling zone	4.38	4.39	Cooper (2004)
Base lower <i>Truncorotalia crassaformis</i> dextral coiling zone	4.40	4.41	Cooper (2004)
HO <i>Globoconella pliozea</i>	4.48	4.49	Cooper (2004)
HO <i>Globoconella mons</i>	4.64	4.65	Cooper (2004)
LO <i>Truncorotalia crassaconica</i>	4.75	4.75	Cooper (2004)
HO <i>Truncorotalia</i> aff. <i>crassaconica</i>	4.75	4.75	Cooper (2004)
LO <i>Globoconella puncticulata</i> s.s. (populations <5% weakly keeled)	5.28	5.30	Crundwell (2004)
Base Opoitian (Wo) Stage	5.28	5.30	Cooper (2004)
HO <i>Globoconella sphericomiozea</i> s.s. (populations >5% weakly keeled)	5.28	5.30	Crundwell (2004)
LO <i>Globoconella pliozea</i>	5.38	5.42	Crundwell (2004)
LO <i>Truncorotalia crassaformis</i>	5.41	5.45	Cooper (2004)
LO <i>Globoconella sphericomiozea</i> s.s. upper-lower Tk proxy (populations >5% unkeeled)	5.53	5.60	Crundwell (2004)
Intra-Kapitean (uTk/ITk boundary)	5.53	5.60	Cooper (2004)
HO <i>Globoconella conomiozea</i> s.s. (populations >5% keeled)	5.53	5.60	Crundwell (2004)
LO <i>Truncorotalia</i> aff. <i>crassaconica</i>	5.57	5.64	Cooper (2004)
LO <i>Globoconella mons</i>	5.84	5.97	Crundwell (2004)
LO <i>Truncorotalia neojuanai</i>	5.84	5.97	Cooper (2004) = <i>Truncorotalia</i> aff. <i>juanai</i>
Top middle <i>Truncorotalia juanai</i> acme	6.86	7.06	Crundwell (2004)
LO <i>Globoconella conomiozea</i> s.s. (populations <10% with <4.5 chambers)	6.87	7.07	Crundwell and Nelson (2007)
Base Kapitean (Tk) Stage	6.87	7.07	Cooper (2004)
HO <i>Globoconella miotumida</i> s.s. (populations >10% with >4.5 chambers)	6.87	7.07	Crundwell and Nelson (2007)
Base middle <i>Truncorotalia juanai</i> acme	7.09	7.21	Cooper (2004)
HO <i>Bolboforma praeintermedia</i> (top BBi Zone)	8.21	8.24	Crundwell and Nelson (2007)
HO <i>Hirsutella</i> cf. <i>ichinosekiensis</i> (non-carinate)	8.24	8.28	Crundwell (2004)
LO <i>Bolboforma praeintermedia</i>	8.25	8.29	Crundwell and Nelson (2007)
HO <i>Bolboforma metzmacheri ornata</i> (BBi/BBm zonal boundary)	8.28	8.32	Crundwell and Nelson (2007)
LO <i>Bolboforma metzmacheri ornata</i>	8.45	8.51	Crundwell and Nelson (2007)
HO <i>Bolboforma metzmacheri</i> s.s. (upper subzone) BBm-593/C	8.78	8.85	Crundwell and Nelson (2007)
Intra-Tongaporutuan (uTt/ITt boundary)	8.88	8.95	Cooper (2004)
HO <i>Globoquadrina dehiscens</i> upper-lower Tt proxy	8.88	8.95	Crundwell and Nelson (2007)
HO <i>Hirsutella</i> cf. <i>ichinosekiensis</i> (weakly carinate)	8.90	8.97	Crundwell (2004)
LO <i>Bolboforma metzmacheri</i> s.s. (upper subzone) BBm-593/C	9.01	9.08	Crundwell and Nelson (2007)
Top Tukemokihi Coiling Zone (TCZ) >20% dextral	9.27	9.36	Crundwell and Nelson (2007)
Top subzone BBm-593/B (small smooth-walled phases)	9.29	9.39	Crundwell (2004)
Base subzone BBm-593/B (small smooth-walled phases)	9.31	9.41	Crundwell (2004)
Base Tukemokihi Coiling Zone (TCZ)	9.31	9.41	Crundwell and Nelson (2007)

Table T3 (continued). (Continued on next page.)

Planktonic foraminiferal datum/New Zealand stage boundary	Age (Ma)		Reference
	Berggren et al. (1995)	GPTS (2008)	
HO <i>Bolboforma metzmacheri</i> s.s. (lower subzone) BBm-593/A	9.34	9.44	Crundwell and Nelson (2007)
<i>Bolboforma metzmacheri</i> s.s. abundance spike (lower subzone) BBm-593/A	9.44	9.53	Crundwell (2004)
LO <i>Bolboforma metzmacheri</i> s.s. (lower subzone) BBm/BBc zonal boundary	9.54	9.62	Crundwell and Nelson (2007)
HO <i>Bolboforma gracilireticulata</i> s.l.	9.61	9.69	Crundwell and Nelson (2007)
LO <i>Bolboforma gracilireticulata</i> s.l.	9.75	9.79	Crundwell and Nelson (2007)
HO <i>Bolboforma pentaspinosa</i>	10.08	10.15	Crundwell and Nelson (2007)
HO <i>Bolboforma capsula</i>	10.13	10.20	Crundwell and Nelson (2007)
LO <i>Bolboforma pentaspinosa</i>	10.15	10.22	Crundwell and Nelson (2007)
LO <i>Bolboforma capsula</i> (BBc/BBg zonal boundary)	10.20	10.27	Crundwell and Nelson (2007)
Top Glomar coiling zone (GCZ)	10.25	10.33	Crundwell (2004)
HO <i>Bolboforma gruetzmacheri</i>	10.31	10.39	Crundwell and Nelson (2007)
HO <i>Hirsutella panda</i> (strongly keeled morphotypes)	10.42	10.50	Crundwell (2004)
LO <i>Bolboforma gruetzmacheri</i>	10.46	10.54	Crundwell and Nelson (2007)
LO <i>Neogloboquadrina pachyderma</i> s.l.	10.48	10.56	Crundwell (2004)
Base Glomar coiling zone (GCZ)	10.48	10.56	Crundwell (2004)
HO <i>Paragloborotalia mayeri</i> s.l.	10.48	10.56	Crundwell (2004)
Top lower <i>Truncorotalia juanai</i> acme	10.50	10.58	Crundwell (2004)
HO <i>Bolboforma subfragoris</i> s.l. = top subzone BBs-593/E (BBg/BBs zonal boundary)	10.50	10.58	Crundwell and Nelson (2007)
Top upper <i>Hirsutella panda</i> acme (>5%)	10.56	10.64	Crundwell (2004)
Top Mapiro Coiling Zone (MCZ)	10.57	10.65	Crundwell (2004)
Base upper <i>Hirsutella panda</i> acme (>5%)	10.58	10.66	Crundwell (2004)
Base Mapiro Coiling Zone (MCZ)	10.60	10.68	Crundwell (2004)
<i>Bolboforma subfragoris</i> s.l. abundance spike (subzone BBs-593/E)	10.61	10.69	Crundwell (2004)
Base <i>Bolboforma subfragoris</i> s.l. subzone BBs-593/E	10.70	10.79	Crundwell (2004)
Top lower <i>Hirsutella panda</i> acme (>5%)	10.73	10.82	Crundwell (2004)
Top <i>Bolboforma subfragoris</i> s.l. subzone BBs-593/D	10.80	10.89	Crundwell (2004)
LO <i>Truncorotalia juanai</i> (base lower <i>Tr. juanai</i> acme)*	10.82	10.91	Crundwell (2004)
Top Kaiti Coiling Zone (KCZ)	10.82	10.91	Crundwell and Nelson (2007)
Base lower <i>Hirsutella panda</i> acme (>5%)	10.82	10.91	Crundwell (2004)
HCO <i>Paragloborotalia mayeri</i> s.l. (>5%)	10.88	10.97	Crundwell (2004)
Base Kaiti Coiling Zone (KCZ) Tt/Sw proxy	10.92	11.01	Crundwell and Nelson (2007)
Base Tongaporutuan (Tt) Stage	10.92	11.01	Cooper (2004)
Base <i>Bolboforma subfragoris</i> s.l. subzone BBs-593/D	10.97	11.06	Crundwell (2004)
Top <i>Bolboforma subfragoris</i> s.l. subzone BBs-593/C	11.17	11.23	Crundwell (2004)
Base <i>Bolboforma subfragoris</i> s.l. subzone BBs-593/C	11.23	11.29	Crundwell (2004)
Top <i>Bolboforma subfragoris</i> s.l. subzone BBs-593/B	11.29	11.36	Crundwell (2004)
Base <i>Bolboforma subfragoris</i> s.l. subzone BBs-593/B	11.47	11.55	Crundwell (2004)
Top <i>Bolboforma subfragoris</i> s.l. subzone BBs-593/A	11.50	11.58	Crundwell (2004)
LO <i>Bolboforma subfragoris</i> s.l. = base subzone BBs-593/A (base BBs Zone)	11.56	11.64	Crundwell and Nelson (2007)
Base Waiauian (Sw) Stage	~12.7	~12.8	Cooper (2004)
HO <i>Menardella praemenardii</i>	~12.7	~12.8	Crundwell (unpubl. data, DSDP Site 593)
HO <i>Paragloborotalia partimlabiata</i>	~12.7	~12.8	Crundwell (unpubl. data, DSDP Site 593)
HO <i>Bolboforma</i> cf. <i>clodiusi</i>	12.83	12.89	Cooper (2004)
HO <i>Globoconella conica</i>		12.98	Crundwell (unpubl. data, ODP Site 1171)
LO <i>Bolboforma</i> cf. <i>clodiusi</i>	13.06	13.09	Cooper (2004)
LCO <i>Paragloborotalia mayeri</i> s.l.		13.33	Crundwell (unpubl. data, ODP Site 1171)
LO <i>Truncorotalia juanai</i>		13.72	Crundwell (unpubl. data, ODP Site 1171)
LO <i>Orbulina universa</i> (population)	16.53	14.62	Cooper (2004)
HO <i>Fohsella peripheroronda</i>	~14.8	~14.8	Cooper (2004)
LO <i>Orbulina suturalis</i> (population)	~15.1	~15.1	Cooper (2004)
Base Lillburnian (Sl) Stage	~15.1	~15.1	Cooper (2004)
LO <i>Praeorbulina circularis</i> (population)	~15.4	~15.4	Cooper (2004)
LO <i>Praeorbulina glomerata</i> (population)	~15.6	~15.6	Cooper (2004)
LO <i>Praeorbulina curva</i> (population)	~15.9	~15.9	Cooper (2004)
Base Clifdenian (Sc) Stage	~15.9	~15.9	Cooper (2004)
<i>Globoconella miozea</i> (coiling transition – 20% dextral threshold)	16.06	16.02	Cooper (2004)
HO <i>Globoconella zealandica</i>	16.7	16.7	Cooper (2004)
LO <i>Globoconella miozea</i>	16.7	16.7	Cooper (2004)
HO <i>Globorotalia praescitula</i>	16.7	16.7	Cooper (2004)
HO <i>Globoconella incognita</i>	18.5	18.3	Cooper (2004)
HO <i>Zeaglobigerina connecta</i>	~18.8	~18.5	Cooper (2004)
LO <i>Globigerinoides trilobus</i>	19.0	18.7	Cooper (2004)
LO <i>Globoconella praescitula</i>	19.0	18.7	Cooper (2004)

Table T3 (continued).

Planktonic foraminiferal datum/New Zealand stage boundary	Age (Ma)		Reference
	Berggren et al. (1995)	GPTS (2008)	
Base Altonian (Pl) Stage	19.0	18.7	Cooper (2004)
HO <i>Catapsydrax dissimilis</i>	19.0	18.7	Cooper (2004)
LO <i>Globoconella incognita</i>	~20.2	~19.8	Cooper (2004)
Base Otaian (Po) Stage	21.7	21.0	Cooper (2004)
HO <i>Chiloguembelina triseriata</i>	~23.5	~22.7	Cooper (2004)
LO <i>Zeaglobigerina connecta</i>	~23.7	~22.9	Cooper (2004)
HO <i>Zeaglobigerina euapertura</i>	23.8	23.0	Cooper (2004)
LO <i>Zeaglobigerina woodi</i>	~24.0	~23.3	Cooper (2004)
HO <i>Globorotaloides testarugosa</i>	~24.0	~23.3	Cooper (2004)
HO <i>Neogloboquadrina opima</i>	~24.5	~23.8	Cooper (2004)
HO <i>Zeaglobigerina laibicrassata</i>	~24.5	~23.8	Cooper (2004)
HO <i>Chiloguembelina cubensis</i>	~24.5	~23.8	Cooper (2004)
LO <i>Globoquadrina dehiscens</i>	25.2	24.6	Cooper (2004)
Base Waitakian (Lw) Stage	25.2	24.6	Cooper (2004)
HO <i>Tenuitella munda</i>	~25.2	~24.6	Cooper (2004)
LO <i>Zeaglobigerina brazieri</i>	~25.5	~24.9	Cooper (2004)
LO <i>Fohsella kugleri</i>	~26.5	~26.1	Cooper (2004)
LO <i>Streptochilus pristinus</i>	~27.2	~26.9	Cooper (2004)
LO <i>Globoquadrina tripartita</i>	27.3	27.0	Cooper (2004)
Base Duntroonian (Ld) Stage	27.3	27.0	Cooper (2004)
HO <i>Antarcticella zeocenica</i>	~27.3	27.0	Cooper (2004)
LO <i>Globigerinopsis obesa</i>	~29.5	~29.6	Cooper (2004)
HO <i>Chiloguembelina ototara</i>	~29.5	~29.6	Cooper (2004)
Intra-Whaingaroan (upper/lower boundary)	30.0	30.1	Cooper (2004)
HO <i>Subbotina angiporoides</i>	30.0	30.1	Cooper (2004)
LO <i>Tenuitella ciperoensis</i>	~30.3	~30.4	Cooper (2004)
LO <i>Zeaglobigerina euapertura</i>	~30.5	~30.6	Cooper (2004)
LO <i>Catapsydrax dissimilis</i>	~30.5	~30.6	Cooper (2004)
HO <i>Zeaglobigerina ampliapertura</i>	~30.5	~30.6	Cooper (2004)
LO <i>Neogloboquadrina opima</i>	~30.5	~30.6	Cooper (2004)
LO <i>Globigerina juvenilis</i>	~30.5	~30.6	Cooper (2004)
LO <i>Zeaglobigerina laibicrassata</i>	~30.5	~30.6	Cooper (2004)
LO <i>Globorotaloides testarugosa</i>	~31.5	~31.7	Cooper (2004)
LO <i>Tenuitella munda</i>	~32.7	~32.9	Cooper (2004)
LO <i>Chiloguembelina cubensis</i>	~33.7	~33.9	Cooper (2004)
Base Whaingaroan (Lwh) Stage	34.3	34.4	Cooper (2004)
Base Runangan (Ar) Stage	36.0	36.0	Cooper (2004)
Base Kaiatan (Ak) Stage	37.0	36.8	Cooper (2004)
Base Bortonian (Ab) Stage	43.0	42.0	Cooper (2004)

Notes: Modified after Cooper (2004); based on Ogg et al. (2008). GPTS = geomagnetic polarity timescale. LO = lowest occurrence, HO = highest occurrence, HCO = highest common occurrence, LCO = lowest common occurrence.

Table T4. Calibrated benthic foraminifer datums used for local correlations with New Zealand stages, Expedition 317. (See table notes.)

Datum	Age (Ma)	Datum	Age (Ma)
HO <i>Bolivinita quadrilatera</i>	0.00	HO <i>Cibicides victoriensis</i>	15.10
HO <i>Loxostomum karrierianum</i>	0.00	LO <i>Hopkinsina mioindex</i>	15.10
HO <i>Notorotalia finlayi</i>	0.00	LO <i>Uvigerina mioshwageri</i>	15.10
HO <i>Notorotalia zelandica</i>	0.00	LO <i>Siphouvigerina notohispida</i>	15.10
HO <i>Rotalia wanganuiensis</i>	0.34	HO <i>Haeuslerella pukeuriensis</i>	~15.10
LO <i>Loxostomum karrierianum</i>	0.34	HO <i>Semivulvulina ihungia</i>	15.10
HO <i>Bolivinita pliozea</i>	0.60	HO <i>Uvigerina miozea</i>	15.10
HO <i>Haeuslerella parri</i>	1.63	HO <i>Bolivina punctatostriata</i>	15.87
HO <i>Notorotalia briggsi</i>	1.63	HO <i>Bolivinella australis</i>	15.87
HO <i>Notorotalia taranakia</i>	1.63	HO <i>Bolivinella bensoni</i>	15.87
HO <i>Uvigerina pliozea</i>	1.63	HO <i>Cibicides amoenus</i>	15.87
LO <i>Notorotalia zelandica</i>	2.40	HO <i>Discorotalia aranea</i>	15.87
LO <i>Rotalia wanganuiensis</i>	2.40	HO <i>Ehrenbergina marwicki</i>	15.87
HO <i>Haeuslerella pliocenica</i>	2.40	HO <i>Haeuslerella decepta</i>	15.87
HO <i>Notorotalia kingmai</i>	2.40–2.99	HO <i>Notorotalia biconvexa</i>	15.87
HO <i>Lenticulina mamilligera</i>	2.99	HO <i>Notorotalia serrata</i>	15.87
HO <i>Cibicides molestus</i>	2.99	HO <i>Notorotalia spinosa</i>	15.87
HO <i>Haeuslerella finlayi</i>	3.62	HO <i>Sigmoilopsis compressa</i>	15.87
HO <i>Hopkinsina mioindex</i>	3.62	HO <i>Spiroloculina novozealandica</i>	15.87
HO <i>Siphouvigerina notohispida</i>	3.62	LO <i>Cibicides victoriensis</i>	~18.71
HO <i>Cibicides finlayi</i>	3.62	LO <i>Bolivinella australis</i>	18.71
LO <i>Notorotalia finlayi</i>	3.62	LO <i>Cibicides thiaracuta</i>	18.71
LO <i>Notorotalia briggsi</i>	3.62	LO <i>Cibicides amoenus</i>	18.71
HO <i>Notorotalia hurupiensis</i>	3.62	LO <i>Haeuslerella pukeuriensis</i>	18.71
HO <i>Haeuslerella morgani</i>	3.62–5.30	LO <i>Notorotalia wilsoni</i>	18.71
LO <i>Notorotalia kingmai</i>	5.30	LO <i>Rectuvigerina ruatoria</i>	18.71
LO <i>Uvigerina pliozea</i>	5.30	LO <i>Semivulvulina ihungia</i>	18.71
LO <i>Haeuslerella parri</i>	~5.30	LO <i>Sigmoilopsis compressa</i>	18.71
LO <i>Haeuslerella finlayi</i>	~6.67	HO <i>Gaudryna reussi</i>	18.71
LO <i>Haeuslerella pliocenica</i>	6.67	HO <i>Haeuslerella hectori</i>	18.71
LO <i>Bolivinita pliozea</i>	6.67–8.95	HO <i>Uvigerina picki</i>	18.71
LO <i>Bolivinella liliei</i>	6.67	LO <i>Bolivina punctatostriata</i>	18.71
HO <i>Cibicides thiaracuta</i>	6.67	LO <i>Textularia miozea</i>	18.71
HO <i>Rectuvigerina ongleyi</i>	6.67	LO <i>Ehrenbergina marwicki</i>	21.03
HO <i>Rectuvigerina pohana</i>	6.67	LO <i>Notorotalia biconvexa</i>	21.03
HO <i>Vulvulina pennatula</i>	6.67	LO <i>Spiroloculina novozealandica</i>	21.03
HO <i>Textularia miozea</i>	6.67	HO <i>Bolivinella subrugosa</i>	21.03
HO <i>Bolivinella rugosa</i>	6.67–11.01	HO <i>Ehrenbergina cf. bicornis</i>	21.03
HO <i>Vulvulina jablonskii</i>	11.01	HO <i>Semivulvulina waitakia</i>	21.03
HO <i>Loxostomum truncatum</i>	8.95–11.01	HO <i>Uvigerina maynei</i>	21.03
LO <i>Uvigerina peregrina</i>	11.01	LO <i>Bolivinella bensoni</i>	24.58
HO <i>Discorotalia tenuissima</i>	11.01	LO <i>Ehrenbergina cf. bicornis</i>	24.58
LO <i>Haeuslerella morgani</i>	~11.01	LO <i>Haeuslerella decepta</i>	24.58
LO <i>Notorotalia taranakia</i>	11.01	LO <i>Haeuslerella hectori</i>	24.58
HO <i>Bolivinella profolium</i>	11.01	LO <i>Rectuvigerina ongleyi</i>	24.58
HO <i>Notorotalia wilsoni</i>	11.01	LO <i>Rectuvigerina rerensis</i>	24.58
HO <i>Quasibolivinella finlayi</i>	11.01	LO <i>Uvigerina miozea</i>	~24.58
HO <i>Rectuvigerina ruatoria</i>	11.01	LO <i>Uvigerina picki</i>	24.58
HO <i>Uvigerina mioshwageri</i>	11.01	LO <i>Vulvulina pennatula</i>	24.58
LO <i>Bolivinita pohana</i>	11.01	HO <i>Rectuvigerina striatissima</i>	24.58
LO <i>Bolivinita quadrilatera</i>	11.01	HO <i>Semivulvulina capitata</i>	~24.58
LO <i>Rectuvigerina pohana</i>	11.01	LO <i>Notorotalia spinosa</i>	27.04
LO <i>Notorotalia hurupiensis</i>	12.76	LO <i>Quasibolivinella finlayi</i>	27.04
LO <i>Uvigerina rodleyi</i>	12.76	LO <i>Semivulvulina waitakia</i>	27.04
LO <i>Bolivinella liliei</i>	12.76	LO <i>Vulvulina jablonskii</i>	27.04
LO <i>Bolivinella profolium</i>	12.76	HO <i>Bolivinella interrupta</i>	27.04
LO <i>Loxostomum truncatum</i>	12.76	HO <i>Notorotalia stachei</i>	27.04
HO <i>Rectuvigerina rerensis</i>	12.76	HO <i>Vulvulina granulosa</i>	27.04

Notes: Modified after Hornibrook et al. (1989) and Cooper (2004); recalibrated to Ogg et al. (2008). HO = highest occurrence, LO = lowest occurrence. Ages cited for each species relate to calibrated ages of New Zealand stage boundaries, and benthic foraminifer datums may not necessarily correlate precisely with stage boundaries. Hence ages are only approximate.

Table T5. Adopted abbreviations for phylogenetically based planktonic foraminiferal genera, Expedition 317. (See table note.)

Abbreviation	Genus
Cs.	<i>Catapsydrax</i>
Fs.	<i>Fohsella</i>
Gc.	<i>Globoconella</i>
Gd.	<i>Globorotaloides</i>
Ge.	<i>Globigerinella</i>
Gg.	<i>Globigerina</i>
Gp.	<i>Globigerinopsis</i>
Gq.	<i>Globoquadrina</i>
Gr.	<i>Globorotalia</i>
Gs.	<i>Globigerinoides</i>
Gt.	<i>Globigerinita</i>
Hr.	<i>Hirsutella</i>
Mn.	<i>Menardella</i>
Nq.	<i>Neogloboquadrina</i>
Or.	<i>Orbulina</i>
Pg.	<i>Paragloborotalia</i>
Pr.	<i>Præorbulina</i>
Sb.	<i>Subbotina</i>
Ss.	<i>Sphaeroidinellopsis</i>
Te.	<i>Tenuitella</i>
Tb.	<i>Turborotalita</i>
Tr.	<i>Truncorotalia</i>
Zg.	<i>Zeaglobigerina</i>

Note: Modified after Kennett and Srinivasan (1983).

Table T6. Selected Neogene benthic foraminifers used to estimate paleodepths in New Zealand waters, Expedition 317. (See table note.)

Paleodepth	Water depth (m)	Benthic foraminifer
Estuarine and subtidal	0–20	<i>Ammonia aoteana</i> <i>Elphidium advenum</i> <i>Elphidium charlottense</i> <i>Elphidium crispum</i> <i>Elphidium excavatum</i>
Inner shelf, including embayments	0–50	<i>Bolivina striatula</i> <i>Discorbis dimidiatus</i> <i>Elphidium novozealandicum</i> <i>Notorotalia hornibrooki</i> <i>Notorotalia inornata</i> <i>Quinqueloculina</i> spp. <i>Virgrinopsis turris</i> <i>Zealorilus parri</i>
Inner shelf	0–50	<i>Notorotalia aucklandica</i> <i>Notorotalia depressa</i> <i>Patellinella inconspicua</i>
Inner to middle shelf	0–100	<i>Bulimina marginata</i> <i>Ehrenbergina mestateri</i> <i>Loxostomum karrerianum</i> <i>Mississippina concentrica</i> <i>Notorotalia finlayi</i> <i>Notorotalia zelandica</i>
Middle shelf	50–100	<i>Hoeglundina elegans</i> <i>Saracenaria italica</i>
Middle to outer shelf	50–200	<i>Anomalinoidea sphericus</i> <i>Lenticulina calcar</i>
Outer shelf	100–200	<i>Globocassidulina canalisutulata</i> <i>Notorotalia profunda</i>
Uppermost bathyal	200–400	<i>Bolivinita quadrilatera</i> <i>Cibicidoides neoperforatus</i> <i>Cibicidoides wuellerstorfi</i> <i>Fursenkoina complanata</i> <i>Globocassidulina subglobosa</i> <i>Karriella cylindrica</i> <i>Melonis affinis</i>
Upper bathyal	400–600	<i>Bolivina robusta</i> <i>Glandulonodosaria</i> spp. <i>Martinotiella</i> spp. <i>Nonionella</i> spp. <i>Orthomorphina</i> spp. <i>Pleurostomella</i> spp. <i>Pyrgo murrhina</i> <i>Siphonodosaria</i> spp. <i>Trifarina anglosa</i> <i>Uvigerina</i> spp.
Middle bathyal	600–800	<i>Bulimina truncana</i> <i>Karriella bradyi</i> <i>Quinqueloculina venusta</i> <i>Sigmilopsis schlumbergeri</i> <i>Vulvulina</i> spp.
Deep middle bathyal	800–1000	<i>Cibicidoides robertsonianus</i> <i>Hopkinsina mioindex</i> <i>Neugeborina ovicula</i> <i>Stilostomella</i> spp. <i>Uvigerina</i> spp. (hispid form)
Lower bathyal	1000–1500	<i>Cibicidoides kullenbergeri</i>
Deep lower bathyal	1500–3500	<i>Laticarinina pauperata</i> <i>Melonis pompilioides</i> <i>Tritaxilina</i> spp.

Note: Modified after Hayward et al. (1999) and B.W. Hayward, unpubl. data.

Table T7. Calibrated Paleogene to recent calcareous nannofossil datums, Expedition 317. (See table notes.)
(Continued on next page.)

Calcareous nannofossil datum	Age (Ma)	Zone/ Subzone (base)	Reference
AB <i>Emiliana huxleyi</i> acme	0.08		Lourens et al. (2004)
LO <i>Emiliana huxleyi</i>	0.29	NN21	Lourens et al. (2004)
HO <i>Pseudoemiliana lacunosa</i>	0.44	NN20	Lourens et al. (2004)
HCO <i>Reticulofenestra asanoi</i>	0.91		Lourens et al. (2004)
LR <i>Gephyrocapsa</i> (>4 μm)	1.01		Lourens et al. (2004)
LCO <i>Reticulofenestra asanoi</i>	1.14		Lourens et al. (2004)
HO <i>Gephyrocapsa</i> (>6.5 μm)	1.21		de Kaenel et al. (1999)
HO <i>Gephyrocapsa</i> (>5.5 μm)	1.26		Lourens et al. (2004)
HO <i>Helicosphaera sellii</i>	1.34		Lourens et al. (2004)
LO <i>Pseudoemiliana lacunosa</i> acme	1.34		de Kaenel et al. (1999)
LO <i>Gephyrocapsa</i> (>5.5 μm)	1.56		Lourens et al. (2004)
HO <i>Calcidiscus macintyreii</i>	1.61		Lourens et al. (2004)
LO <i>Gephyrocapsa</i> (>4 μm)	1.69		Lourens et al. (2004)
Pliocene/Pleistocene boundary	1.806		Lourens et al. (2004)
HO <i>Discoaster brouweri</i>	1.93	NN19	Lourens et al. (2004)
LCO <i>Discoaster triradiatus</i>	2.14		Lourens et al. (2004)
HO <i>Discoaster pentaradiatus</i>	2.39	NN18	Lourens et al. (2004)
HO <i>Discoaster surculus</i>	2.49	NN17	Lourens et al. (2004)
HO <i>Reticulofenestra amplus</i>	2.78		Kameo and Bralower (2000)
HO <i>Discoaster tamalis</i>	2.80		Lourens et al. (2004)
HO <i>Reticulofenestra minutula</i> (circular)	3.36		Kameo and Bralower (2000)
HO <i>Sphenolithus</i> spp.	3.54		Lourens et al. (2004)
HO <i>Reticulofenestra pseudoumbilicus</i>	3.70	NN16	Lourens et al. (2004)
LCO <i>Discoaster asymmetricus</i>	4.13		Raffi et al. (2006)
HO <i>Amaurolithus primus</i>	4.50		Raffi et al. (2006)
HO <i>Ceratolithus acutus</i>	5.04		Lourens et al. (2004)
LO <i>Ceratolithus rugosus</i>	5.05	NN13	Lourens et al. (2004)
HO <i>Triquetrorhabdulus rugosus</i>	5.28		Lourens et al. (2004)
Miocene/Pliocene boundary	5.332		Lourens et al. (2004)
LO <i>Ceratolithus larrymayeri</i>	5.34		Lourens et al. (2004)
LO <i>Ceratolithus acutus</i>	5.35		Lourens et al. (2004)
HO <i>Discoaster quinqueringus</i>	5.58	NN12	Lourens et al. (2004)
HCO <i>Nicklithus amplificus</i>	5.98		Lourens et al. (2004)
X <i>Nicklithus amplificus</i> / <i>Triquetrorhabdulus rugosus</i>	6.79		Lourens et al. (2004)
LO <i>Nicklithus amplificus</i>	6.91		Lourens et al. (2004)
LO <i>Amaurolithus</i> spp.	7.36		Lourens et al. (2004)
LO <i>Discoaster berggrenii</i>	8.29		Lourens et al. (2004)
HO <i>Catinaster calyculus</i>	9.67		Lourens et al. (2004)
HO <i>Discoaster hamatus</i>	9.69	NN10	Lourens et al. (2004)
HO <i>Catinaster coalitus</i>	9.69		Lourens et al. (2004)
LO <i>Discoaster hamatus</i>	10.55	NN9	Lourens et al. (2004)
LO <i>Catinaster calyculus</i>	10.76		Lourens et al. (2004)
LO <i>Catinaster coalitus</i>	10.89	NN8	Lourens et al. (2004)
HO <i>Coccolithus miopelagicus</i>	11.02		Raffi et al. (2006)
HCO <i>Discoaster kugleri</i>	11.58		Lourens et al. (2004)
LCO <i>Discoaster kugleri</i>	11.86	NN7	Lourens et al. (2004)
HO <i>Coronocyclus nitescens</i>	12.12		Lourens et al. (2004)
HO <i>Calcidiscus premacintyreii</i>	12.45		Lourens et al. (2004)
HCO <i>Cyclicargolithus floridanus</i>	13.33		Lourens et al. (2004)
HO <i>Sphenolithus heteromorphus</i>	13.53	NN6	Lourens et al. (2004)
HO <i>Helicosphaera ampliaperata</i>	14.91	NN5	Lourens et al. (2004)
AE <i>Discoaster deflandrei</i>	15.66		Raffi et al. (2006)
LO <i>Discoaster signus</i>	15.70		Raffi et al. (2006)
LCO <i>Sphenolithus heteromorphus</i>	17.71		Lourens et al. (2004)
HCO <i>Sphenolithus belemnus</i>	17.95	NN4	Lourens et al. (2004)
HO <i>Triquetrorhabdulus carinatus</i>	18.28	NN3	Lourens et al. (2004)
LO <i>Sphenolithus belemnus</i>	19.03		Lourens et al. (2004)
LO <i>Helicosphaera ampliaperata</i>	20.43		Lourens et al. (2004)
X <i>Helicosphaera euphratis</i> / <i>Helicosphaera carteri</i>	20.92		Lourens et al. (2004)
HCO <i>Triquetrorhabdulus carinatus</i>	22.09		Raffi et al. (2006)
LO <i>Sphenolithus disbelemnus</i>	22.76		Lourens et al. (2004)
Oligocene/Miocene boundary	23.03		Lourens et al. (2004)
HO <i>Sphenolithus delphix</i>	23.11		Lourens et al. (2004)
LO <i>Sphenolithus delphix</i>	23.21		Lourens et al. (2004)

Table T7 (continued).

Calcareous nannofossil datum	Age (Ma)	Zone/ Subzone (base)	Reference
HO <i>Sphenolithus ciperoensis</i>	24.4	NN1	Blaj et al. (2009)
X <i>Triquetrorhabdulus longus</i> / <i>Triquetrorhabdulus carinatus</i>	24.7		Blaj et al. (2009)
HO <i>Sphenolithus distentus</i>	26.8	NP25	Blaj et al. (2009)
HO <i>Sphenolithus predistentus</i>	26.9		Blaj et al. (2009)
LO <i>Sphenolithus ciperoensis</i>	27.1	NP24	Blaj et al. (2009)
LO <i>Sphenolithus distentus</i>	30.0		Blaj et al. (2009)
HO <i>Reticulofenestra umbilicus</i> (>14 μm)	32.0	NP23	Blaj et al. (2009)
HO <i>Isthmolithus recurvus</i>	32.5		Villa et al. (2008)
HO <i>Coccolithus formosus</i>	32.9	NP22	Blaj et al. (2009)
Eocene/Oligocene boundary	33.8		Pälike et al. (2006b)
HO <i>Discoaster saipanensis</i>	34.4	NP21	Blaj et al. (2009)
HO <i>Discoaster barbadiensis</i>	34.8		Blaj et al. (2009)
HO <i>Reticulofenestra reticulata</i>	35.2		Backman (1987)
LO <i>Isthmolithus recurvus</i>	36.6	NP19	Backman (1986)
LO <i>Chiasmolithus oamaruensis</i>	37.0	NP18	Berggren et al. (1995)
HO <i>Chiasmolithus grandis</i>	37.1		Backman (1987)
LO <i>Dictyococcites bisectus</i> (>10 μm)	38.0		Berggren et al., 1995
HO <i>Chiasmolithus solitus</i>	40.4	NP17	Berggren et al., 1995
LO <i>Reticulofenestra reticulata</i>	42.0		Berggren et al., 1995
HO <i>Nannotrinita</i> spp.	42.3		Backman (1987)
LO <i>Reticulofenestra umbilicus</i> (>14 μm)	42.5		Backman (1987)
HO <i>Nannotrinita fulgens</i>	43.4		Backman (1986)
HO <i>Chiasmolithus gigas</i>	44.0	NP15c	Backman (1986)
LO <i>Sphenolithus furcatolithoides</i>	45.8		Jovane et al. (2007)
LO <i>Chiasmolithus gigas</i>	46.1	NP15b	Agnini et al. (2006)

Notes: Based on Ogg et al. (2008). AB = acme beginning, LO = lowest occurrence, HO = highest occurrence, HCO = highest common occurrence, LR = lowest entrance, LCO = lowest common occurrence, X = crossover event, AE = acme end.

Table T8. Replicate analyses of a carbonate sample to establish typical precision of carbonate analyses, Expedition 317.

Analysis no.	Sediment mass (g)	CaCO ₃ (wt%)	Inorganic carbon (wt%)
1	7.92	65.2	7.83
2	8.74	66.5	7.99
3	10.6	66.8	8.02
4	12.93	67.7	8.13
5	12.88	66.2	7.95
6	10.63	67.8	8.13
7	11.86	65.2	7.83
8	9.58	68.5	8.23
9	8.72	65.6	7.88
10	9.74	66.1	7.93
11	13.07	64.9	7.79
	Mean:	66.4	
	Standard deviation:	1.19	
	Coefficient of variation:	0.018	

Table T9. Replicate analyses of a rock standard to establish typical precision of total carbon, total nitrogen, and total sulfur contents of sediment samples, Expedition 317. (See table note.)

Analysis no.	N (wt%)	C (wt%)	S (wt%)
1	0.533	3.60	1.56
2	0.644	3.68	1.65
3	0.536	3.55	1.58
4	0.577	3.67	1.63
5	0.585	3.61	1.62
6	0.601	3.71	1.60
7	0.581	3.62	1.65
8	0.597	3.64	1.63
9	0.599	3.60	1.58
10	0.593	3.67	1.65
Mean:	0.58	3.64	1.62
Standard deviation:	0.032	0.046	0.032
Coefficient of variation:	0.06	0.01	0.02

Note: Rock standard from Weatherford Laboratories (#99986; PWDR5).



Table T10. Replicate analyses of a rock standard to establish typical precision of source rock analyzer (SRA) parameters, Expedition 317. (See table notes.)

Rock standard	S ₁ (mg HC/g rock)	S ₂ (mg HC/g rock)	S ₃ (mg HC/g rock)	T _{max} (°C)	TOC _{SRA} (wt%)	Hydrogen index (mg HC/g TOC)	Oxygen index (mg C/g TOC)	Pyrolysis carbon	Production index
Specification:	0.16	8.41	0.39	418	3.11	270.4	12.5	0.71	1.87
Lower limit:	0.08	7.15	0.29	413	2.33				
Upper limit:	0.24	9.67	0.49	423	3.89				
Tolerance (%):	50	15	25	5	25				
Analysis no.									
1	0.19	8.46	0.39	415.8	3.07	275.6	12.7	0.72	2.20
2	0.21	8.39	0.37	415.3	3.13	268.1	11.8	0.71	2.44
3	0.19	8.37	0.37	413.3	3.06	273.5	12.1	0.71	2.22
4	0.18	8.39	0.39	413.6	2.97	282.5	13.1	0.71	2.10
5	0.18	8.36	0.37	416.0	3.02	276.8	12.3	0.71	2.11
6	0.18	8.34	0.38	413.6	2.94	283.7	12.9	0.71	2.11
7	0.17	8.54	0.45	417.3	2.86	298.6	15.7	0.72	1.95
8	0.17	8.42	0.43	418.5	2.82	298.6	15.2	0.71	1.98
Mean:	0.18	8.41	0.39	415.4	2.98	282.2	13.2	0.71	2.14
Standard deviation:	0.013	0.065	0.030	1.89	0.11	11.26	1.46	0.005	0.15
Coefficient of variation:	0.071	0.008	0.077	0.005	0.036	0.040	0.110	0.007	0.072

Notes: Rock standard from Weatherford Laboratories (#99986; PWD5). Specification, lower and upper limits, and tolerance are as specified by Weatherford Laboratories. HC = hydrocarbon, TOC_{SRA} = total organic carbon from SRA. Pyrolysis carbon = $[0.83 \times (S_1 + S_2)/10]$, production index = $[S_1/(S_1 + S_2) \times 100]$.

**Table T11.** Source rock and elemental analysis data for 10 decarbonated sediment samples, Hole U1351A. (See table notes.)

Core, section, interval (cm)	Depth CSF-A (m)	IC (wt%)	TC (wt%)	TN (wt%)	TS (wt%)	TOC _{DIFF} (wt%)	TOC _{SRA} (wt%)	S ₁ (mg HC/g rock)	S ₂ (mg HC/g rock)	S ₃ (mg CO ₂ /g rock)	T _{max} (°C)	Hydrogen index (mg S ₂ /g TOC)	Oxygen index (mg S ₃ /g TOC)
317-U1351A-													
Original data													
1H-1, 11	0.11	3.51	4.22	0.53	0.04	0.71	1.31	0.27	1.13	1.25	429.7	86.3	95.4
1H-1, 25	0.25	3.32	4.06	0.61	0.06	0.74	1.37	0.22	1.01	1.16	422.0	73.7	84.7
1H-2, 43	1.92	1.68	2.49	0.54	0.26	0.81	1.35	0.22	1.05	1.19	422.5	77.8	88.1
2H-3, 98	6.68	0.29	0.67	0.52	0.37	0.38	0.83	0.05	0.20	0.23	416.4	24.1	27.7
2H-4, 50	7.70	1.70	0.99	0.53	0.48	-0.71	1.07	0.05	0.21	0.29	419.4	19.6	27.1
3H-2, 77	14.47	1.77	2.32	0.48	0.23	0.55	1.05	0.10	0.52	0.71	421.1	49.5	67.6
4H-2, 127	20.97	0.95	1.23	0.43	0.17	0.28	1.00	0.04	0.15	0.25	401.6	15.0	25.0
4H-3, 76	21.96	3.54	3.95	0.60	0.26	0.41	1.42	0.10	0.57	0.94	423.1	40.1	66.2
5H-2, 34	26.94	3.70	3.81	0.61	0.08	0.11	1.01	0.07	0.35	0.69	413.7	34.7	68.3
5H-2, 54	27.14	3.76	4.04	0.56	0.06	0.28	0.98	0.06	0.36	0.69	425.7	36.7	70.4
Decarbonated data													
						Difference							
1H-1, 11	0.11	—	0.88	0.35	0.42	-0.17	0.94	0.42	1.32	0.70	417.5	140.4	74.5
1H-1, 25	0.25	—	0.95	0.38	0.40	-0.21	1.03	0.40	1.27	0.76	421.2	123.3	73.8
1H-2, 43	1.92	—	0.77	0.32	0.69	0.04	1.00	0.37	1.07	0.36	415.0	107.0	36.0
2H-3, 98	6.68	—	0.31	0.39	0.53	0.07	0.68	0.12	0.22	0.05	405.3	32.4	7.4
2H-4, 50	7.70	—	0.30	0.34	0.73	-1.01	0.44	0.11	0.21	0.05	402.4	47.7	11.4
3H-2, 77	14.47	—	0.53	0.33	0.69	0.02	0.75	0.26	0.61	0.18	416.7	81.3	24.0
4H-2, 127	20.97	—	0.18	0.00	0.50	0.10	0.32	0.11	0.16	0.04	416.7	50.0	12.5
4H-3, 76	21.96	—	0.62	0.35	1.05	-0.21	0.93	0.33	0.73	0.21	411.2	78.5	22.6
5H-2, 34	26.94	—	0.29	0.30	0.55	-0.18	0.61	0.11	0.26	0.13	414.7	42.6	21.3
5H-2, 54	27.14	—	0.36	0.35	0.56	-0.08	0.69	0.20	0.43	0.12	414.7	62.3	17.4

Notes: Inorganic carbon (IC) from coulometric measurement of acid-evolved CO₂. Total carbon (TC), total nitrogen (TN), and total sulfur (TS) from elemental analysis of sediments. TOC_{DIFF} = total organic carbon from difference between TC and IC. TOC_{SRA} = total organic carbon from source rock analyzer pyrolysis (see Table T18 in the "Site U1351" chapter). T_{max} = pyrolysis temperature at which the evolution rate of S₂ is at a maximum. Difference is between TOC_{DIFF} (original data) and TOC_{decarbonated} TC (decarbonated data).

Table T12. Replicate analyses of an interstitial water sample to establish typical precision of Dionex ICS-3000 Ion Chromatograph for a typical anion (chloride) and cation (sodium), Expedition 317.

Analysis no.	Chloride (mM)	Sodium (mM)
1	326.9	278.8
2	327.7	278.4
3	326.3	279.4
4	327.4	279.3
5	327.9	277.9
6	327.1	279.3
7	326.5	278.0
Mean:	327.1	278.7
Standard deviation:	0.611	0.649
Coefficient of variation:	0.002	0.002

Table T13. Nominal concentrations and acceptable 2% limits in IAPSO seawater for sodium, potassium, magnesium, calcium, chloride, and sulfate by ion chromatography, Expedition 317.

Analyte	Concentration (mM)	2% error acceptable range (mM)
Sodium	480	470.4–489.6
Potassium	10.44	10.23–10.65
Magnesium	54	52.92–55.08
Calcium	10.55	10.34–10.76
Chloride	559	547.82–570.18
Sulfate	28.9	28.32–29.48

Table T14. Replicate analyses of elemental concentrations of IAPSO seawater standard to establish typical precision of the Teledyne Prodigy high-dispersion ICP-AES, Expedition 317. (See table notes.)

Analysis no.	Li (μM)	B (μM)	Si (μM)	Sr (μM)	Ba (μM)
Data set 1					
1	22.9	397.2	142.8	80.1	1.8
2	23.8	412.8	152.3	86.4	1.8
3	24.9	417.8	159.0	86.9	2.0
4	26.7	433.6	169.0	92.5	2.2
5	25.2	426.5	159.7	91.2	1.9
6	26.6	432.4	163.0	93.3	2.1
7	24.8	421.6	152.4	91.1	1.8
Mean:	25.0	420.3	156.9	88.8	1.9
2σ:	2.7	25.4	17.0	9.3	0.3
Data set 2					
1	27.1	418.6	152.2	89.3	1.6
2	26.2	411.8	148.0	88.7	1.5
3	26.7	415.8	148.9	88.9	1.6
4	26.4	410.1	148.1	88.8	1.5
5	27.1	410.0	150.5	88.7	1.7
Mean:	26.7	413.2	149.6	88.9	1.6
2σ:	0.8	7.6	3.5	0.4	0.1
Expected values:	25.9	431	103	93.3	0.106

Notes: Data set 1 was run on 5 December 2009; data set 2 was run on 13 December 2009. Expected values are as published in Burton (1996).

The Ba content of seawater is essentially zero (Murray et al., 2000), so it is uncertain why the measured Ba values in IAPSO seawater are slightly higher than this, as well as higher than some interstitial water samples analyzed during Expedition 317.

Table T15. Artificial salt solution used as the basis for all enrichment media, Expedition 317. (See table note.)

Component	Concentration
Distilled water	1000 mL
NaCl	30 g/L
KBr	0.09 g/L
CaCl ₂ ·2H ₂ O	1.47 g/L
MgCl ₂ ·6H ₂ O	5.67 g/L
KCl	0.6 g/L
MgSO ₄ ·7H ₂ O	5.62 g/L
Tris	1.20 g/L
SrCl ₂ ·6H ₂ O	0.02 g/L
The pH was adjusted to 7.5 with 1M HCl	
After autoclaving, the following were added from sterile stock solutions:	
NH ₄ Cl (1M)	4.67 mL/L
KH ₂ PO ₄ (1M)	1.5 mL/L
Trace element solution	1.0 mL/L
Vitamin mixture	1.0 mL/L

Note: The trace element solution and vitamin mixture was described by Widdel et al. (1983).

Table T16. Culture media used for cultivations at 70°C, Expedition 317. (See table note.)

Medium	Components	Concentration	Comments
317-1: Methanogen medium (hydrogenotrophy)	Na ₂ S	0.1% (wt/vol)	SS prepared under 5% H ₂ , 5% N ₂ , 90% N ₂ (biogas) headspace
317-2: Methanogen medium	Na ₂ S	0.1% (wt/vol)	SS prepared under 5% H ₂ , 5% N ₂ , 90% N ₂ (biogas) headspace
	Ethanol	0.5% (vol/vol)	
	Methanol	0.5% (vol/vol)	
317-3: Methanogen medium (methylotrophy)	Na ₂ S	0.1% (wt/vol)	SS prepared under 5% H ₂ , 5% N ₂ , 90% N ₂ (biogas) headspace
	Methylamine	0.01M	
317-4: Medium for heterotrophic sulfate-reducers	Na ₂ S	0.1% (wt/vol)	SS prepared under 5% H ₂ , 5% N ₂ , 90% N ₂ (biogas) headspace
	Pyruvate	0.01M	
	Succinate	0.01M	
317-5: Medium for fermenters	Na ₂ S	0.1% (wt/vol)	SS prepared under 5% H ₂ , 5% N ₂ , 90% N ₂ (biogas) headspace
	Peptone	0.05% (wt/vol)	
	Yeast	0.05% (wt/vol)	

Note: SS = artificial salt solution.

Table T17. Downhole measurements made by wireline tool strings, Expedition 317. (See table notes.)

Tool string	Tool	Measurement	Sampling interval (cm)	Approximate vertical resolution (cm)
Triple combination	HNGS	Spectral gamma ray	15	20–30
	GPIT	Tool orientation	3.8	15
	HLDS	Bulk density	2.5 and 15	38
	DIT	Resistivity	15	240/180/92
	APS	Porosity	5 and 15	36
Formation MicroScanner-sonic	HNGS	Spectral gamma ray	15	20–30
	GPIT	Tool orientation	3.8	15
	FMS	Microresistivity	0.25	0.5
	DSI	Acoustic velocity	15	107
Versatile Seismic Imager	SGT	Total gamma ray	5 and 15	30
	VSI	Acoustic travel time	Stations at 20 m	NA

Notes: All tool names are trademarks of Schlumberger. Sampling interval is based on optimal logging speed. NA = not applicable. For definitions of tool acronyms, see Table T18.

Table T18. Acronyms and units used for downhole wireline tools and measurements, Expedition 317. (See table note.)

Tool	Output	Description	Unit
APS	APLC	Accelerator Porosity Sonde Near/array limestone porosity corrected	%
	STOF	Computed standoff	Inch
	SIGF	Formation capture cross section	Capture units
DIT		Dual Induction Tool	
	IDPH	Deep induction resistivity	Ωm
	IMPH	Medium induction resistivity	Ωm
	SFLU	Spherically focused resistivity	Ωm
DSI		Dipole Sonic Imager	
	DTCO	Compressional wave slowness (Δt)	$\mu\text{s}/\text{ft}$
	DTSM	Shear wave slowness (Δt)	$\mu\text{s}/\text{ft}$
FMS		Formation MicroScanner	
	C1, C2	Orthogonal hole diameters	Inch
	P1AZ	Pad 1 azimuth Spatially oriented resistivity images of borehole wall	Degrees
GPIT		General Purpose Inclinometry Tool	
	DEVI	Hole deviation	Degrees
	HAZI	Hole azimuth	Degrees
	F _x , F _y , F _z A _x , A _y , A _z	Earth's magnetic field (three orthogonal components) Acceleration (three orthogonal components)	Degrees m/s^2
HLDS		Hostile Environment Litho-Density Sonde	
	RHOM	Bulk density	g/cm^3
	PEFL	Photoelectric effect	barns/e ⁻
	LCAL	Caliper (measure of borehole diameter)	Inch
	DRH	Bulk density correction	g/cm^3
HNCS		Hostile Environment Natural Gamma Ray Sonde	
	HSGR	Standard (total) gamma ray	gAPI
	HCGR	Computed gamma ray (HSGR minus uranium contribution)	gAPI
	HFK	Potassium	wt%
	HTHO	Thorium	ppm
	HURA	Uranium	ppm
SGT		Scintillation Gamma Ray Tool	
	GR	Total gamma ray	gAPI
	ECGR	Environmentally corrected gamma ray	gAPI
	EHGR	High-resolution environmentally corrected gamma ray	gAPI
VSI		Versatile Seismic Imager	
		Acoustic travel time	ms

Note: For the complete list of acronyms used in IODP and for additional information about tool physics and use, consult IODP-USIO Science Services, LDEO, at iodp.ldeo.columbia.edu/TOOLS_LABS/tools.html.